ESTIMATION OF SOIL MOISTURE USING MICROWAVE REMOTE SENSING DATA

by

TARENDRA LAKHANKAR

A dissertation submitted to the Graduate Faculty in Engineering in partial fulfillment of the requirements for the degree of Doctor of Philosophy, The City University of New York

2006

UMI Number: 3231970

Copyright 2006 by
Lakhankar, Tarendra

All rights reserved.

UMI Microform 3231970
Copyright 2006 by ProQuest Information and Learning Company.
All rights reserved. This microform edition is protected against
unauthorized copying under Title 17, United States Code.

ProQuest Information and Learning Company
300 North Zeeb Road
P.O. Box 1346
Ann Arbor, MI 48106-1346

© 2006

TARENDRA LAKHANKAR

All Rights Reserved

This manuscript has been read and accepted for the
Graduate Faculty in Engineering in satisfaction of the
dissertation requirement for the degree of Doctor of Philosophy.

Date

Prof. Hosni Ghedira
Professor of Civil Engineering
Chair of Examining Committee

Date

Dean Mumtaz K. Kassir
Executive Officer

Supervisory Committee

Prof. Reza Khanbilvardi

Prof. Vasil Diyamandoglu

Prof. Shayesteh Mahani

Prof. Reginald Blake

THE CITY UNIVERSITY OF NEW YORK

Abstract

ESTIMATION OF SOIL MOISTURE USING MICROWAVE

REMOTE SENSING DATA

By

Tarendra Lakhankar

Adviser: Professor Hosni Ghedira

Knowledge of soil moisture helps to derive parameters, such as evaporation, transpiration, infiltration, runoff and drainage classes, which are very useful in several agricultural and hydrological applications. Active and passive remote sensing sensors have shown the capability to estimate soil moisture based on the large contrast between the dielectric properties of wet and dry soil. However, the retrieval of soil moisture from microwaves system is mostly influenced by the characteristics of the vegetation cover. Indeed, having accurate information of the spatial distribution of vegetation (i.e. NDVI and vegetation optical depth) improves the soil moisture retrieval from microwave data.

The major objective of this research is to develop an algorithm to produce spatial retrieval of soil moisture using active microwave data. The algorithm will be developed using a combination of parametric and non-parametric tools such as neural networks, fuzzy logic, maximum likelihood etc. The study area is located in Oklahoma (97d35'W, 36d15'N). The active microwave data from RADARSAT-1 acquired in SCANSAR mode were used in combination with the soil moisture data generated from passive

Electronically Scanned Thinned Array Radiometer (ESTAR) during the SGP97 campaign operated by NASA.

This study will evaluate the contribution of vegetation in minimizing its effect on the accuracy of soil moisture retrieval. Based on our research, we found that the presence of higher vegetation cover reduces the accuracy of soil moisture retrieval. The empirical model to limit the effect of vegetation cover to maximize the accuracy of soil moisture retrieval has been proposed. The final product of this study, which has been produced, is a soil moisture map using active microwave data with different level of accuracy. This research also highlights the impact of spatial heterogeneity in land surface conditions on soil moisture retrieval from microwave data. Sensitivity of soil moisture retrieval in spatial heterogeneous area is positively correlated with the type of land-cover.

Acknowledgement

First and foremost, I would like to express my deep and sincere gratitude to my supervisor, Professor Hosni Ghedira, for his support and encouragement throughout my doctoral study. Prof. Hosni, you are a fantastic mentor, and a nice person. Without you, this thesis would have been impossible to be complete.

I would also like to thank, Professor Reza Khanbilvardi, for his guidance, encouragement and financial support over the last three years. It is my privilege to work with Prof. Reza and NOAA-CREST on such a nice project. I am grateful to Prof. Shayesteh Mahani for carefully following my work and useful comments and corrections. I also would like to thank Professor Vasil Diyamandoglu and Reginald Blake for their remarkable advices and for serving in my PhD committee. Special thanks to Dr. Shakila Merchant for her cheer and encouragement.

I wish to express my thanks to my colleagues Amir Azar, Juan Arevalo, Cecelia Hernandez, Heather Glickman, Yajaira Mejia, Bernard Mhando, Kallol Gangul, Rouzbeh Nazari, Nasim and Nasim at City College of New York for all the discussions, cooperation and for the wonderful time we have shared during various conference visits. Heather and Cecelia your last minute help in dissertation correction are very much appreciated. I also would like to thank Yevgeniy Leykin, Sanchia Peterson, Carla and all civil engineering staff for their love. My loving thanks are due to Rabi Khan and his family, for incorporating us in his house and lived like single happy family in New York.

Last but certainly not least, I am short of words, to express my loving gratitude to my wife, Aparna, for her patience, understanding and support throughout this study, and to my daughter, Astha, who sacrificed 3 years without her mom and dad, are a never-ending source of love, pride and inspiration to me. This study would not be possible without inspiration and loving support of my parents, brothers and in-laws.

Table of Content

ABSTRACT IV

ACKNOWLEDGEMENT VI

TABLE OF CONTENT VII

LIST OF FIGURES XI

LIST OF TABLES XIV

NOMENCLATURE XV

ACRONYMS XVI

1 INTRODUCTION 1

1.1 BACKGROUND 1

1.2 THESIS OBJECTIVES 4

1.3 THESIS HYPOTHESES 5

1.4 THESIS OVERVIEW 6

2 LITERATURE REVIEW 7

2.1 SOIL MOISTURE MEASUREMENT 8

2.2 SOIL MOISTURE SATELLITE MISSIONS 11

2.3 MICROWAVE REMOTE SENSING 13

2.4 MICROWAVE REMOTE SENSING AND SOIL MOISTURE 15

2.5 ACTIVE MICROWAVE MODELS FOR SOIL MOISTURE RETRIEVAL 16

2.5.1 Theoretical Models 17

2.5.2 Empirical Backscattering Models 17

2.5.3 Semi-empirical Backscattering Models 19

2.5.4 Linear Relationship 22

2.5.5 Modified Linear Relationship 23

2.5.6 Michigan Microwave Canopy Scattering (MIMICS) Model 24

2.5.7 An Optical/Microwave Synergistic Model 25

2.6 Effect of Vegetation on Soil Moisture Estimation 26

3 MICROWAVE THEORY AND SOIL MOISTURE 29

3.1 Introduction 29

3.2 Passive Microwave Theory 30

3.3 Active Microwave Theory 31

3.3.1 Frequency and Wavelength 34

3.3.2 Incidence angle 35

3.3.3 Polarization 37

3.4 Soil Surface Parameters 39

3.4.1 Dielectric Constant 39

3.4.2 Surface Roughness 40

3.4.3 Soil Texture 42

3.4.4 Topography 43

3.4.5 Observation depth 45

3.5 Vegetation Parameters 46

3.5.1 Normalized Difference Vegetation Index (NDVI) 46

3.5.2 Vegetation Optical Depth 48

3.5.3 Leaf Area Index (LAI) 50

4 NON-PARAMETRIC METHODS 52

4.1 Neural Network System 52

4.2 Fuzzy Logic Method 56

4.3 Remote Sensing and Neural Network System 60

5 STUDY AREA AND DATA ACQUISITION 64

5.1 SGP'97 Experiment 64

5.2 Soil Moisture Data 66

5.2.1 Field Soil moisture data 66

5.2.2 Truth Soil moisture Data 71

5.3 VEGETATION AND ANCILLARY DATA 73
5.3.1 NDVI *73*
5.3.2 Vegetation optical depth *73*
5.3.3 Soil Texture *74*
5.3.4 Land-cover data *75*
5.4 ACTIVE MICROWAVE DATA FROM RADARSAT-1 SATELLITE 75
5.4.1 Data Acquisition *77*
5.4.2 Data Pre-processing *78*
5.4.3 Image Registration *79*
5.5 TEXTURAL ANALYSIS SAR DATA 80

6 METHODOLOGY AND ALGORITHM DEVELOPMENT 85

6.1 INTRODUCTION 85
6.2 NEURAL NETWORK ALGORITHM 85
6.2.1 Neural Network Architecture *86*
6.2.2 Neural Network Training *91*
6.2.3 Effect of Threshold Limit *96*
6.2.4 Neural Network output *99*
6.3 FUZZY LOGIC ALGORITHM 100
6.4 MULTIPLE REGRESSION ANALYSIS 108
6.5 ASSESSMENT AND VALIDATION 112
6.5.1 Categorical Assessment *112*
6.5.2 Quantitative Assessment *117*
6.5.3 Model Validation *121*

7 EFFECT OF VEGETATION ON SOIL MOISTURE RETRIEVAL 125

7.1 INTRODUCTION 125
7.2 EFFECT OF NORMALIZED DIFFERENCE VEGETATION INDEX (NDVI) 125
7.3 EFFECT OF VEGETATION OPTICAL DEPTH 131

7.4 Effect of Sub-pixel Variability of Land Cover 133

7.5 Sub-pixels Variability of SAR backscatter and NDVI 135

8 CONCLUSIONS 138

SUGGESTED FUTURE WORK 143

APPENDICES 145

Appendix A: IEM Model 145

Appendix B: Sampling location and Vegetation type and growth stage 146

Appendix C: Vegetation Plant Height, Water Content and Biomass at SGP sites 147

Appendix D: Leaf Area Index measured at SGP97 sites 148

Appendix E: Optimization of NN architecture for nodes in single hidden layer 149

CONFERENCE PROCEEDING AND PRESENTATION 151

REFERENCES 153

List of Figures

Figure 1: Tensiometer for soil moisture measurement 9

Figure 2: A neutron probe for soil moisture measurements (Courtesy: United Nations website) 10

Figure 3: Time-Domain Reflectory (TDR) Soil Moisture Probe 10

Figure 4: Operating frequency and launching year of satellite missions 13

Figure 5: Backscatter contribution from vegetation cover 20

Figure 6: Details of RADARSAT-1 incidence angle, swath width and beam modes 33

Figure 7: Backscatter from forest area to L, C, and X band wavelength 35

Figure 8: Effect of incidence angle of RADARSAT-1 beam mode S1 and S7 on backscatter 36

Figure 9: Horizontal and vertical polarization 37

Figure 10: Backscatter from relative surface roughness 41

Figure 11: Backscatter response to soil moisture at different soil textures (Ulaby et al. 1981) 43

Figure 12: Effect of topography on radar backscatter 44

Figure 13: Penetration depth as a function of moisture content for loamy soil (Ulaby et al. 1996) 45

Figure 14: Spectral reflectance of green and dry vegetation 47

Figure 15: Typical Neural Network (3 Input layer, 2 Hidden Layer, 3 Output layer) 53

Figure 16: A typical fuzzy logic system (Wang and Jamshidi 2004) 58

Figure 17: SGP'97 study region (Jackson et al. 1999) 65

Figure 18: Test sites in the El Reno (ER) area. Coordinates are UTM. 67

Figure 19: Test sites in the Central Facility (CF) area. Coordinates are UTM. 68

Figure 20: Test sites in the Little Washita (LW) area. Coordinates are UTM. 68

Figure 21: SAR backscattering and L-Band SM for vegetated and harvested area (July 02 data) 69

Figure 22: SAR backscattering and L-Band SM for vegetated and harvested area (July 12 data) 69

Figure 23: Landsat Thematic Mapper false color composite image of study area (SGP'97 website) 70

Figure 24: Relationship of SAR backscattering values with truth soil moisture data 72

Figure 25: Path of Radarsat-1 satellite (Courtesy: Canadian Space Agency) 77

Figure 26: Details of study area with reference to soil moisture and SAR images 80

Figure 27: Textural images generated from SAR image. 84
Figure 28: Effect of number of training pixel on classification accuracy 89
Figure 29: Effect of training pixels on variance of the accuracy for 25 runs of model 89
Figure 30: Accuracy of test data with combination of hidden nodes in two hidden layers 90
Figure 31: Accuracy of data with combination of hidden nodes in single hidden layer 90
Figure 32: Standard deviation of accuracy of test data with variation in nodes in the hidden layer 91
Figure 33: Role of each training data set in the training process (Ghedira and Bernier, 2004) 93
Figure 34: Data selection methodology for model development 95
Figure 35: Methodology applied in soil moisture estimation 96
Figure 36: Effect of threshold limit on soil moisture maps (Area A, July 12 data) 98
Figure 37: Effect of threshold limits on pixel classification 99
Figure 38: Data and clusters in selected two dimensions of the input space (SM and Backscatter) 104
Figure 39: Data and clusters in selected two dimensions of the input space (SM and NDVI) 104
Figure 40: Effect of cluster radii on retrieval accuracy for different datasets 105
Figure 41: Sugeno Rule used for prediction of soil moisture 106
Figure 42: Soil moisture map using fuzzy logic method (July 12, 1997) 107
Figure 43: Soil moisture map using the multiple regression method (July 12, 1997) 111
Figure 44: Comparison between neural network (a) and fuzzy logic (b) output 118
Figure 45: BOX plot shows RMSE for 100 models runs of NN, FL and MR output 120
Figure 46: Comparison of soil moisture retrieval from fuzzy model with truth values (July 02 data) 123
Figure 47 Comparison of soil moisture retrieval from fuzzy model with truth values (July 12 data) 123
Figure 48 Comparison of soil moisture retrieval error and its relationship with NDVI (July 02 data) 124
Figure 49 Comparison of soil moisture retrieval error and its relationship with NDVI (July 12 data) 124
Figure 50: Effect of NDVI classes on SAR backscattering and soil moisture relationship 126
Figure 51: Effect of NDVI class on soil moisture classification accuracy 127
Figure 52: Effect of NDVI and soil texture as an input on accuracy of soil moisture retrieval 128
Figure 53 Correlation between NDVI and soil moisture retrieval error (July 02, 1997 data) 129
Figure 54 Correlation between NDVI and soil moisture retrieval error (July 12, 1997 data) 129

Figure 55: Effect of plant height on absolute error in soil moisture retrieval.....130

Figure 56: Relationship between NDVI and vegetation optical depth for the study area 131

Figure 57: Effect of vegetation optical depth class on classification accuracy 132

Figure 58: Example of heterogeneity classes 134

Figure 59: SAR variability as function of NDVI values (Area A on July 2nd 1997).....136

Figure 60: SAR variability as function of NDVI variability (Area A on July 2nd 1997) 137

List of Tables

Table 1: Details of active microwave sensors 12

Table 2: Wavelengths and frequencies used in microwave remote sensing 14

Table 3: Characteristics of RADARSAT-1 satellite 33

Table 4: Parameter used for ESTAR soil moisture estimation for different land cover categories 74

Table 5: Details of soil texture data used as input parameter 75

Table 6: Characteristics of RADARSAT-1 beam mode **(**Courtesy: Canadian Space Agency**)** 76

Table 7: Main characteristics of used RADARSAT-1 scenes 77

Table 8: GLCM based features 83

Table 9: Relationship between SAR Textural images using Correlation Coefficients 83

Table 10: Neural network training parameters 94

Table 11: RMSE and correlation values for input variable used in neural network model 100

Table 12: RMSE and correlation values for input variable used in fuzzy logic model 106

Table 13: RMSE and correlation values for input variable used in regression model 110

Table 14: Confusion matrix using SAR for 200 test pixels 114

Table 15: Confusion matrix using SAR, NDVI and optical depth for 200 test pixels 114

Table 16: Normalized Confusion matrix using SAR for 200 test pixels 115

Table 17: Normalized Confusion matrix using SAR, NDVI and optical depth for 200 test pixels 115

Table 18: Z-test of classification results using a 95% confidence level (Z-Score<1.96) 117

Table 19: ANOVA test for RMSE for 100 models runs of NN and FL output 119

Table 20: Model validation using RMSE and correlation coefficient (in bracket) 122

Table 21: Average values of NDVI for different land cover in study area 135

Table 22: Effect of heterogeneity of pixel on accuracy of classification 135

Table 23: Correlation coefficient for SAR variability and NDVI values 136

Table 24: Correlation coefficient for SAR variability and NDVI variability 137

Nomenclature

ε	Dielectric constant
ε’	Real part of the dielectric constant of a soil-water-air mixture
ε “	Imaginary part of the dielectric constant of a soil-water-air mixture
εa	Dielectric constant of air
εi	Dielectric constant of ice
εw	Dielectric constant of water
θ	Incidence angle
λ	wavelength
ρ_b	bulk density
σ	Backscatter coefficient
τ	Vegetation optical depth
e_s	surface emissivity
b	vegetation absorption parameter
T_{sky}	reflected sky brightness
T_{soil}	thermometric temperature of the soil
T_{atm}	thermometric temperature of the atmosphere
T_S	soil surface temperature
M_v	Volumetric soil moisture
$\hat{K}$	Kappa Coefficient
R	surface reflectivity
R_t	target range
T_B	brightness temperature
G_r and G_t	received and transmitted antenna gain
P_r and P_t	received and transmitted power

Acronyms

ASCAT	METOP's Advanced SCATterometer
AVHRR	Advanced Very High Resolution Radiometer
CMIS	Cross-Track Microwave Imaging Sensor
ENVISAT	Environmental Satellite (ESA)
ERS	ESA Remote Sensing satellite
ESA	European Space Agency
ESTAR	Electronically Scanned Thinned Array Radiometer (L band)
FIFE	First ISLSCP Field Experiment
GCP	Ground Control Point
GIS	Geographical Information System
GPS	Global Positioning System
HAPEX	Hydrologic Atmospheric Pilot Experiment
HH	Horizontal like-polarization
HV	Horizontal-vertical cross-polarization
VV	Vertical like-polarization
HYDROS	Hydrosphere State Mission
HAPEX	Hydrologic Atmospheric Pilot Experiment
ISLSCP	International Satellite Land Surface Climatology Project
LAI	Leaf Area Index
MACHYDRO	Multi-sensor Aircraft Campaign for Hydrology
METOP	Europe’s first operational polar-orbiting weather satellite
NASA	National Aeronautics and Space Administration
NDVI	Normalized Difference Vegetation Index
NERC	Natural Environment Research Council
NPOESS	National Polar-orbiting Operational Environmental Satellite System
OXSOME	OXford County SOil Moisture Experiment
PBMR	Push Broom Microwave Radiometer
RADARSAT	Canadian Radar Satellite

RAR	Real aperture radar
RMSE	Root mean square error
SAR	Synthetic Aperture Radar
SGP	Southern Great Plains Mission (NASA)
SIR-C/X-SAR	Shuttle Imaging Radar-C and X-Band Synthetic Aperture Radar
SMEX	Soil Moisture Experiments
SMOS	Soil Moisture and Ocean Salinity mission
SSM/I	Special Sensor Microwave/Imager (Radiometer)
TM	Thematic Mapper
VIIRS	Visible Infrared Imager / Radiometer Suite

1 Introduction

1.1 Background

In a remote sensing context, soil moisture represents the amount of water in the top layer of the soil surface; generally the upper 5 to 10 cm below natural ground surface. The temporal and spatial variations of soil moisture represent two key parameters for various hydrological modeling processes. With the actual field measurement techniques, it is very difficult to have a spatial measurement of soil moisture, as it varies spatially and its value is generally affected by the heterogeneity of soil surface characteristics. The water content of the upper soil layer, or soil moisture, is being increasingly used as input for various hydrological modeling processes. Presently, most of the hydrological models that require soil moisture information use point measurements or spatial distribution of soil moisture derived from physically-based models.

Spatial distribution of soil moisture is being increasingly used as input to hydrological models. Having an accurate estimation of soil moisture with acceptable resolution and revisit times is indispensable for an efficient hydrological modeling and for improved soil wetness forecasts. Indeed, the of many environmental phenomena such as flooding and drought extent cannot be captured by ground measurements alone, which explain the increasing importance of remote sensing in conjunction with ground-based observations in natural resource management and especially in water resources monitoring and forecasting. Additionally, improved estimates of spatial and temporal variation of surface moisture will significantly enhance our ability to more accurately predict the

magnitude and the timing of extreme events and natural hazards such as extreme weather, floods, and droughts.

Active and passive remote sensing systems and especially those operating in the microwave region of the electromagnetic spectrum have shown the ability to measure the spatial variation of soil moisture content in the near-surface layer under a variety of topographic and land cover conditions. Spaceborne active microwave sensors are able to provide high spatial resolution (up to 10 m), but have low temporal resolution and are more sensitive to surface characteristics than passive systems. However, passive microwave sensors provide low spatial resolutions (40 to 50 km) with a higher temporal resolution (12 to 24 hrs). Most of the applications of active microwave in soil moisture retrieval are based on the hypothesis that the signal backscattered from the observed scene is widely dependent of the dielectric contrast that exists between wet and dry soils. Indeed, under the same land cover condition, the stronger radar backscattering values are observed for high soil moisture. However, soil moisture estimation based on active microwave data only may face several challenges since the microwave sensors are sensitive to other land cover characteristics such as vegetation density, surface roughness, and soil texture (Engman and Chauhan 1995; Hall et al. 1995; Ulaby et al. 1981; Ulaby et al. 1986b).

This study is motivated by the recent and intensive research activities currently underway by the European and US scientific communities to design the two upcoming satellite missions fully dedicated to soil moisture mapping from space: ESA[1]'s Soil Moisture and

[1] European Space Agency

Ocean Salinity Mission (SMOS) and NASA's Hydrosphere Sate Mission (HYDROS) exclusively dedicated for soil moisture retrieval. SMOS mission is designed to use a L-band interferometric radiometer to make measurements at a spatial resolution of about 40 km and HYDROS will combine a passive radiometer (40 km) and an active scatterometer (3 and 10 km). The expected launch dates for these missions are 2007 and 2010, respectively. These two missions are first-of-a-kind exploratory measurements and aim to measure soil moisture with an accuracy of 0.04 m^3 m^{-3} (4%).

The accuracy of satellite-derived soil moisture is usually affected by the presence of vegetation which significantly modifies and attenuates the outgoing microwave radiation of the soil and makes the retrieval of realistic soil moisture from satellite-based sensors difficult and inaccurate. Soil moisture estimation by active remote sensing involves the measurement of backscattering which may be affected by both vegetation canopy and soil moisture. The vegetation canopy may affect the backscattered energy by contributing to the volume backscatter of the observed scene and by attenuating the soil component of the total backscatter (Ulaby *et al*. 1981; Kasischke *et al*. 2003). The total amount of attenuation and backscatter depends on several vegetation parameters, such as vegetation height, leaf area index, and vegetation water content; and on sensor-related characteristics such as angle of incidence, frequency, and polarization. Indeed, it is expected that the presence of high and dense vegetation decreases the correlation between the backscattering and the soil moisture.

An accurate retrieval of soil moisture from microwave sensors under the complex conditions explained above seems difficult using a simple linear or non-linear algorithm. However, a combination of parametric and non-parametric tools may serve as a better

alternative. Parametric models such as maximum likelihood are based on statistical assumptions where coefficients of linear and non-linear models are assumed to be a function of the input variables. On the other hand, non-parametric models, such as artificial neural network and fuzzy logic do not require a priori assumptions about statistical behavior of the data or about any specific relationship between variables. These models use the data itself to extract the relationship between the input and output. In this study, we focus on the development of a soil moisture retrieval algorithm by using tools such as neural networks, fuzzy logic and multiple linear regression models to produce high-accuracy soil moisture maps from active microwave data.

1.2 Thesis Objectives

The primary intent of this study is to produce spatial soil moisture maps from satellite active microwave data, which will be used as an additional input to the advanced hydrologic prediction system (AHPS) operated by NOAA National Weather Service. Adding an accurate estimation of soil moisture distribution to the AHPS will improve its flood forecasting accuracy and flash flood warning capabilities. AHPS was designed to provide forecasts of river levels and river flow volumes in time frames ranging from hourly to seasonally at local and regional scale. The main objectives of this thesis are:

- The first objective of this study was focused on developing an appropriate algorithm for soil moisture mapping from active microwave data. To produce soil moisture maps, an algorithm based on Fuzzy Logic and Neural Network will be developed, optimized and validated. The algorithm uses active microwave data acquired from RADARSAT-1 satellite operating at 5.3 GHz with 25 m spatial resolution.

- The second objective of this study was to assess the effect of vegetation on soil moisture retrieval. The measured backscatter from microwave sensors is sensitive to the structure and the density of vegetation. The normalized difference vegetation index (NDVI) and vegetation optical depth will be used as additional inputs to the Fuzzy Logic and Neural Network algorithm.
- The third objective of this study is to review the effect of sub-pixels variability of land cover on soil moisture retrieval. The variability of land cover within small area is expected to have an effect on soil moisture accuracy.

A multiple linear regression model has been also proposed to retrieve soil moisture from Radarsat-1 data. The choice of the study areas for this work was driven mainly by the availability of intensive field data collected by NASA, USDA, NRC and around 25 other institutions and organizations during Southern Great Plains Mission in 1997.

1.3 Thesis Hypotheses

The research study presented in this thesis is based on the four following hypotheses:

- First, soil moisture can be estimated from active microwave backscattering based on the large contrast in the dielectric constant between wet and dry soils.
- Second, the relationship between radar backscattering and soil moisture may be affected significantly by the presence of vegetation and its characteristics: density, structure, moisture content etc.
- Third, non-statistical models (i.e. neural network and fuzzy logic), are more suitable to define the relationship between radar backscattering and soil moisture and to assimilate additional information to the model (i.e. vegetation related information).

- Fourth, taking into account the level of land cover heterogeneity during the mapping Process could improve the soil moisture retrieval in heterogeneous areas.

1.4 Thesis Overview

This dissertation is structured as follows: In Chapter 2 the scientific background of the application of microwave in soil moisture retrieval is discussed. A review of previous relevant research and their contributions to the problem of interest are presented in Chapter 3. In Chapter 4, a detailed description of neural network and fuzzy logic methods has been given. Chapter 5 describes the study area, the collection and processing of satellite and field data. The development, calibration, and validation of the retrieval algorithm are presented in Chapter 6. The findings of this research and results discussion are presented in chapter 7. Chapter 8 concludes the dissertation.

2 Literature Review

Life cannot exist without water. Water covers 71 percent of the earth surface; of that amount, oceans make up 97.2 percent; polar ice 2.15 percent and groundwater represents 0.63 percent. Soil moisture is the amount of water in the top layer of the earth surface; that within reach of plant roots constitutes 0.005 percent of global water. Despite its small amount, soil moisture plays an important role in the interaction mechanisms between hydrosphere, biosphere and atmosphere as well as disciplines such as meteorology, hydrology, agriculture and climate change. In the agricultural field, soil moisture plays a dominant role in determining crop yield potential for irrigation management. Information on saturated soil conditions, which have reached field capacity, can serve as early warning tool for possible flooding. Soil moisture content is important for watershed modeling that ultimately provides information on hydroelectric and irrigation capacity. In meteorology and climate change, soil moisture directly affects the partitioning of energy at the surface between latent and sensible heating. Evaporation will predominate at higher soil moisture, adding to atmospheric moisture content.

The spatial and temporal distribution and quantification of soil moisture over large regions enhances estimates of evapo-transpiration through the influence on partitioning of available energy at the ground surface into sensible and latent heat exchange (Entekhabi et al. 1994). The weather predictions models require extensive information about the interaction of land surface processes. The partitioning of precipitation between runoff and infiltration is necessary for flood forecasting. Soil moisture information is important economically due to water conservation benefits through rational irrigation scheduling,

and by increasing crop yield through optimal soil moisture conditions at the time of pre-planting and during the growing season. Erosion prediction through hydrological modeling and a better understanding of the relationship between erosion and runoff producing zones require soil moisture information. Economical and environmental benefits can be achieved by selecting suitable pesticides for soil moisture dependent insects and diseases. Global climate change can be monitored through broader knowledge of high or low soil moisture content (Engman 1991; Engman and Chauhan 1995).

2.1 Soil Moisture Measurement

Traditionally soil moisture has been characterized as a point based measurement. The widely used techniques for point based measurement are Gravimetric, Hygrometric, Tensiometric, Nuclear, and Electromagnetic methods. In the thermo-gravimetric method a soil sample is removed and its weight is calculated before and after it has been dried in an oven at 105°C for 24 hours. All other methods are ultimately calibrated on this standard method for soil wetness. The hygrometric and Tensiometric methods use soil water potential as a measure of soil moisture (Figure 1). The nuclear method shown in Figure 2 based on neutron scattering, measures the slowdown of fast neutrons emitted into the soil. Radioactive technique based on gamma attenuation is also a nuclear method used for soil moisture measurement. The dependence of resistivity of soil on the soil water potential is used as basis for electromagnetic methods for soil moisture measurement. The widely used electromagnetic method is Time-Domain Reflectory (TDR), in which the velocity of propagation of a high frequency voltage pulse in the soil is measured and related to the soil dielectric properties. A typical TDR soil moisture

measuring probe is shown in Figure 3. The soil moisture content can be estimated since the dielectric constant of a soil increases with the water fraction.

The traditional field measurement techniques of soil moisture estimation yield a point measurement, but it is difficult to obtain adequate data to represent this average. Soil moisture measurement over large areas using traditional field techniques is neither suitable nor cost effective. Furthermore, these traditional techniques generate point measurement data that do not always represent the spatial distribution of soil moisture over the region, for soil moisture varies in space and in time and its value is generally affected by the variability of soil properties, topography, land cover, evapo-transpiration and precipitation. Hence, it is necessary to look for technologies such as remote sensing as an alternative to produce spatial distribution of soil moisture estimates.

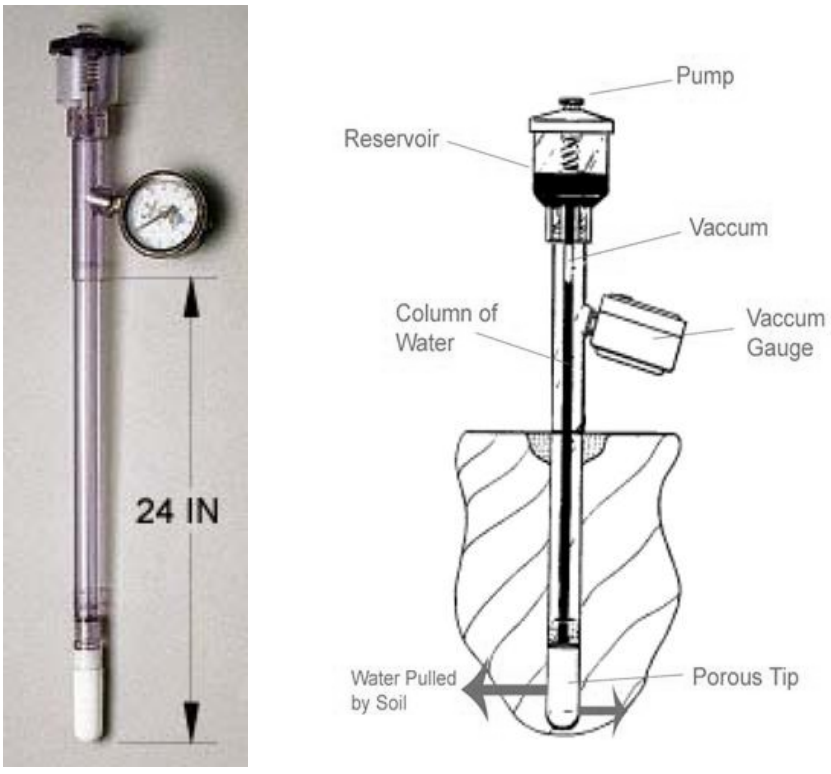

Figure 1: Tensiometer for soil moisture measurement

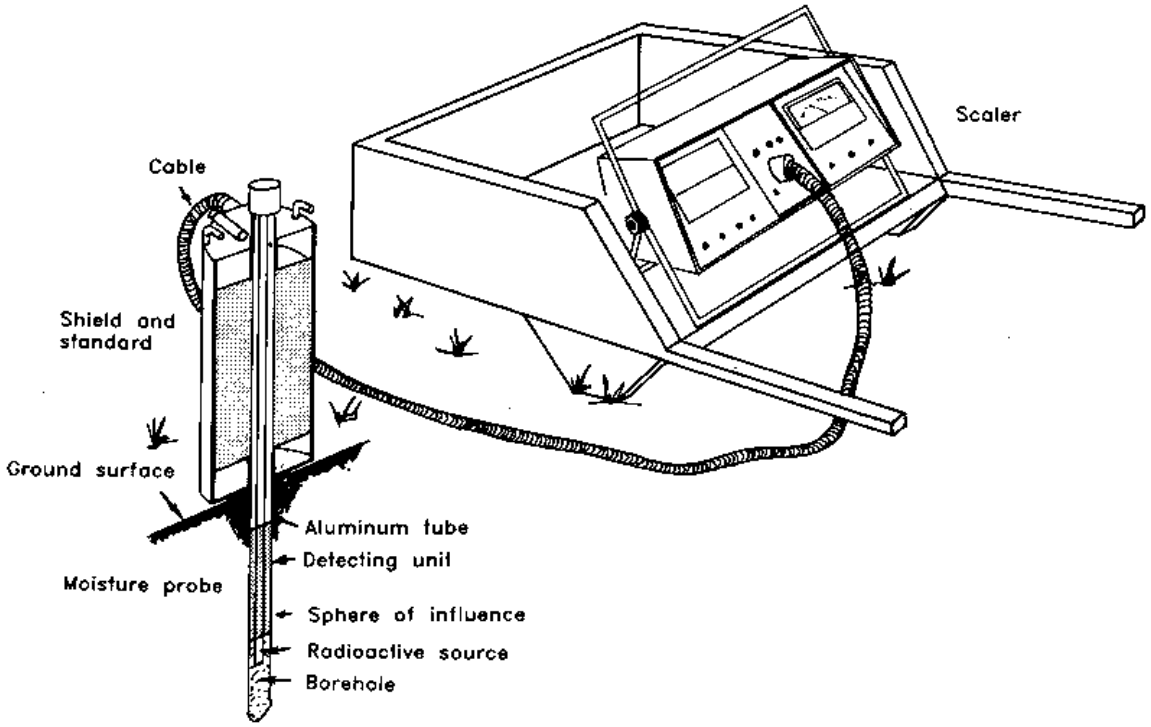

Figure 2: A neutron probe for soil moisture measurements (Courtesy: United Nations website)

Figure 3: Time-Domain Reflectory (TDR) Soil Moisture Probe

Since the early sixties, satellite remote sensing has developed as a prominent tool to monitor and compute environmental processes in both spatial and temporal terms. In addition to point measurements, soil moisture can be measured using remote sensing. Remote sensing methods can collect spatial data over large areas on a routine basis, providing a potential capability to make spatially and temporally comprehensive measurements of the near-surface soil moisture content and other environmental parameters.

2.2 Soil Moisture Satellite Missions

Knowledge of the state of soil moisture and its spatial and temporal dynamics is in increased demand because of technological and methodological progress in meteorologic, climatologic and hydrologic applications. Hydrological study missions such as: FIFE'87-89, MANSOON'90, OXSOME'90, MACHYDRO'90, HAPEX'90-92, WASHITA'92, SGP'97, SGP'99, SMOSREX'01-06, SMEX'02, SMEX03, and SMEX'04 were carried out to explore the potential of microwave remote sensing for estimation of soil moisture and other hydrological parameters (Jackson et al. 1999; Jacobs et al. 2004; O'Neill et al. 1993; Rosnaya et al. 2006; Schmugge 1998). The details of active microwave sensors that show high capabilities in soil moisture retrieval are given in Table 1.

Table 1: Details of active microwave sensors

Sensor	Frequency	Polarization	Year Launched
SEASAT	L	HH	1978
JERS-1	L	HH	1992
SIR-C	X, C, L	HH, VV, HV	1994
ERS-1	C	VV	1991
ERS-2	C	VV	1995
RADARSAT-1	C	HH	1995
ENVISAT	C	HH, VV, HV	2002
PALSAR	L	HH, VV	2002
HYDROS	L	HH, VV, HV	2010*
METOP-ASCAT	C	VV	2006*

* Expected to launch

In the coming years, several experimental and operational satellite missions will be available to observe global hydro-meteorological processes. ESA's Soil Moisture and Ocean Salinity Mission (SMOS) and NASA's HYDROS are expected to provide a flow of high quality coarse resolution soil moisture data. SMOS will make passive measurements at a spatial resolution of about 40 km. However, HYDROS will combine a passive radiometer (40 km) and active radar (3 and 10 km). As a lower microwave frequency is advantageous for soil moisture retrieval, both missions will operate in L-band. These two missions are expected to measure soil moisture with an accuracy 0.04 m3/m3. In addition to these two soil moisture missions other operational radiometers systems such as Advanced Microwave Scanning Radiometers (AMSR), Conical scanning Microwave Imager/Sounder (CMIS) have been found to be capable of soil moisture retrieval. Advanced Microwave Scanning Radiometer (AMSR-E), the latest generation of radiometers was launched in 2002 onboard of AQUA satellite. AMSR-E acquires data

at 6 passive frequencies ranging from 6.9 GHz (C-Band) to 89.0 GHz, with a spatial resolution ranging between 56 km (6.9 GHz) and 5.4 km (89 GHz). The Aquarius satellite that will carry an integrated L-band radiometer (1.413 GHz) and scatterometer (1.26 GHz) is expected to be operational in 2008. The CMIS uses a dual-primary reflector to measure across a large frequency range of 6 to 190 GHz (Scipal and Wagner 2004). The EUMETSAT's Polar System METOP will be a continuation of ERS scatterometer mission carrying the Advanced Scatterometer ASCAT. The METOP satellite series, with Advanced Scatterometer onboard, will be the first operational satellite system dedicated to the retrieval of soil moisture information. The operating frequency and launching years of these missions are shown in Figure 4.

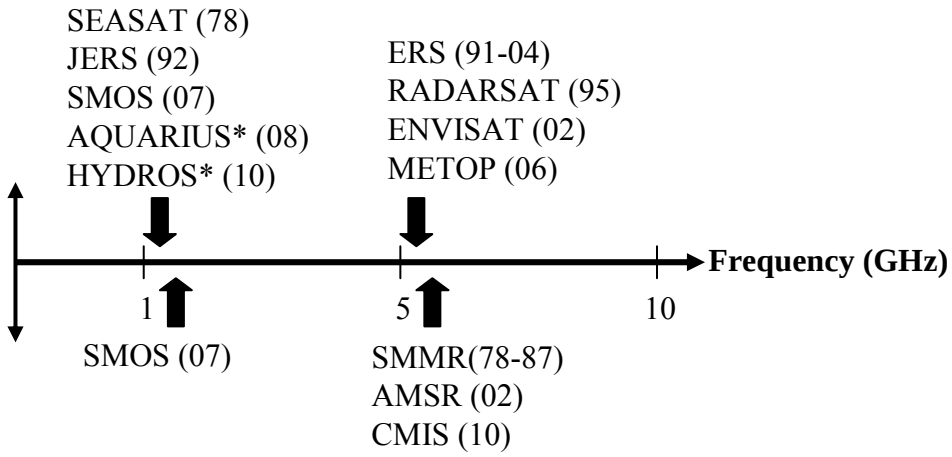

Figure 4: Operating frequency and launching year of satellite missions

2.3 Microwave Remote Sensing

The microwave region of the electromagnetic spectrum is in the frequency range of 0.3 to 300 GHz and sub-divided in various bands (Table 2). The unique characteristics of

microwave energy compared to the classic remote sensing systems are the ability to penetrate the atmosphere under various conditions including clouds, light rain, snow and smoke; as well as the ability of low frequency to penetrate vegetation up to a certain level. Microwave radiation is independent of solar radiation and can be used during both night-time and day-time hours; high frequency microwaves are partially absorbed by vegetation, therefore emitted signatures contain information on vegetation properties (Ulaby et al. 1981).

The greatest advantage of the microwave region of the spectrum is its ability to observe the earth's surface under all weather conditions. This is not possible in the visible or infrared region. The measurement of soil moisture using microwave systems is based on the large contrast between the dielectric properties of liquid water ($\varepsilon \approx 80$) and of dry soil ($\varepsilon \approx 4$). Microwave remote sensing can be used in either active or passive mode. Each mode has its distinct advantages over the other.

Band Designations	Wavelength (cm)	Frequency (GHz)
K_a	0.75 - 1.18	40.0 – 26.5
K	1.19 – 1.67	26.5 – 18.0
K_u	1.67 – 2.4	18.0 – 12.5
X	2.4 – 3.8	12.5 – 8.0
C	3.9 – 7.5	8.0 – 4.0
S	7.5 – 15.0	4.0 – 2.0
L	15.0 – 30.0	2.0 – 1.0
P	30.0 – 100	1.0 – 0.3

Table 2: Wavelengths and frequencies used in microwave remote sensing

The passive microwave systems are based on the measurement of the natural thermal emission in the form of brightness temperature from the earth surface. Thermal emission is the product of surface temperature and surface emissivity. On the other hand, the active microwave systems generate their own radiation, which is transmitted toward the earth surface, and measures the reflected energy called backscatter coefficient. The total backscatter measure consists of backscatter from vegetation and soil with an attenuation factor caused by the vegetation canopy. The details of active and passive microwave theory are discussed in the subsequent sections.

The space based passive microwave sensors generally have very low resolution ranging from 25 km to ~50 km. However, passive sensors deployed on aircrafts at lower altitude usually produce higher resolution, generally between 100 and 1000 m. The active microwave sensors can generate higher spatial resolution data compared to passive microwave sensors, and offer resolution up to 8 m (fine mode of RADARSAT-1), and 3 m (future RADARSAT-2) even from spacecrafts. This high spatial resolution data have larger application in the agricultural field, where crop growth and production is highly dependant on available surface soil moisture (Doraiswamy et al. 2004). Apart from soil moisture application, microwave remote sensing has been successfully used for rice crop inventory (Chakraborty and Panigrahy 2000).

2.4 Microwave Remote Sensing and Soil Moisture

Remote sensing technology is spatial in nature, and creates a greater capability to estimate soil moisture using the microwave region of the electromagnetic spectrum. A number of experiments conducted using truck mounted sensors, aircrafts, and spaceborne

sensors (ERS-1, ERS-2, JERS-1, SIR-C/X-SAR and RADARSAT-1) demonstrated that soil moisture can be measured accurately from the upper ~5 cm of the soil surface. Both active and passive microwave sensors have demonstrated a strong potential to retrieve spatial and temporal variability of soil moisture for different land surface classification.

The potential of microwave remote sensing in estimating soil moisture is based on the dielectric properties of soil. This relationship is highly influenced by surface parameters such as surface roughness, soil textures, and vegetation cover conditions (vegetation density, vegetation water content, leaf area index, etc). The spatial validation of this relationship is challenging because point measurements of soil moisture cannot be related to the spatial variability of the soil moisture profile. Recent research has focused on retrieval of soil moisture by reducing the influence of these parameters.

The two microwave frequencies C (3.9-7.5 cm) and L-band (15-30 cm) are the most dominant in past and current studies of soil moisture estimation. As discussed in chapter 2, with its higher penetration depth, the L-band has been used wildly in dense vegetation area to retrieve soil moisture. However, the C-band sensors demonstrate better performance in agricultural areas with shallow vegetation density. Optical sensors are generally used to retrieve vegetation related parameters, such as NDVI, vegetation water content, and green leaf area index to complement the microwave data (Doraiswamy et al. 2004; Jackson et al. 2004; Walthall et al. 2004).

2.5 Active Microwave Models for Soil Moisture Retrieval

A number of studies have been carried out to investigate the relationship between radar backscattering and soil moisture for different study areas. Various theoretical (Fung et al.

1992) and empirical models (Dubois et al. 1995; Oh et al. 1992; Shi et al. 1997) have been developed to retrieve the soil moisture from active microwave data. The theoretical models are based on the science of diffraction of electromagnetic waves with the observed surface, to predict the backscattering coefficient for a given configuration (frequency, polarization and incidence angle) and surface characteristics (dielectric properties and surface roughness). Some of these models are discussed in the following sub-sections.

2.5.1 Theoretical Models

Fung et al. (1992) have developed an Integral Equation Model (IEM) based on electromagnetic spectrum model for bare soil surfaces (see Appendix A). Five year later, Shi et al. (1997) simplified the complex IEM to infer soil moisture and surface roughness over bare and short vegetated fields. The simplification was made using regression analysis of estimated backscatter and surface parameters such as soil moisture, surface roughness and correlation functions. Further, the IEM model has been used by many researchers (Baghdadi et al. 2002; Chen et al. 1995; Rao et al. 1993; Satalino et al. 2002; Schoups et al. 1998; Zribi and Dechambre 2002; Zribi et al. 2003) to retrieve soil moisture and/or surface roughness and to validate data obtained from field studies.

2.5.2 Empirical Backscattering Models

Oh et al. (1992) proposed an empirical model for co-polarized and cross-polarized backscatter to relate soil moisture to dielectric constant. The model is given by the following equation:

$$\sigma^0_{hh}(\theta, \varepsilon_r, ks) = g\sqrt{p}\cos^3\theta\left[\Gamma_v(\theta) + \Gamma_h(\theta)\right] \tag{3.1}$$

$$\sigma_{vv}^{0}(\theta,\varepsilon_r,ks)=\frac{g\cos^3\theta}{\sqrt{p}}\left[\Gamma_v(\theta)+\Gamma_h(\theta)\right] \tag{3.2}$$

$$\sigma_{hv}^{0}(\theta,\varepsilon_r,ks)=q*\sigma_{vv}^{0}(\theta,\varepsilon_r,ks) \tag{3.3}$$

Where, ε_r = real part of the dielectric constant,
s = rms height of surface,

$g=0.7\left[1-\exp\left(-0.65(ks)^{1.8}\right)\right]$

$\sqrt{p}\doteq\sqrt{\frac{\sigma_{hh}^{0}}{\sigma_{vv}^{0}}}=1-\left(\frac{2\theta}{\pi}\right)^{\left[1/3\Gamma_0\right]}*e^{-ks}$, and

Fresnel reflectivity of the surface at nadir, $\Gamma_0=\left|\frac{1-\sqrt{\varepsilon_r}}{1+\sqrt{\varepsilon_r}}\right|^2$

The applicability of the model proposed by Oh et al (1992) has been further tested (Chen et al. 1995; Dawson et al. 1997). Further, Chen et al. (1995) proposed a simple empirical linear regression model as fallows:

$$\ln(M_v)=C_1*\sigma_{(hh/vv)}^{0}+C_2*\theta+C_3*f+C_4 \tag{3.4}$$

with the coefficients C_1 = -0.09544, C_2 = -0.00971, C_3 = 0.029238, C_4 = -1.74678. The units of parameter are $\sigma_{(hh/vv)}^{0}$ in dB; incidence angle θ in degrees, frequency f in GHz, and C4 is an offset constant value.

Dubois et al. (1995) used a ground-based scatterometer data of Oh *et al.* (1992) to generate an empirical model for co-polarized SAR system. The model calculates the backscatter coefficient of bare surface as function of dielectric constant, surface roughness (range 0.3-3 cm), incidence angle (range 30-65°) and frequency (range 1.5–11 GHz). The authors defined the backscattering in HH and VV polarize cross-sections as:

$$\sigma_{hh}^{0}=10^{-2.75}\frac{\cos^{1.5}\theta}{\sin\theta^5}10^{0.028\varepsilon\tan\theta}(ks\sin^{1.4}\theta)\lambda^{0.7} \tag{3.5}$$

$$\sigma_{vv}^{0} = 10^{-2.75} \frac{\cos^3 \theta}{\sin \theta} 10^{0.046 \varepsilon \tan \theta} (ks \sin^3 \theta)^{1.1} \lambda^{0.7} \quad (3.6)$$

Where, θ is the incidence angle, ε is the real part of the dielectric constant, *s* is the RMS height of the surface, *k* is the wave number ($k=2\pi/\lambda$) and λ is the wavelength in cm. The Dubois-model claims best results with sparsely vegetated area (NDVI < 0.4). A detailed comparison between these empirical models can be found in Wang *et al.* (1997). The use of Dubois-model for sparse vegetated area (NDVI < 0.11), showed better correlation between backscatter from C-band than from L-band (Neusch and Sties 1999). The empirical models derived above have used field experiments to validate their results, but many of them are applicable only to similar radar parameters and surface conditions present at the time of the experiments.

2.5.3 Semi-empirical Backscattering Models

The major challenge to the above theoretical and empirical models is the modeling of backscatter behavior under the vegetation canopy. The incorporation of vegetation parameters in the above models generates large number of variables and makes their inversion process more difficult. A simple approach in the form a semi-empirical *water-cloud* model (WCM) was developed by Attema and Ulaby (1978) based on a first-order solution of a radiative transfer model. The formulation of this model has been chosen for simplicity in radar data inversion and adequacy to represent plants with leaf dimensions smaller than the sensor wavelength.

In the WCM, the canopy is represented as a uniform cloud of spherical droplets that are held in place structurally by dry matter. The canopy is represented by bulk variables such as leaf area index or vegetation water content. The vegetation is considered as a

homogeneous horizontal cloud, uniformly distributed above the soil surface where multiple scattering between canopy and soil can be neglected. The cloud density is assumed to be proportional to the volumetric water content of the canopy. The height of the canopy layer is considered as a significant variable in the model.

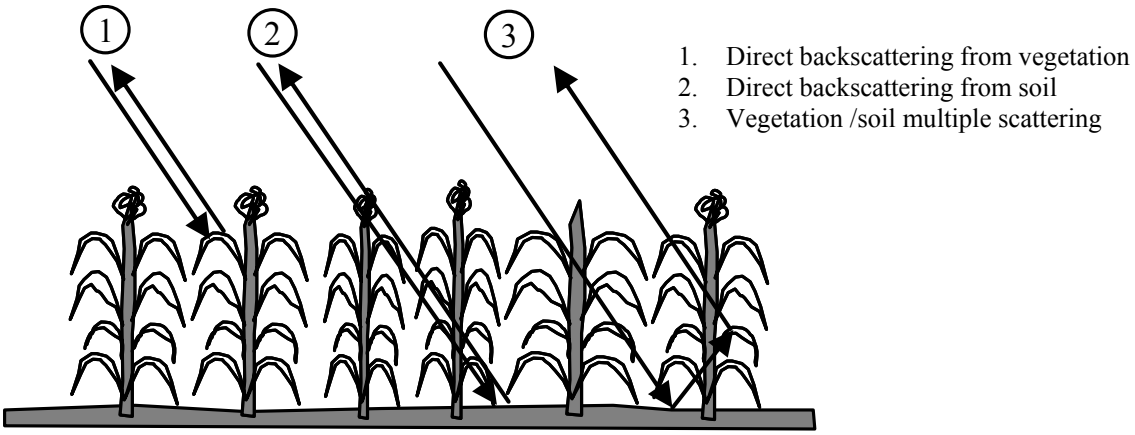

Figure 5: Backscatter contribution from vegetation cover

In this context, as shown in Figure 5, the total backscatter from a vegetated soil surface consists of three types of contributions: backscatter from bare soil surface (σ^0_{soil}), direct backscatter of the vegetation layer (σ^0_{canopy}) and multiple backscattering ($\sigma^0_{soil+canopy}$) involving the vegetation canopy and ground surfaces (Karam et al. 1992; Ulaby et al. 1996). For the given incidence angle, the total backscatter coefficient is given by:

$$\sigma^0 = \sigma^0_{canopy} + \sigma^0_{soil+canopy} + \tau^2 * \sigma^0_{soil} \tag{3.7}$$

where $\tau^2 = e^{(-2B*M_v*Wc)}$ (3.8)

and backscatter from canopy is given by:

$$\sigma^0_{canopy} = A * M_v * \cos\theta \left(1 - \tau^2\right) \tag{3.9}$$

where τ^2 is the two-way vegetation transmissivity, M_v is the volumetric soil moisture content, W_c is the vegetation water content in kg/m2 and θ is the radar incidence angle. The vegetation related parameters (A and B) are determined from experimental observations, representing the vegetation scattering and the vegetation attenuation, respectively.

Bindlish and Barros (2001) subsequently modified water-cloud model by introducing the vegetation correlation length, α, and neglecting soil-vegetation interaction. The modified model is expressed as:

$$\sigma^0 = \sigma^{0*}_{canopy} + \tau^2 * \sigma^0_{soil} \tag{3.10}$$

$$\sigma^{0*}_{canopy} = \sigma^0_{canopy}\left(1 - e^{-\alpha}\right) \tag{3.11}$$

where σ^{0*}_{canopy} is the backscatter contribution of the vegetation corrected for the effects of orientation and geometry of the canopy. The parameter, α, measured directly at the ground, is a function of the average distance between vegetation canopies within a pixel. In the water-cloud model the soil backscatter from bare soil, σ^0_{soil}, is computed through regression analysis where the measured backscatter is assumed as a linear function of the volumetric soil moisture (Ulaby et al. 1986b).

2.5.4 Linear Relationship

The theoretical and empirical models discussed above are complex in nature and require many inputs that are not always available. Many researchers used a linear regression model to simplify the complex relationship between radar backscattering and soil moisture (Bernard et al. 1982; Geng et al. 1996; Glenn and Carr 2003; Kasischke et al. 2003; Meade et al. 1999; Moeremans and Dautrebande 2000; Pultz et al. 1990; Quesney et al. 2000; Srivastava et al. 2003; Ulaby 1974; Ulaby et al. 1981; Wood et al. 1993). However, this relationship between backscatter and soil moisture (top 5 cm surface) is a complex phenomenon that varies based on various soil surface parameters. Some of the researchers proposed the linear relationship between radar backscatter and soil moisture for specific land cover conditions (Moeremans and Dautrebande 2000; Quesney et al. 2000; Wood et al. 1993). The simplified linear relationship between radar backscatter (σ_0) of soil with varying moisture content for a composite surface can be given by:

$$\sigma_0 = a * M_v + b \qquad (3.12)$$

Where, a, b are empirical coefficients and M_v is the volumetric soil moisture. Backscatter coefficient (σ_0), and is generally used in unit decibel format (dB) or a simple digital number (DN).

In the early eighties, Bernard *et al.* (1982) used a C-band scatterometer that was mounted on a crane to determine the soil moisture in agricultural areas. The experiment was carried out on three different types of soil surface; wheat stubble, sugar beat and corn. Similar studies carried out by Wood *et al.* (1993) for corn, oat and pasture land, used

different type of polarization and found that the backscattering coefficient is highly correlated to soil moisture using linear regression model for all types of vegetation.

This linear relationship is better correlated in the case of bare soil surface. However, the presence of vegetation on the soil surface reduces the sensitivity between the backscatter and soil moisture (Boisvert et al. 1995b; Glenn and Carr 2003; Moeremans and Dautrebande 2000). In the same way, L-band radiometric sensitivity to soil moisture variation is higher in the burned watershed than unburned watershed (Wang et al. 1989). In the context of vegetation sensitivity, researchers (Shoshany et al. 2000; Svoray and Shoshany 2004; Taconet et al. 1996) modify this linear relationship by considering vegetation as an additional input. This approach will be discussed in next section.

2.5.5 Modified Linear Relationship

Some researches have observed that the relationship between backscatter and soil moisture is complex and nonlinear, and a simple regression model is not the best representation of this relationship. To improve this relationship, researchers used other factors such as vegetation cover, vegetation water content, and temporal SAR backscatter. Taconet et al. (1996) used a vegetation correction factor to calculate the soil moisture from C-band radar backscatter:

$$\sigma_0 = a * V_{sm} + b + c * W_{veg} \tag{3.13}$$

where c coefficient represents the attenuation by the canopy. The authors have found that, by using the vegetation corrected factor, the correlation improves significantly (11%) compared to the linear relationship of backscatter and soil moisture.

In other study, Shoshany et al (2000) proposed the Normalized Backscatter Soil Moisture Index (NBMI), where the ratio of backscatter values of two different days was used as explanatory variable in a simple linear regression model to estimate soil moisture. The proposed NBMI reduces the common multiplicative effect of difference in soil type and surface roughness on radar backscatter.

$$\mathrm{NBMI} = \frac{\sigma_{\mathrm{t1}} - \sigma_{\mathrm{t1}}}{\sigma_{\mathrm{t1}} + \sigma_{\mathrm{t1}}} \tag{3.14}$$

$$V_{sm} = a * \left(\frac{\sigma_{t1}}{\sigma_{t2}} \right) + b \tag{3.15}$$

NDVI has also been used along with NBMI to improve the soil moisture estimation accuracy (Svoray and Shoshany 2004). The authors noted that, at larger scale, the degree of spatial variation of soil moisture depends on the drying rate attributed to the intrinsic soil properties of watershed area.

2.5.6 Michigan Microwave Canopy Scattering (MIMICS) Model

Ulaby et al. (1990) proposed the Michigan Microwave Canopy Scattering (MIMICS) model to simulate the radar backscatter from forest canopy in frequency ranging from 1-10 GHz and wide range of incidence angles. The MIMICS is a first-order radiative transfer model, where canopy was divided into three layers: crown layer, trunk layer and underlying surface. These three layers have been characterized as: crown layer by size, shape and dielectric constants of leaves and branches; trunk layer by size and density of trunks in the area and finally underlying surface by dielectric constant and surface roughness. The backscattering from these three components has been combined to estimate the total backscatter. The authors have simulated this model on both X and L

frequencies. The MIMICS model has shown better performance with L-band than X-band, because the X-band interacts more with crown layer of the tree than the trunk layer (Ulaby et al. 1990). Recently, Roo *et al.* 2001 developed a forward scattering model based on MIMICS model for shallow vegetation by eliminating the backscatter term used for trunk layer component.

2.5.7 An Optical/Microwave Synergistic Model

The effect of vegetation density on radar backscatter is dominant in densely vegetated areas. The optical imagery obtained at the same time with SAR imagery allows a better understanding of the interactions of the SAR signal with soil and plant surfaces (Chauhan et al. 2003; Moran et al. 2002). The synergistic model developed by Wang *et al.* (2000) proposed a temporal differential backscatter coefficient as a function of NDVI. In another similar study, the synergy between NDVI (TM) and SAR (ERS-2) data has been used by (Wang et al. 2004) for soil moisture estimation. The difference between backscatter from dry and wet season minus NDVI relationship is used to generate iso-moisture equations to estimate soil moisture. The author noted that vegetation contributed more at the dry soil surface (M_v < 10%), and less at wet soil surface (M_v> 10%).

The synergistic use of two active microwave instruments (SAR and wind scatterometer) of ERS satellites has been used by Zribi *et al.* (2003) for soil moisture estimation over bare soil areas at a larger scale. The authors have used a series of temporal images to reduce the effect of forest vegetation on measuring soil moisture from SAR data and found a correlation coefficient of 0.8 for soil moisture estimation.

Studies conducted by Narayan et al. (2004) have used active and passive sensors to estimate soil moisture under high vegetation water content during SMEX02 mission. The

study also evaluates the performance of linear regression techniques for soil moisture estimation. A higher correlation between brightness temperature and soil moisture has been found when vegetation water content is lower than 1.0 kg/m^2 using L and S band.

Based on the above reviews, we may conclude that a single SAR data cannot be considered a reliable source to correlate with soil moisture based on dielectric constant. It is imperative to consider other parameters such as: NDVI, vegetation optical depth, soil texture, vegetation type and textural information of SAR data as an input to estimate soil moisture. These large variables cannot be simplified in small or empirical equations and need to have parametric and non-parametric tools like neural network and fuzzy logic to solve the complex problems that exist between soil moisture and microwave backscatter.

2.6 Effect of Vegetation on Soil Moisture Estimation

The vegetation cover has a great influence on the soil moisture estimation with microwave remote sensing systems. A good application of SAR imagery in soil moisture monitoring requires a basic knowledge of radar scattering from different types of land cover and their interaction with the soil moisture and the contribution of soil moisture to the total backscatter. For example, the SAR backscattering from agricultural land is influenced by crop structure, type, amount of vegetation, and canopy water content. These parameters are responsible to make the relationship between SAR backscattering and soil moisture more complex.

In the presence of vegetation, the backscattering signal from vegetated areas depends on: soil moisture content, surface roughness, and the vegetation canopy overlying the soil. However, instrument characteristics such as, angle of incidence, polarization, and

frequency play an important role on identifying the soil moisture contribution to the total backscatter (Ulaby *et al.* 1981). The vegetation effect on the total backscatter measured by the sensor is mainly due to the macrostructure of vegetation canopy such as height of canopy and number of plants or trees per unit area; and the microstructure, which refers to geometry, moisture contents, and vegetation volume fraction of canopies. The penetration depth radar beam is lower at higher soil moisture contents in vegetation canopies.

The total backscattering is composed of backscatter from vegetation and soil, and attenuation / backscatter caused by vegetation (σ_c) canopy. The vegetation canopy affects the backscattered energy in two ways: first, the vegetation layer attenuates the soil backscatter contribution and second, the vegetation canopy contributes its own backscatter (Ulaby *et al.* 1981; Kasischke *et al.* 2003). The total amount of attenuation and backscatter depends on some structural and physical vegetation parameters which include vegetation height, leaf area index, and vegetation water content. The equation of measured radar backscatter (σ) from vegetated area has been defined as:

$$\sigma = \sigma_c + t\,\sigma_b \tag{3.16}$$

Where σ_c is the canopy backscatter contribution, σ_b backscatter contribution from bare soil and t is the two way transmission coefficient. Since longer microwave wavelength signals (L-band) can penetrate the vegetation cover, the effect of vegetation on backscattering decreases as the wavelength increases. Longer wavelengths become advantageous in the extraction of information from soil surface in vegetated areas (Ulaby *et al.* 1986a). Quesney *et al.* (2000) found that the crop conditions (crop water content,

crop structure, etc) play an important role in soil moisture estimation. However, the strong vegetation attenuation of radar signal reduces the accuracy of soil moisture estimation.

The sensitivity of backscattering to the forest vegetation density is more in L and P bands, and less in C band (Table 2). However, the structural properties of crown have more effect on the C band. Indeed, for a dense area the backscatter from vegetation is higher than that of bare surface (Dubois et al. 1995). The horizontal polarizations (HH and HV) have shown higher sensitivity to biomass and the linear dependence of backscatter on biomass is related to the wavelength of signal (Dobson et al. 1992).

The microwave signal is attenuated in large quantity by vegetation at higher incidence angle. The vegetation component of the scattering coefficient is low at higher incidence angles; hence for soil moisture estimation, the optimum configuration is when the incidence angle is close to nadir. Further, the microwave signal is less sensitive to leaf area index (LAI) at higher incidence angle. At higher incidence angle, the radar viewing to the canopy is more through the sides, which reduce the sensitivity to LAI. At a higher incidence angle the rough canopy, due to higher dry matter, which is dominant, generate more scattering than canopy moisture (Brakke et al. 1981).

The backscatter is also sensitive to thickness of leaves apart from moisture content of leaves and the dimension of leaves (Schoups et al. 1998). The high correlation up to 99% has been found in wheat field having low leaf area index. However, the backscatter from pasture field with large leaf area index can not be correlated to the soil moisture (Wickel et al. 2001).

3 Microwave Theory and Soil Moisture

3.1 Introduction

Microwave remote sensing is currently gaining popularity for its application in mapping spatial and temporal distribution of soil moisture. Recent advances have demonstrated the spatial and temporal soil moisture estimation ability of remote sensing in the near-surface layer under a variety of topographic and land cover conditions using both active and passive microwave measurements. Microwave systems are used to measure soil moisture on the basis of the large contrast that exists between the dielectric constant values for dry and wet soils. Additionally, the microwave radiation is not sensitive to atmospheric variables, and can penetrate through clouds. Also, microwave signal can penetrate, to a certain extent, the vegetation canopy and retrieve information from ground surface (Engman 1991; Kasischke et al. 1997; Oldak et al. 2002).

Microwave systems are classified into two categories: passive and active. The passive sensors measure the natural thermal emission in the form of brightness temperature from the land surface. On the other hand, the active microwave systems generate their own radiation which is transmitted toward the earth surface, and measures the reflected energy called backscatter coefficient. This chapter provides a descriptive outline of the theory of active and passive microwave remote sensing and their application in soil moisture mapping. The soil surface characteristics and microwave instruments parameters which affect the backscatter mechanism are also presented. The relationship between backscatter from Synthetic Aperture Radar (SAR) data and soil moisture is a complex relationship that varies based on: radar system configuration such as frequency (§2.4.1),

incidence angle (§2.4.2), and polarization (§2.4.3); and soil surface parameters such as dielectric constant (§2.5.1), surface roughness (§2.5.2), soil texture (§2.5.3), topography (§2.5.4), observation depth (§2.5.5), and vegetation cover (§3.2).

3.2 Passive Microwave Theory

The principle of passive microwave remote sensing is based on the thermal radiation measurement from the land surface, and depends on physical temperature and the surface emissivity. The passive sensors measure the natural thermal emission of the land surface at microwave wavelength. The microwave brightness temperature of the land surface is a function of the thermodynamic temperature of the soil and surface emissivity:

$$T_B = R \cdot \tau \cdot T_{sky} + (1 - R) \cdot \tau \cdot T_{soil} + T_{atm} \qquad (2.1)$$

Where R is the surface reflectivity, τ is the atmospheric transmissivity, T_{sky} is the contribution from the reflected sky brightness, T_{soil} is the thermometric temperature of the soil, and T_{atm} is the average thermometric temperature of the atmosphere. The surface emissivity (e_s) can be approximately calculated by dividing brightness temperature (T_B) by soil surface temperature (T_S).

The active and passive microwave response to soil moisture is a repeal phenomenon. In the case of passive microwave system, the brightness temperature decreases with the increasing soil moisture. However, in the case of active microwave system, the stronger radar backscattering values are observed at higher soil moisture (Ulaby et al. 1986b).

At the longer wavelength (>10 cm) the atmospheric transmission will be about 99% and the T_{atm} and T_{sky} contribution are less than 5° K; therefore, the second term in the

equation (2.1) becomes the major contributor to the observed brightness temperature. However, the surface emissivity of soil surface is affected by vegetation cover and surface roughness. For bare soil, the measured brightness temperature is directly related to soil water content and temperature of surface emission.

The vegetation cover emits its own microwave energy and may scatter or attenuate the energy emitted by soil surface. Therefore, the measured brightness temperature contains the information about soil moisture as well as vegetation characteristics. Various models have been developed to estimate soil moisture under the vegetation cover (Burke and Simmonds 2001; Engman and Chauhan 1995; Schmugge 1998).

3.3 Active Microwave Theory

Active microwave systems generate their own radiation transmitted towards earth surface and measure the returning radiation. The ratio of strength of received and transmitted signal (backscattering coefficient) depends on surface reflectivity and the antenna characteristics such as incidence angle, wavelength, and polarization. This coefficient is the average value of the scattering cross-section per unit area, "the amount of energy that is scattered back to the receiving sensor per unit area". The strength of backscattered signal (backscatter coefficient or sigma naught, σ^o) is usually expressed in decibels using a logarithmic scale because of the large dynamic range of its values. The relationship between backscattering coefficient and other radar parameters is given by radar equation (Ulaby *et al.* 1986):

$$\sigma^0 = \frac{P_r (4\pi)^3 R_t^4}{P_t G_t G_r \lambda^2 A} \qquad (2.2)$$

Where,

σ^0 = Backscatter coefficient
P_r and P_t = received and transmitted power,
G_r and G_t = received and transmitted antenna gain,
λ = wavelength,
R_t = target range
A = target area

The most widely used active remote sensing systems are: RADAR (RAdio Detection And Ranging), LIDAR (LIght Detection And Ranging), and SONAR (SOund Navigation And Ranging). The radar images are obtained from aircraft or spacecraft using the continuous-strip mapping capability of side-looking radar (SLAR). The SLAR is classified in two types: real aperture radar (RAR) and synthetic aperture radar (SAR) (Jensen, 2000).

The radar spatial resolution is a function of the pulse length and the antenna beam width, which is governed by the length of the antenna. Thus, finer spatial resolution is the obtained by increasing the length of the antenna. For example, 10 m resolution requires a 4 km long antenna. Therefore, to produce the desired resolution, the SAR system uses forward motion of the spacecraft to synthesize a much longer antenna to generate high resolution images even from space. The antenna length is simulated by appropriate processing of a large number of return signals along the flight trajectory (Jensen 2000; Ulaby et al. 1986b).

The SAR data in ScanSAR mode from RADARSAT-1 satellite has been used in this study. The characteristics of RADARSAT-1 satellite have been summarized in Table 3. The details of beam modes and incidence angles used by RADARSAT-1 satellite are shown in Figure 6.

Table 3: Characteristics of RADARSAT-1 satellite

Frequency	5.3 GHz (C Band)
Wavelength	5.6 cm
Orbit	Sun-synchronous
Polarization	HH
Altitude	798 Km
Inclination	98.6°
Incidence angle	20 – 46°
Nominal Swath Width	300 km
Coverage	Global: 4,5 days; North America: 3 days

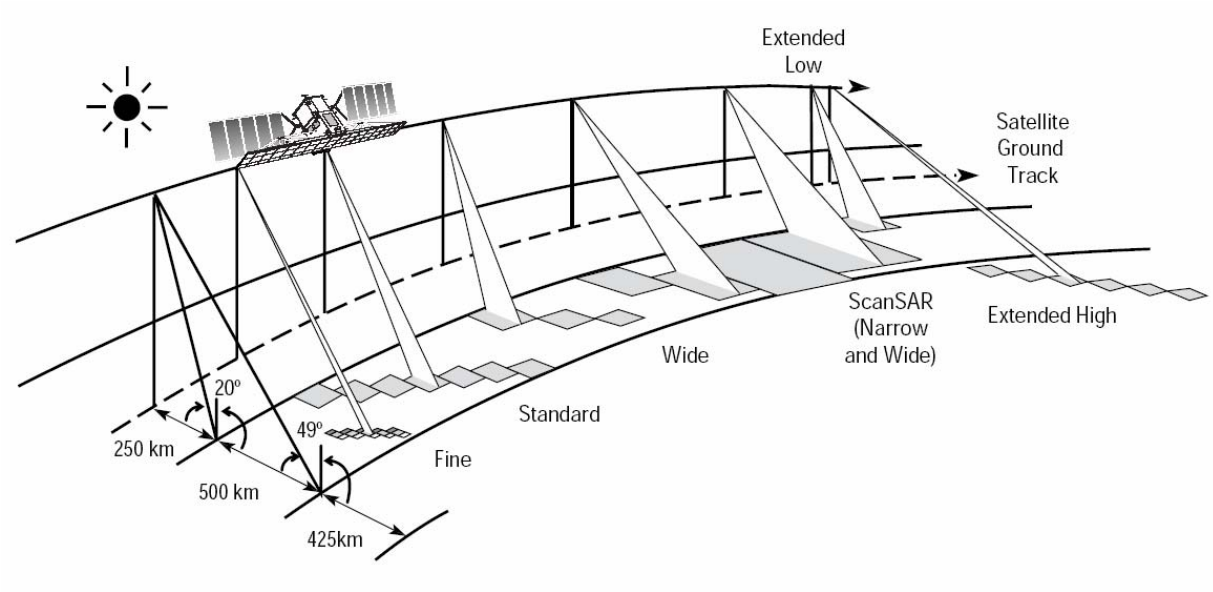

Figure 6: Details of RADARSAT-1 incidence angle, swath width and beam modes

The potential of active microwave sensors in spatial soil moisture monitoring depends on the ability of the applied methodology to define the complex relationship that exists between the backscattered energy and the characteristics of the observed scene. The relationship between backscatter from Synthetic Aperture Radar (SAR) and soil moisture is a complex phenomenon that varies based on: radar configurations (frequency,

polarization, and incidence angles) and soil surface parameters such as surface roughness, topography, soil texture and vegetation cover.

The backscattering from soil surface is affected by dielectric constant and surface roughness. The backscattering of the radar signal from ground surface occurs in the form of volume scattering and surface scattering. Surface scattering occurs on the border surface of homogeneous media due to surface roughness. Volume scattering occurs when radiation is transmitted from one medium to another medium, and usually consists of multiple bounces and reflections from different components within the volume. High vegetation density areas are more inclined to volume scattering (Ulaby et al. 1981; Ulaby et al. 1986b).

3.3.1 Frequency and Wavelength

The frequency of incident radiation has a direct relationship with the penetration depth in the surface and the relative roughness of the surface. The L and C bandwidths (see Table 2), are the most commonly used wavelengths for soil moisture estimation. The longer wavelengths penetrate deeper in the soil surface and/or vegetation canopy. For example, the active microwave system operating in the X-band (see Table 2) can only penetrate the top layer of canopy and retrieves information about the top layer and the crown of the trees (Karam et al. 1992). However, a L-band sensor is able to penetrate leaves and small branches and can interact with tree trunks and branches and eventually soil surface. The illustration in Figure 7 shows the backscatter contribution from the forest cover at different wavelengths.

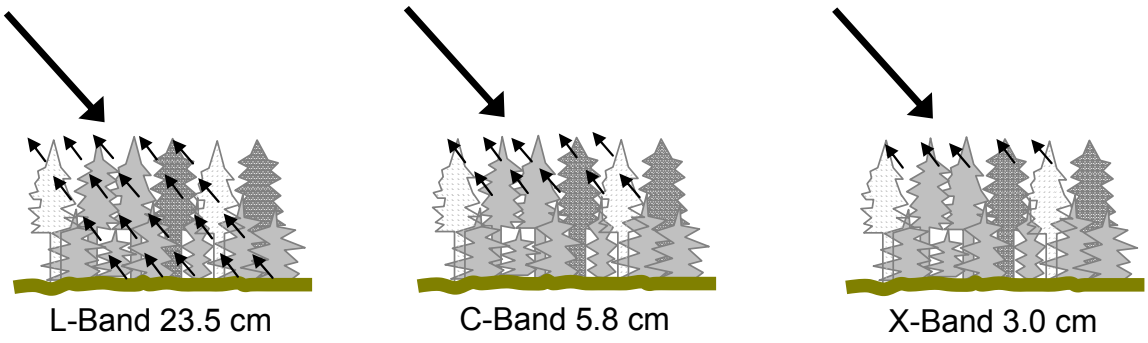

Figure 7: Backscatter from forest area to L, C, and X band wavelength

In sparse vegetation, L band interacts more with underlying surface rather than vegetation, reducing its sensitivity to vegetation (Dubois et al. 1995; Wang et al. 1982). The same principle applies to other targets such as soil, ice, and water. The penetration depth of the radar signal is related to the frequency and moisture content of the observed target. Microwaves do not penetrate water surfaces more than a few millimeters (Ulaby et al. 1986b). The higher backscattering coefficient has been observed for C band than L band for similar soil moisture condition at fixed incidence angle (Mo et al. 1984).

3.3.2 Incidence angle

The incidence angle (θ) is the angle between radar beam and target object shown in Figure 8. The incidence angle describes the angular relationship between the radar beam and the ground surface layer or a target. The incidence angle changes across the radar image swath for the same image from one end (near-range) to other (far-range). The incidence angle causes variation in radar backscatter. For example, for the same observed surface, a higher incidence angle returns less backscattering than a lower incidence angle.

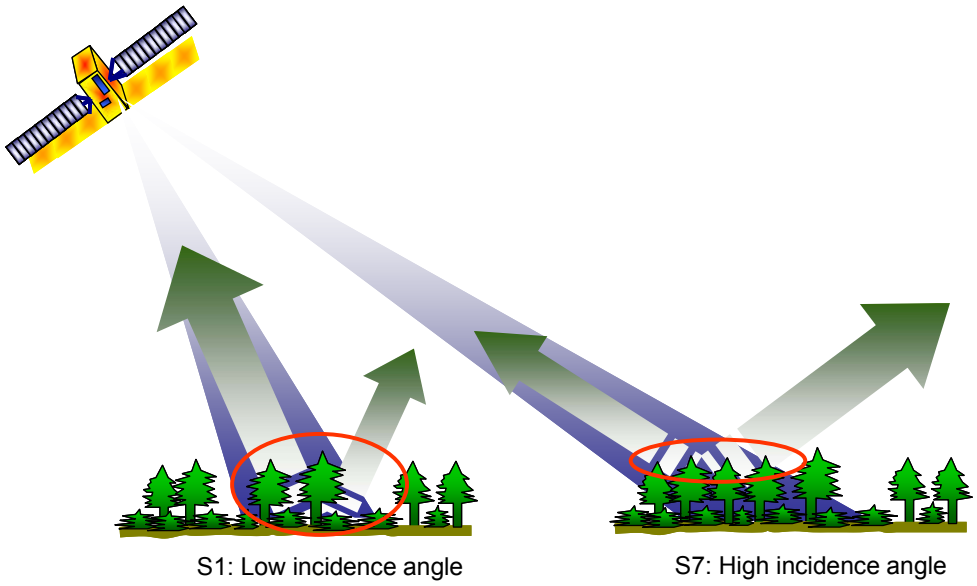

Figure 8: Effect of incidence angle of RADARSAT-1 beam mode S1 and S7 on backscatter

The incidence angle, usually considered different in the case of an inclined surface, is the angle between the incident radar beam and a line that is normal to inclined surface. This local incidence angle is important in case of imaging terrain features to analyze brightness, or image tone of pixel element (Ulaby et al. 1986b). The sensitivity of microwave sensor to soil moisture decreases when the incidence angle increases (Mo et al. 1984). Further, the sensitivity decreases more rapidly by the presence of vegetation because, at higher incidence angle, the vegetation intercepts the radar signal and attenuates it (Figure 8). Thus, the energy backscattered by vegetation reduces the contribution of soil to the total backscattering (Ghedira et al. 2000; Mo et al. 1984).

The optimal soil moisture can be derived using a low incidence angle because it increases the vegetation penetration depth and minimizes the effect of vegetation and surface roughness on backscatter signal (Ulaby et al. 1986b). However, the low incidence angle beam mode is restricted in spatial and temporal scales. As shown in Figure 6, Standard and ScanSAR modes of RADARSAT-1 use a wide range of incidence angles (20°-49°),

and represent a good compromise between spatial coverage and incidence angles due to their high repetition time (Boisvert et al. 1995b).

3.3.3 Polarization

The orientation of the electric field of electromagnetic waves may be either horizontally (H) or vertically (V) polarized. The H polarized waves travel parallel to the soil surface and the V polarized waves travel perpendicular to the soil surface (Figure 9). The RADAR systems are capable of measuring the backscattering response from target using different polarization configurations such as co-polarized (HH and VV) and cross-polarized (HV and VH). The first term corresponds to the transmitted radiation from antenna, the second term to the received radiation by the antenna, for example, C-HV refers to C-band transmitted in H polarization and receiving in V polarization. The responses for HV and VH are identical due to reciprocity property of radar scattering (Ulaby et al., 1996).

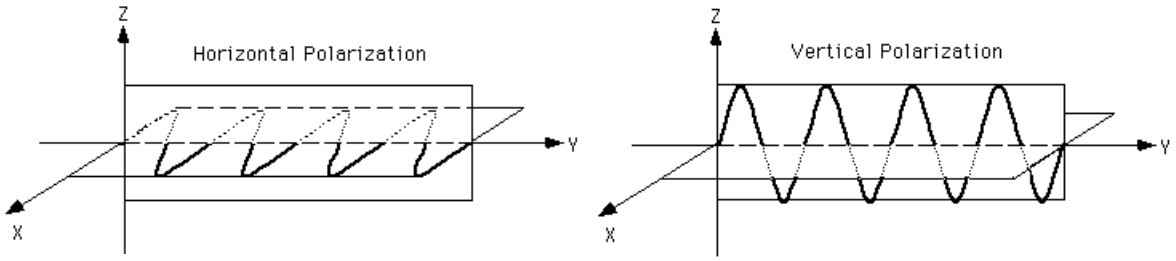

Figure 9: Horizontal and vertical polarization

In addition to measuring radiation in multi-polarized magnitudes (HH, VV, HV) of the scattering response, polarimetric radar can measure the phase differences between the multi-polarized backscattered waves, such as:

Co-polarized phase difference: $$\Phi_C = \Phi_{HH} - \Phi_{VV} \quad (2.3)$$

Cross-polarized phase difference: $$\Phi_X = \Phi_{HV} - \Phi_{VV} \quad (2.4)$$

The co-polarized phase difference Φ_c is an important parameter in image classification process. However, a cross-polarized phase difference may not found to be important in various applications. Overall, polarimetric radar is capable of producing five image products Φ_{HH}, Φ_{VV}, Φ_{HV}, Φ_C, and Φ_X (Ulaby et al. 1996).

These polarization configurations are used to retrieve more accurate information from different layers of the target surface (Ulaby et al. 1996; Ulaby et al. 1986b). Different polarizations can have different penetration depths for the same frequency and the soil dielectric constant. For example, for the same soil and land cover conditions, VV polarization has higher penetration depth than HH polarization (Boisvert et al. 1995a). The VV and HV polarization are very sensitive to the incidence angle. While the effect of incidence angle on backscattering coefficient for HH polarization is weaker than VV and HV polarization (Karam et al. 1992). At L-band, the polarization is dominant on scattering mechanism. For VV polarization, the direct backscatter from the ground dominates the canopy backscatter. However, the ground and canopy backscatter amount are comparable in HH polarization (Roo et al. 2001). Based on these variation in response from vegetation to the L-band polarization Dubois et al. (1995) proposed SAR based vegetation index (SBVI) as fallows:.

$$\mathrm{SBVI} = \frac{\sigma_{L-HV}}{\sigma_{L-VV}} \tag{2.5}$$

The need of multi-polarization and multi-frequency SAR information is required for accurate retrieval of soil moisture from vegetated and roughly surface area (Bindlish and Barros 2000; Blyth 1997; Oh et al. 1992).

3.4 Soil Surface Parameters

3.4.1 Dielectric Constant

The dielectric constant is a response of a medium to an applied electrical property. The physical parameters that affect the dielectric constant are soil moisture, soil texture, bulk density, salinity, organic matter, and temperature. The change in soil dielectric constant is more influenced by change in soil moisture content than other soil characteristics listed above. The increase in soil moisture results in the increase in dielectric constant (Ulaby et al. 1986b). The dielectric constant is related to the soil moisture by a polynomial relationship and is usually denoted by symbol ε. The dielectric constant is a complex number consisting real (ε') and imaginary (ε'') parts shown in equation below:

$$\varepsilon = \varepsilon' - j\varepsilon'' \tag{2.6}$$

The real part refers to the relative permittivity, and the imaginary part refers to the dielectric loss factor. The dielectric constant of soil and water at 1 GHz and at room temperature is approximately 4 and 80 respectively. Ulaby et al. (1986b) suggested the following model (Eq. 2.7) to estimate the dielectric constant for soil based on density of solid material (ρ_{ss}), bulk density (ρ_b), the dielectric constant of solid materials (ε_{ss}), the volumetric soil moisture content (m_v) and the dielectric constant of free water (ε_{fv}).

$$\varepsilon_{soil} = 1 + \frac{\rho_b}{\rho_{ss}}\left(\varepsilon_{ss} - 1\right) + m_v^{\beta}\left(\varepsilon_{fw} - 1\right) \quad (2.7)$$

The dielectric constant for vegetation is modeled by considering the vegetation as a mixture of dry vegetation, bound water and free water, and given by (Ulaby and Al-Rayes 1987):

$$\varepsilon_{veg} = \varepsilon_r + \varepsilon_{bd}.v_{bd} + \varepsilon_f.v_f \quad (2.8)$$

where v_f and v_{bd} are the fractions of free and bound water in the vegetation, ε_f and ε_{bd} are the dielectric constants of vegetation bulk matter for bound and free water. The term ε_r is the residual non-dispersive contribution to the dielectric constant including the effect of dry vegetation matter. Estimation of the dielectric constant for a plant canopy, by assuming a canopy height of 1 m, and a canopy volume fraction of between 0 to 1%, is given by:

$$\varepsilon_{canopy} = \left[1 + v_f.\left(\varepsilon_{veg} - 1\right)\right]^{\frac{1}{\beta}} \quad (2.9)$$

where the value of β indicates the type of model used (β = 1 for linear model and β = 0.5 for refractive model). The term v_f is the vegetation volume fraction (Schmugge and Jackson 1992; Ulaby et al. 1986b).

3.4.2 Surface Roughness

The surface roughness is a measure of the irregularities of the surface geometry which has a significant effect on the variation of radar backscattering amount. The degree of roughness or smoothness of a surface depends on the wavelength of the incidence energy. A surface can be considered smooth at L band (21 cm) and rough at C band (5 cm).

A rough surface has a larger scattering than a smooth surface at same wavelength. According to the Rayleigh criterion (Ulaby et al. 1986b):

A surface is considered smooth if:

$$h < \frac{\lambda}{8 * \cos\theta}, \tag{2.10a}$$

and considered rough if:

$$h > \frac{\lambda}{8 * \cos\theta} \tag{2.10b}$$

Where,

h = mean height of surface variation,
λ = wavelength,
θ = incidence angle (Figure 10).

Surface roughness increases the backscattering by increasing the total emitting surface as shown in Figure 10. The change in surface roughness results in reducing the sensitivity of soil moisture and backscatter relationship (Boisvert et al. 1995a). The effect of surface roughness on radar backscatter can be minimized by selecting a low incidence angles (Ulaby et al. 1986b).

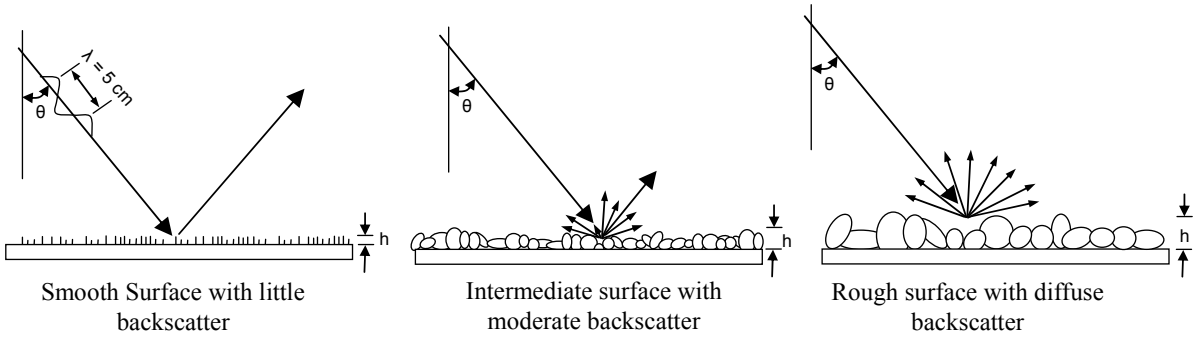

Figure 10: Backscatter from relative surface roughness

Inland and calm water bodies are considered relatively smooth, where most of the incidence energy is reflected away from the radar and only a slight portion of the signal returns to the sensor. However, land surfaces tend to have a higher roughness. In radar images water bodies have dark tone (low backscatter) except those with wind stress or current. This difference between the respective properties of land and water can be very useful for such applications as flood extent measurement or coastal zones erosion (Ulaby et al. 1986b).

3.4.3 Soil Texture

Soil texture is the relative composition of the three major soil classes: sand, silt and clay. The reliance of the dielectric constant on soil texture is a function of variation of water molecule pressure at which it held between soil particles. Previous studies showed a strong linear correlation between the backscatter and soil moisture at a particular soil texture. The plot illustrated in Figure 11 shows that the backscattering coefficient increases when the clay content of the soil decreases at any given value of soil moisture (Ulaby et al. 1986b).

The sensitivity of soil texture to dielectric constant is lower in dry soil, and higher in wet soil conditions (Bindlish and Barros 2002). On the temporal and spatial scale, soil texture is closely related to soil moisture and radar backscatter. Different soil textures have distinct patterns of soil moisture content and soil moisture drainage (Mattikalli et al. 1998). Further, precipitation is responsible for soil moisture variability at a larger scale and soil texture controls this variability at a smaller scale (Oldak et al. 2002).

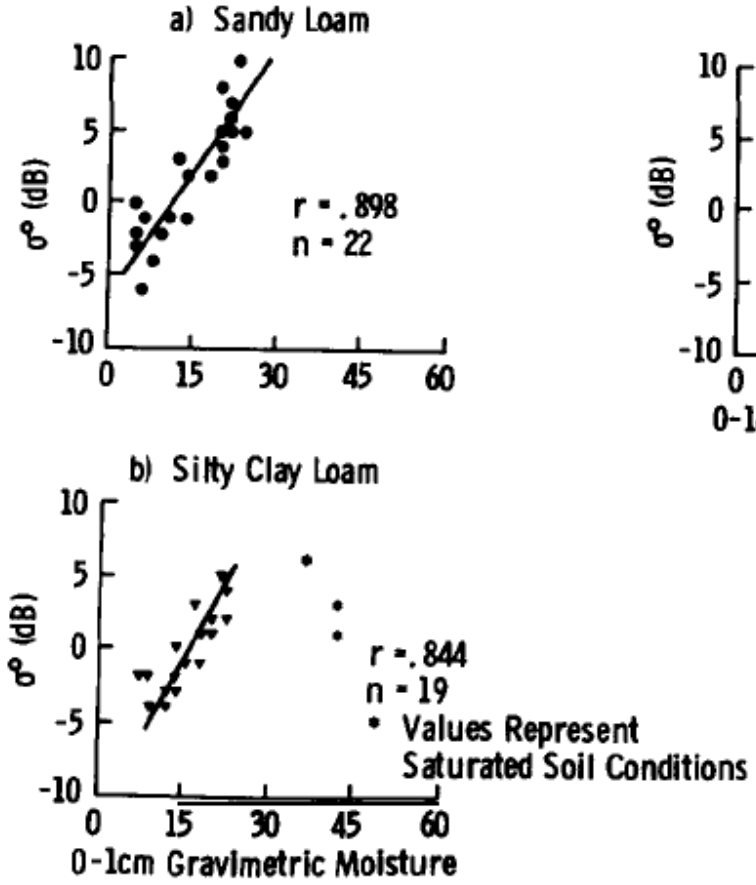

Figure 11: Backscatter response to soil moisture at different soil textures (Ulaby et al. 1981)

3.4.4 Topography

The orientation of surface topography to the radar sensor influences the radar backscatter. The local incidence angle due to variation in topography interferes with backscattering from the soil surface. The surface facing the sensor produces higher radar backscatter due to its geometry. However, a surface facing to the opposite direction to the sensor produces a limited or no backscatter for similar surface soil moisture conditions (Dubois et al. 1995; Glenn and Carr 2003). The HH polarized signals and longer wavelength are

most sensitive to the local topographic effect. The topography effect is observed better for sparser forests with relatively smooth ground surfaces. The topography errors for moderate relief lead to smaller than 1 dB, while for high relief areas the errors on the order of 5 dB or more (van-Zyl 1993).

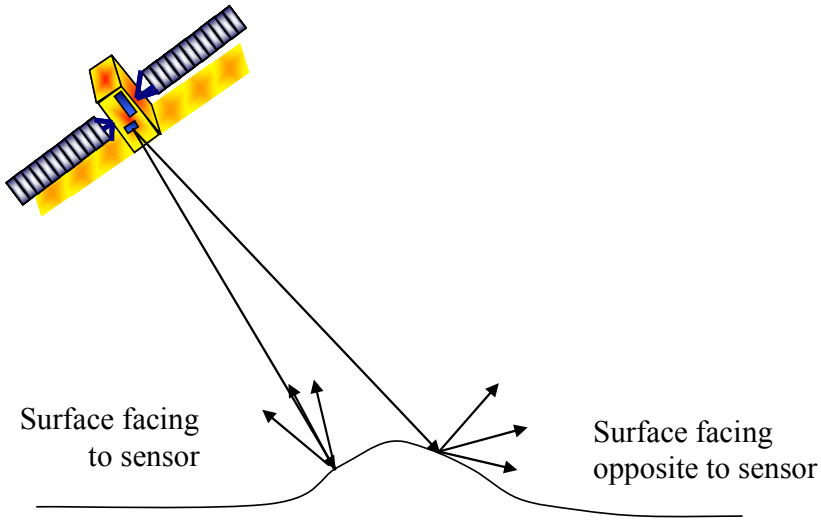

Figure 12: Effect of topography on radar backscatter

The local incidence angle of an individual pixel is calculated using the geometry of the sensor and topographic information from a Digital Elevation Model by:

$$\cos \vartheta = \cos S * \cos Z + \sin S * \sin Z * \cos (T - A) \qquad (2.11)$$

Where ϑ is the local incidence angle (degrees), S is the slope of the pixel (degrees), Z is the zenith angle of the sensor (the angle between the radar and the normal to the horizontal surface), T is the actual flight track of the remote sensing sensor (degrees), and A is the aspect angle of the pixel position (degrees). T and A are defined to be zero to the north and increase counter clockwise (Robinson 1966).

3.4.5 Observation depth

The penetration of microwave energy into the ground depends on the dielectric constant of the upper layer, frequency and radar polarization. The depth of penetration of microwave radiation at a particular wavelength is proportional to the surface soil moisture as shown in Figure 13. A longer wavelength beam penetrates deeper into the soil medium provides information from the deeper soil layer. The penetration depth is also influenced by soil moisture; the penetration depth decreases with increased soil moisture content. A beam with VV polarization penetrates deeper in the soil surface than HH polarization for similar soil moisture content (Ulaby et al. 1986b).

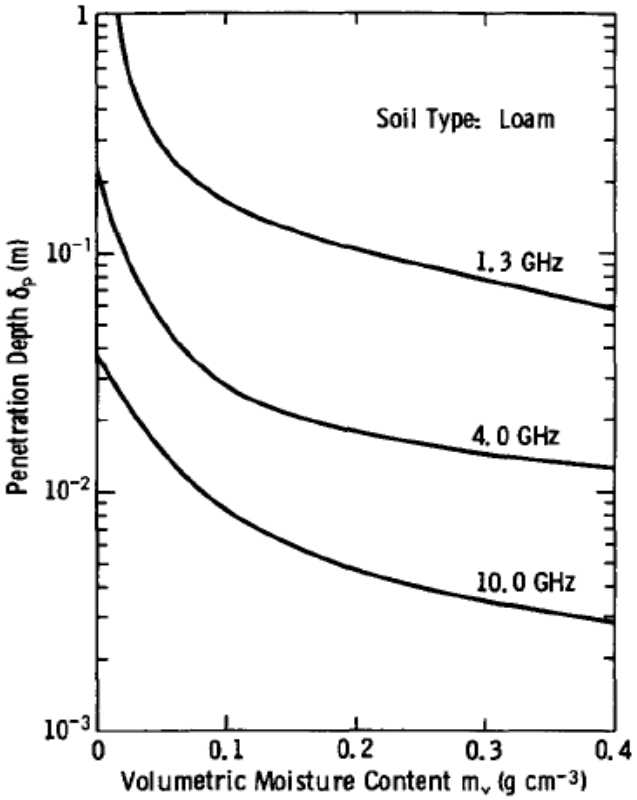

Figure 13: Penetration depth as a function of moisture content for loamy soil (Ulaby et al. 1996)

3.5 Vegetation Parameters

Vegetation cover is the most important factor that influences the retrieval of soil moisture from active microwave remote sensing. The degree of its influence on the retrieval of soil moisture depends upon physical and structural properties of vegetation cover. Various vegetation indices have been developed based on multi-spectral measurements from remote sensing satellites, to study quantitative and qualitative status of the vegetation. The following subsection will be discussing some of the vegetation indices commonly used in the soil moisture retrieval from microwave remote sensing.

3.5.1 Normalized Difference Vegetation Index (NDVI)

The spectral behavior of vegetation is used to calculate the NDVI, which exploits the spectral properties of vegetation cover. The NDVI is considered to be a function of the vegetation strength. As it can be seen in Figure 14, healthy plants absorb light for photosynthesis in the visible part of the spectrum (especially red and blue) and strongly reflect light in the near-infrared part of the spectrum. The green chlorophyll in the leaves does absorb larger visible light and the mesophyll cells scatter light in near-infrared wavelengths. Inactive vegetation (winter deciduous trees), dry vegetation, bare soil and snow do not show this spectral response.

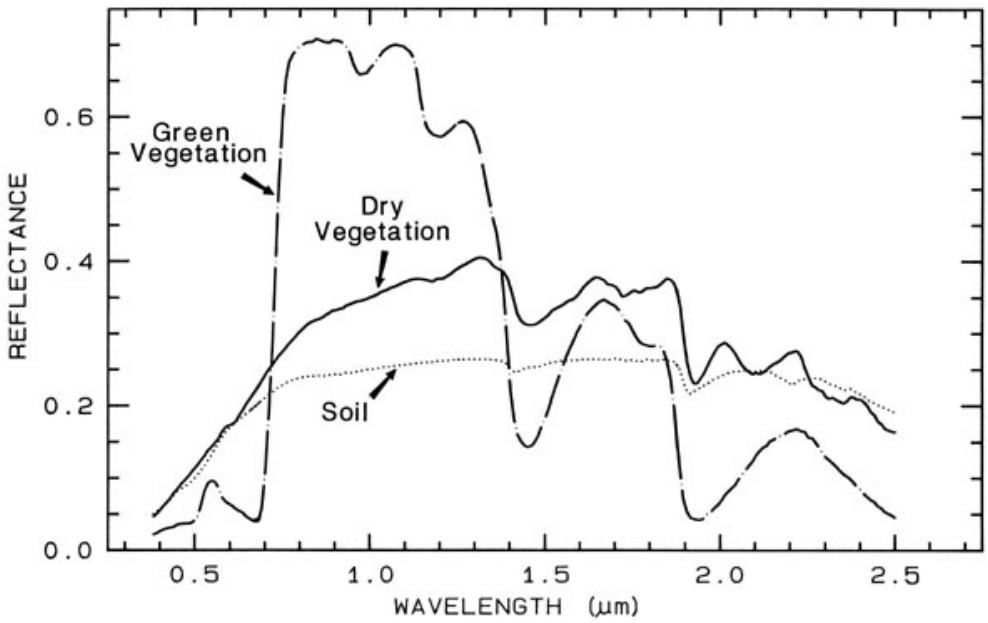

Figure 14: Spectral reflectance of green and dry vegetation

Mathematically, NDVI is defined as the normalized difference between the reflectance in the visible (red) and the near infrared band. The visible (RED) band represents the absorption band of chlorophyll and NIR represents a maximum of vegetation reflectance related to the mesophyll structure. The contrast between vegetation and soil is large in NIR and visible (red) band. The NDVI is calculated using following equation:

$$NDVI = \frac{NIR - RED}{NIR + RED} \tag{2.12}$$

NDVI values are related to the optical properties of vegetation and are mainly sensitive to leaf water and chlorophyll content. The NDVI gives an estimation of the health of vegetation. The negative value means little or no vegetation (high reflectance at RED band) and a value close to one indicates high density of green leaves (high absorbance at RED band). A regression curve between the cross-polarization ratios for L-band data and NDVI is generated by Dubois et al. (1995) shows an alternate method for computing

NDVI. Farrar et al. (1994) have established the relationship between NDVI to the precipitation and soil moisture content. NDVI responds to the change of soil moisture at different root-zone depths in different climate and vegetation conditions suggested that root-zone soil moisture can be estimated using NDVI (Farrar et al. 1994).

3.5.2 Vegetation Optical Depth

Vegetation optical depth (V_d) is directly related to the vegetation water content (W_C) and biomass. The vegetation water content contributes to the microwave emission of the surface and also attenuates the emission of the soil (Jackson and Schmugge 1991; Jackson et al. 1999). The vegetation optical depth was defined by the authors as follows:

$$V_d = b * W_C \tag{2.13}$$

Where, b is an empirically derived parameter related to the nature of the vegetation cover. The parameter b is specified based on land cover classification from published data. The values (Table 4) of vegetation water content and parameter b were used to retrieval soil moisture from ESTAR data during SGP'97 study (Jackson et al. 1999). The emissivity from ground surface depends on vegetation optical depth, and acts as an attenuating layer with transmissivity (γ) and incidence angle (θ). The vegetation optical depth (V_d) is the function of vegetation dielectric properties, the plant shape or structure, the wavelength, polarization, and incidence angle (θ) measured from nadir (Jackson and Schmugge 1991). The transmissivity is defined as:

$$\gamma^2 = e^{\left[-2 * V_d * (\sec\theta)\right]} \tag{2.14}$$

The vegetation water content represents a potential mechanism in retrieval of vegetation optical depth. However, vegetation water content (and, indeed, the value of b) cannot be

derived from remotely sensed data. NDVI in particular is used as a surrogate measure of vegetation optical depth for surface soil moisture retrieval (Burke et al. 2001). A quadratic relationship between the ground-based vegetation water content measurement and remotely sensed NDVI values used to specify the regional based vegetation water content for the SGP97 mission. The relationship between vegetation water content and remote sensed NDVI was established by optimizing a polynomial function (Jackson et al. 1999). The relationship is given by:

$$\text{If NDVI} = 0.5; \quad W_c\ (kg/m^2) = 1.9134 * (NDVI)^2 - 0.3215 * (NDVI) \tag{2.15}$$

$$\text{If NDVI} > 0.5; \quad W_c\ (kg/m^2) = 4.2857 * (NDVI) - 1.5429 \tag{2.16}$$

Further, the research carried out by Ceccato et al. (2002) reported the limitation of NDVI in estimating the vegetation water content. The authors have found that each plant has a different relationship between chlorophyll content and vegetation water content, and a decrease in chlorophyll does not imply a decrease in vegetation water content or vice versa. The vegetation data collected during the SMEX02 mission (Jackson et al. 2004), have been used to retrieve different relationships between NDVI and vegetation water content for soybeans and corn. The optical depth value varies more than NDVI in the time domain due to its inherent characteristics. A study carried out by Du et al. (2000) showed that the radiometric sensitivity decreases with increasing the vegetation optical depth. Anderson et al. (2004) have found that the vegetation water content and canopy heights are directly correlated with leaf area index (LAI). In other study Rosnaya et al. (2006) have found that the LAI and V_d established for green vegetation are more correlated compared to mulch and standing biomass.

3.5.3 Leaf Area Index (LAI)

LAI is a bio-physical parameter considered as a function of vegetation density and cover. LAI is a dominant variable in various land surface processes such as photosynthesis, transpiration, energy balance and ecological and hydrological modeling processes. The LAI value is a dimensionless parameter varying from 0 to 16 describing the number of leaf layers in a plant canopy. LAI is derived by measuring the total projected leaf area in the canopy per unit surface area covered by canopy (Wang et al. 2005).

$$\mathrm{LAI} = \frac{\text{leaf area } (\mathrm{m}^2)}{\text{surface area } (\mathrm{m}^2)} \tag{2.17}$$

LAI = 0 indicates no leafs; LAI = 1, indicates that, the leaf area equals the horizontal ground surface, LAI = 2 means that the leaf area is double the size as the ground surface area; LAI = 16 indicates the maximum value reached in evergreen forests.

The measurement of LAI includes direct and indirect methods. The direct method is a little destructive and requires, taking apart a certain area of canopy and counting the total area of leaves. Direct estimation approaches include area harvest, leaf litterfall, and allometry equations (involving leaf area to stem diameter data). The indirect method includes measures of light transmission within leaf areas using a photometer. The commercially available instruments include: Decagon ceptometer, Li-Cor LAI-2000 plant canopy analyzer, DEMON and TRAC. Decagon ceptometer and Li-Cor LAI-2000 assume foliage is randomly distributed in the canopy (Gower et al. 1999).

Remote sensing derived NDVI values are most widely used to relate LAI. The detailed theoretical relationships between vegetation indices and LAI was given by (Myneni et al. 1995). The relationship indicates that the broadleaf forests tend to have higher NDVI than conifer forests of the same LAI. The LAI can be estimated from the temporal values of NDVI, due to the fact that NDVI represents the relative seasonal changes in vegetation rather than vegetation amount, which considered as a significant relationship between NDVI and LAI. By considering a liner relationship between NDVI and LAI and the maximum NDVI value in a season corresponds to the maximum LAI of vegetation cover (Fassnacht et al. 1997; Justice et al. 1986). LAI can be inferred from NDVI as fallows:

$$LAI_i = LAI_{max} * \frac{NDVI_i - NDVI_{min}}{NDVI_{max} - NDVI_{min}} \quad (2.18)$$

Where max, min and 'i' are the maximum, minimum and period values observed, respectively. Maximum and Minimum NDVI values can be observed by multi-temporal images.

4 Non-Parametric Methods

The learning-based approaches such as neural network and fuzzy logic, which can be considered an alternative to classical modeling techniques for hydrological and meteorological applications, exploit the statistical relationships between hydrologic inputs and outputs without explicitly considering the physical process relationships that exist between them. Neural networks were historically inspired by the biological functioning of the human brain and fuzzy logic by the attempt to simulate human "vagueness" of reasoning. In practice many characteristics of these approaches, such as the ability to learn and generalize, the ability to cope with noise, which maintains robustness, can be of great help in many engineering tasks. Relating to the philosophy of data modeling, important progress has been made in data fusion, i.e. the operation of combining information from multiple sensors and data sources, by eventually exploiting the potential of several alternative models such as neural networks, fuzzy logic, and the maximum likelihood classifier. These techniques are the most commonly used in remotely sensed image classification, and have recently been used in soil moisture inversion. Image classification involves the grouping of image data into a finite number of discrete classes. In this study, neural network and fuzzy logic have been used to predict soil moisture from radar, soil and vegetation data.

4.1 Neural Network System

A Neural network is a highly interconnected system of simple processing elements (called nodes) that is designed to mimic the highly parallel human biological neurons.

These nodes are usually organized into a sequence of layers with random connections between successful layers. The strength of these connections is given through the connecting weights of the network. Each node calculates a summation of weighted inputs and then outputs its transfer function value to other nodes. The typical neural network structure is shown in Figure 15. There are two main phases in the operation of a network: training and testing. Training is the process of adapting the connection weights in response to training samples presented at the input layer and the desired response at the output layer. This learning phase is an iterative process which continues until the neurons have reached a convergence stage to that particular set of training. Testing refers to how the trained neural network processes an input vector presented and creates a response at the output layer (Western and Bloschl 1999).

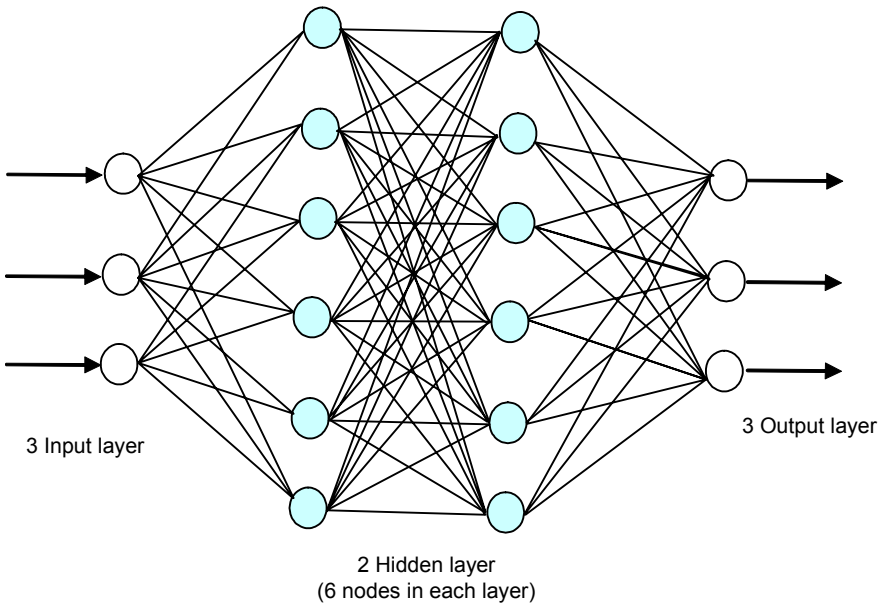

Figure 15: Typical Neural Network (3 Input layer, 2 Hidden Layer, 3 Output layer)

Neural networks (NN) have been applied to a wide range of problems in remote sensing and have produced an improved accuracy compared to traditional statistical methods. They have been increasingly used since 1988 for the classification of remotely sensed images (Benediktsson et al. 1990; Carpenter et al. 1999; Low et al. 1999; Paola and Schowengerdt 1995). The rapid increase of NN applications in remote sensing is due mainly to their ability to perform more accurately than other classification techniques. This success of NN is based on the fact that a single neuron can be compared with a multi-variance linear regression model, which works without any a priori statistical assumptions of the data set. A large combination of several neurons in hidden layers allows for further capability to solve complex problems in remote sensing. Moreover, the learning capability of NN from existing examples makes the classification adaptive and objective. A significant advantage of the NN approach is that it does not require a well-defined physical relationship for systematically converting an input to an output. The other advantages of NN over conventional classification techniques are: the ability to handle data acquired at different levels of measurement precision, and its fast processing time after the network is trained (Foody and Arora 1997). Furthermore, neural networks can provide an alternative to conventional statistical methods, such as maximum likelihood or Bayesian methods. A useful review of the application of neural networks in remote sensing may be found in (Benediktsson et al. 1990; Paola and Schowengerdt 1995). The major advantages of the neural network method over traditional classifiers are (Ghedira et al. 2000):

- Adaptability: Neural network are easily adaptable to different types of data and input configuration. Moreover, neural networks can easily incorporate ancillary data which would be difficult or impossible with conventional techniques.

- No assumption about data distribution: The traditional parametric classification methods, such as, the Maximum Likelihood classifier make unreasonable assumptions about the statistical proprieties of the data, specifically that they are normally (or Gaussian) distributed for each ground cover class. However, this assumption is not always satisfied.

- Problem and model complexity: Neural network deal with large amounts of training data and use its complex configuration to find the best nonlinear function between the input and the output data without the constraint of linearity or pre-specified non-linearity which is required in regression analysis.

- Robustness and quality of prediction estimation: Neural networks are able to assign more than one label of land cover classes to each pixel in an image. This property resolves the mixed pixel problem usually observed in image classification.

Given this list of advantages of neural networks have been wildly used by remote sensing community in many applications. Researchers have modified several internal parameters of neural networks for specific needs, creating various newer versions of the model. Multi-layer perceptron trained by the back-propagation algorithm is the most common neural network used in remote sensing for image classification. This type of neural network has been successfully applied to image processing and has shown great potential in the classification of different remotely sensed data. Further, neural network

technology has provided many promising results in the field of hydrology and water resources.

Multi-layer perceptron neural network trained by backpropagation algorithm adjusts its weights to minimize the root mean square error between observed outputs and predicted values. The backpropagation algorithm uses a gradient descent method to find a local minimum on the error surface. The partial derivative of the square error for each weight has been calculated to obtain the direction in which the error decreases. The direction opposite to these partial derivatives (slope) in which the error decreases is called the steepest descent direction. The standard backpropagation algorithm adjusts the weights along the steepest descent direction. Although the error in the steepest descent direction decreases most rapidly, it usually converges slowly and tends to be stranded due to oscillation. Therefore many backpropagation variants have been created to improve performance by optimizing direction and step size. Some examples include backpropagation with momentum, conjugate gradient, Quasi-Newton and Levenberg-Marquardt.

4.2 Fuzzy Logic Method

The basic principle of fuzzy set theory was formulated in linguistic form by Dr. Lotfi Zadeh in 1965. This linguistic approach is an approximate and effective means of describing the behavior of systems that are imprecise and vague, and too complex to be analyzed with precise mathematical approaches. A strong advantage of the fuzzy approach over traditional methods is that it does not require a detailed mathematical description of the system. The expert knowledge is used in fuzzy modeling to build a

linguistic description of the system's behavior. Fuzzy systems provide a computational framework in which linguistic knowledge is expressed in the form of fuzzy IF-THEN rules. Fuzzy modeling is modified to generate new techniques by other researchers, adding more objectivity in constructing fuzzy models (Chiu 1997; Hayajneh and Radaideh 2003).

A typical Fuzzy system includes the processes are: fuzzification, inference system, and Defuzzification (Figure 16). The fuzzification comprises the process of transforming crisp values of image data into grades of membership in linguistic terms. Defuzzification involves the process of transposing the fuzzy crisp outputs in the form of image data. The fuzzy inference system is based on the concepts of fuzzy set theory, fuzzy if-then rules, and fuzzy reasoning. The widely employed fuzzy model is the Mamdani type, in which fuzzy sets consists of IF-THEN rules for both input and output. Another fuzzy model was Takagi–Sugeno model, which is associated with rules based on a special format that is characterized with functional type consequents instead of the fuzzy consequents used by Mamdani. The Takagi–Sugeno model was proposed by Takagi and Sugeno (Takagi and Sugeno 1985). In the Sugeno model, a system with ''m'' inputs can be represented as a set of ''n'' rules in the following format:

Ri: IF $x_1 = A_1^i$ AND $x_2 = A_2^i$, AND $x_m = A_m^i$ THEN

$$y_i = a_{i0} + a_{i1} x_i + \ldots\ldots + a_{im} x_m \qquad (4.1)$$

where $a_{i0}, a_{i1}, \ldots, a_{im}$; i=1,2, . . . , n are regression parameters to be estimated using the least squares estimation (LSE) algorithm. The output of each rule is a linear combination of input variables plus a constant term, and the final output is the weighted average of each rule's output.

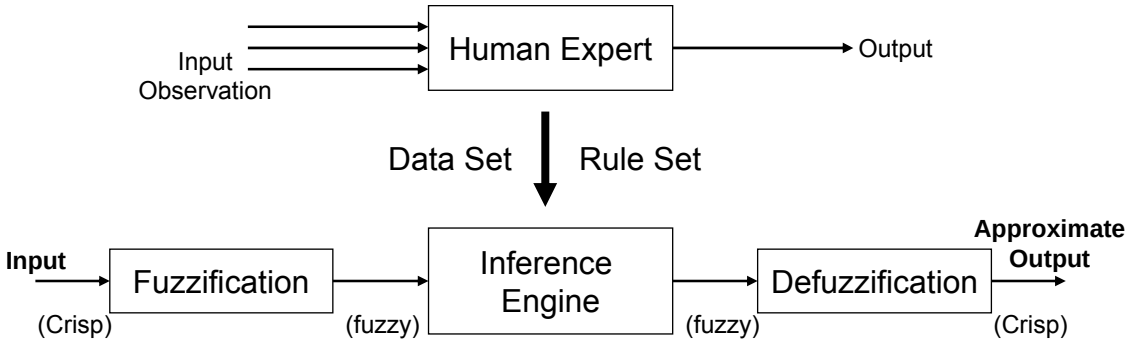

Figure 16: A typical fuzzy logic system (Wang and Jamshidi 2004)

The input–output data is use by fuzzy techniques to enhance human knowledge or to even breed new knowledge. The models development from input–output data consists of two major steps. The first is structure identification; this involves initial rule generation in the form of IF-THEN statements. The second is parameter identification, which consists of setting membership functions or parameters responsible for reasoning processes based on certain objective criterion. The identification of membership functions involves setting up a rough estimate of initial fuzzy rules from identified cluster centers. Membership functions and other fuzzy rule parameters are then optimized with respect to some output error criterion. The above procedure is used to extract rules for function approximations (Chiu 1997).

In the classical fuzzy logic, an element is expressed in binary terms: 0 or 1, yes or no, black and white; in terms of Boolean algebra. A fuzzy set generalizes the Boolean set by allowing partial membership in a set, with values ranging from 0 to 1. The fuzzy logic technique based on fuzzy set theory has been applied in many areas where the relationship between variables is not empirically defined. The elements of a fuzzy set have different degrees of membership values. The membership value ranges between 0 and 1, depending upon partial or full membership.

A mathematical function defines the degree of an element's membership in a fuzzy set. Fuzzy logic has been used widely in the areas of: process control, management and decision making, operations research, economics and engineering. The advantage of fuzzy logic is in dealing with uncertainty and imprecision in a decision-making process, and thus offers a new approach for classifying remotely sensed images (Nedeljkovic 2004).

In the remote sensing application, pixels in an image can be partitioned into a series of fuzzy sets by assigning to each individual entity a ‘‘grade of membership’’ in each of the sets. These fuzzy membership values range between 0 (no membership) and 1 (type specimen) and specify the degree to which each individual can be regarded as belonging to a specific fuzzy set. Therefore, the defining membership functions of fuzzy sets have a strong influence under the data-driven similarity relation model used in this study. The value of the membership function depends on the classification method used (Chiu 1997).

A clustering technique is used in this study for automatic generation of rules, in which each cluster represents a group of associated data in a data space. Fuzzy identification of systems invariably use fuzzy partitioning in data space based on certain measures. Each data point in a data space is assumed to have an equal contribution towards system identification. Therefore, the grouping of data into clusters is determined by density of the data based on a search criterion. The relative positioning of data into different clusters depends on the measure it scored with reference to different cluster centers. A data point that scored the highest search measure represents a cluster center (Demirli and Muthukumaran 2000).

4.3 Remote Sensing and Neural Network System

In microwave remote sensing, the NN technique combined with electromagnetic model has been proved as a dominant role in an inversion problem. The retrieval of soil moisture using neural networks was studied by (Aires et al. 2005; Atluri et al. 1999; Baghdadi et al. 2002; Dawson et al. 1997; Frate et al. 2003; Sahebi et al. 2004; Satalino et al. 2002; Zhao et al. 2003). The advantage of NN technique is that all surface parameters included and trained in neural network acts as an empirical mapping relation between radar backscatter and land surface parameters.

The neural network method coupled with Integral Equation Model (IEM) is used by researchers to estimate soil moisture. Satalino *et al*. (2002) used multilayer perceptron NN architecture to retrieve the soil moisture by inversion IEM model. The authors classified the soil moisture in 2 classes to reliable retrieval of soil moisture using neural network. Meade et al. (1999) used multi-layers back propagation and feedforward neural network to estimate soil moisture from ERS-1 and ERS-2, C-band SAR data. The ground measured soil moisture along with vegetation type was used to train the neural network for SAR data and found poor correlation between SAR data with field measured soil moisture. It is important to note that, the vegetation type along with SAR data is not enough to improve the relationship between backscatter and soil moisture.

NN with backpropagation and Levenberg-Marquardt training algorithms is used for soil moisture prediction at regional agricultural study. The input variables used in the model are calibrated surface temperature, and brightness temperature at L-Band and S-Band. The network trained with Levenberg-Marquardt algorithm has been found much faster than that trained with backpropagation (Atluri et al. 1999).

Frate et al (2003) studied the retrieval of soil moisture from microwave radiometry using a NN technique, and shows that the NN is capable of solving the problem of remote sensing inversion. To solve this problem, the authors use the L-Band with two polarization radiometric data and the electromagnetic model. The authors found that in the upper layer of soil within the first centimeters, the L-Band is more sensitive to moisture content, and the soil emissivity is sensitive to moisture in low frequencies. As summary, the study suggest that a good retrieval of soil moisture can be obtained if a consideration of vegetation cover and roughness are made, as well as an assumption of the growing cycle of the crop. However, with this NN there is no requirement to the vegetation roughness and cover status.

Other researches also demonstrated the efficacy of the application of NN to soil moisture retrieval, but with different input parameters. Zhao et al (2003) studied the retrieval of soil moisture content using as input to the NN, data obtained from the advanced microwave scanning radiometer (AMSR/E). The developed NN model also showed a good correlation on the estimation of soil moisture, and demonstrated that the microwave emissivity from soil is dependent on near-surface soil moisture content. On the other hand, Sahebi et al (2004) used synthetic aperture radar (SAR) satellite data in combination to a neural network to solve the inversion problem. Using backscattering coefficient and incident angle from SAR data as input to the NN, the authors estimate the surface roughness and soil dielectric constant. The combination of three radar configurations (VV 23º, HH 39º, and HH 47º) from SAR data was done, obtaining high accuracy for soil moisture and surface roughness estimates (Baghdadi et al. 2002).

In a global scale, (Aires et al. 2005) studied the retrieval of soil moisture using passive microwave (SSM/I) and a NN consisting of multi-layer perceptron (MLP). It was found that the relationship between the differences in polarization of SSM/I are more sensitive to vegetation than to soil moisture. Therefore, the retrieval of soil moisture is complex and can be obtained thru a relationship of the correlation between vegetation and soil moisture. Thus, leading that the soil moisture retrieval should be retrieved locally for the specific surface conditions, and cannot be generalized for all surface types. In addition, the research found that the large errors are mainly in wetlands and mountainous areas, due that the developed NN does not work well in the detection of wetland, and the microwave satellite data (passive and active) are sensitive to topography, which contaminate the retrieval. However, the NN can produce accurately results in global scale if observations from various wavelengths are considered. At the global level, the soil moisture predicted by using neural network from SSM/I and ERS-1 data with RMS error of 5% of volumetric soil moisture.

In terms of NN configuration, Atluri et al (1999) compared Levenberg-Marquardt (LM) algorithm and backpropagation algorithms. The LM algorithm worked faster than the backpropagation algorithm with higher accuracy in classifying soil (grass or bare smooth), and predicting the soil temperature and moisture. The developed NN was able to predict accurately the soil moisture at higher depths; at surface, the accuracy was low due to environmental factors such as the variation in the soil moisture due to sunlight, and therefore evaporation.

For detection, (Topouzelis et al. 2004) used NN in combination with SAR images to detect oil spills, and (Alhumaidi et al. 1997) used NN to detect ice covered ocean

surfaces. By comparing two types of NN, the multilayer perceptron (MLP) and Radial Basis Function (RBF), the reliability of the LMP image classification was found to be higher than for RBF, although RBF works faster than LMP (Topouzelis et al. 2004).

Another technique used in remote sensing is fuzzy logic, which is mainly used for pattern recognition and image classification (Nedeljkovic 2004; Wang and Jamshidi 2004). Nedeljkovic (2004) compared the fuzzy logic technique with the maximum likelihood (ML) classifier, and found ML faster in image classification than using fuzzy logic. However, since the input data for ML and fuzzy logic must be the same, fuzzy logic perform better than ML; because fuzzy logic uses simplest rules for image classification, which make it less time consuming, if a consideration of all the process is made.

5 Study Area and Data Acquisition

5.1 SGP'97 Experiment

The Southern Great Plain mission (SGP'97) was an interdisciplinary research campaign which conducted large-scale mapping of surface soil moisture in the summer of 1997 in Oklahoma USA (Figure 17) and represents the study area of this research. This area has been the focus of much remote sensing and soil moisture experimentation carried out by various government agencies during the last 15 years. This study area is shown in the false color composite image generated from a Landsat thematic Mapper (TM) image taken on July 25, 1997 (Figure 23). Many of the sites used during SGP97 were also a part of meteorological observation networks: Atmospheric Radiation Measurement Program (ARM), Cloud and Radiation Testbeds (CART), Agricultural Research Service (ARS), Oklahoma Mesonet, and the USDA Natural Resources Conservation Service's (NRCS) two soil moisture and soil temperature (SMST) analysis network (SCAN) sites.

The SGP'97 experiment was performed over a one-month (June 18 - July 17) period with the objective of testing formerly established soil-moisture retrieval algorithms for the ESTAR (Electronically Scanned Thinned Array Radiometer) Instrument (Jackson et al. 1999). The ESTAR is a synthetic aperture, L-band passive microwave radiometer operated at a frequency of 1.413 GHz with horizontal polarization (Vine et al. 1994; Vine et al. 2001). The ESTAR instrument demonstrates a great potential to estimate surface soil moisture maps during experiments such as Walnut Gulch'91, Washita'92, etc. This instrument is one of the most efficient soil moisture mapping devices currently available. The experiment was carried out using airborne and truck-mounted sensors to extend the

soil moisture retrieval algorithms developed for fine resolution truck and aircraft-based sensors to the coarser resolutions expected from satellite platforms.

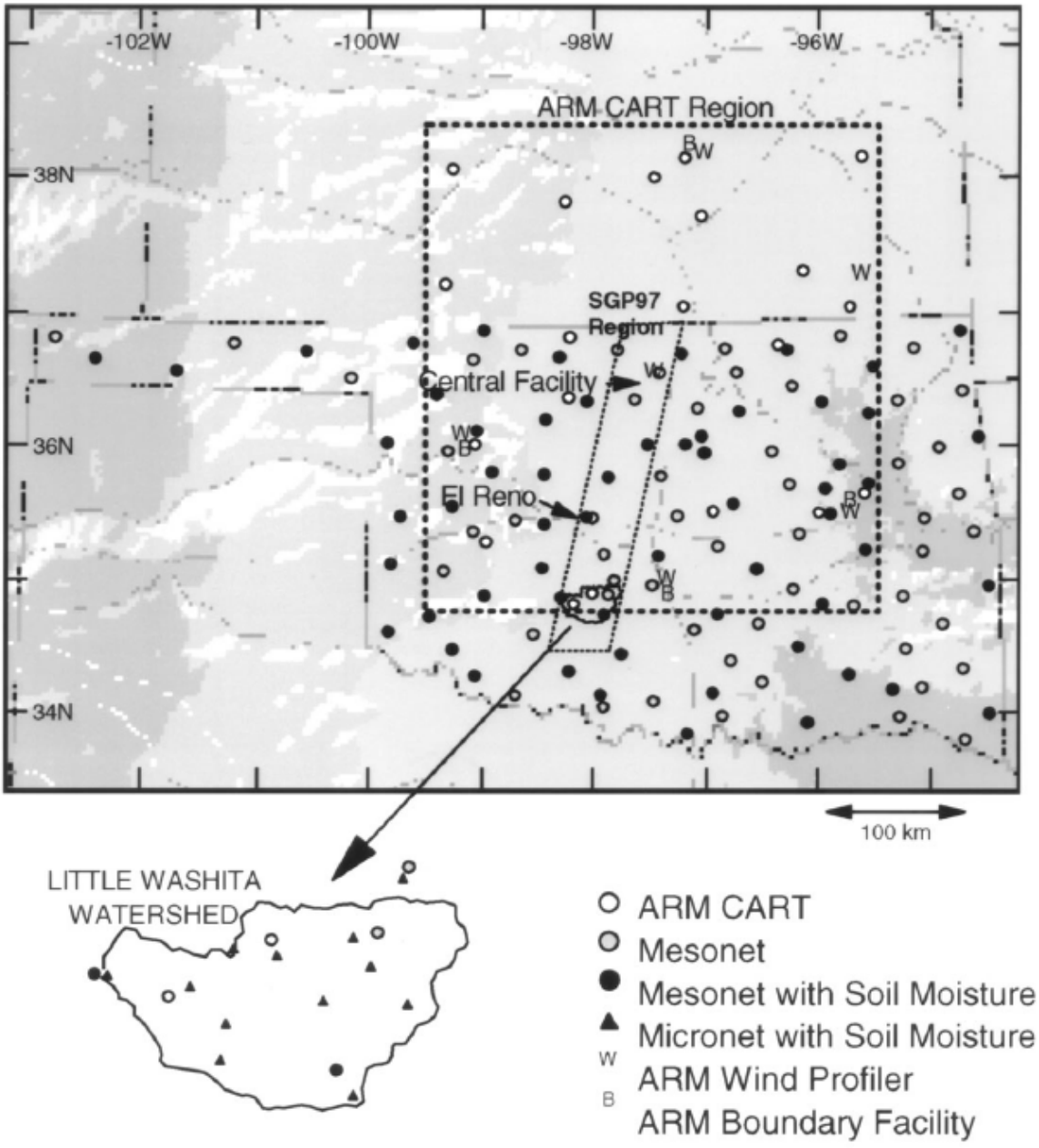

Figure 17: SGP'97 study region (Jackson et al. 1999)

The SGP region has a relatively homogeneous geography, variable surface flux properties, stable humidity, large seasonal variation in temperature, and moderately rolling topography with maximum relief of 200 m. The study area has a sub-humid climate with annual average rainfall of 75 cm. The soil type widely varies from clay to sand. The predominant vegetation covers are Pasture/Rangeland (approx 49%), wheat (35%), summer legume (5%), Alfalfa (3%), and Forage (4%). In-situ measurements of soil moisture, temperature, surface roughness, and vegetation cover were conducted in 50 different locations. Field soil moisture and other vegetation data such as NDVI and vegetation optical depth have been collected, compiled, and used in different steps of this research.

5.2 Soil Moisture Data

Two types of soil moisture data has been used in this study. First, the field data measured gravimetrically on site during the SGP97 mission. Second, calibrated soil moisture data derived from a passive radiometer used as an input to the neural network and fuzzy logic models. The details about these datasets are discussed in following sections.

5.2.1 Field Soil moisture data

Gravimetric soil moisture measurements of the surface layer have been taken from 50 sites located in study area. For each sampling site an average of 14 samples of soil moisture were measured. The number of samples taken from each site varied based on heterogeneity of land surface. The sample location from each site was kept 100 m apart and spatially distributed within a grid size of approximately 0.8 square kilometers. Samples were coded for location for identification such as: Little Washita (LW), El Reno

(ER), and Central Facility (CF). Jackson et al. (1999) shows detailed information about sampling site location used to measure gravimetric soil moisture and other parameters during the SGP97 mission. Four measurements of Bulk density were performed for each field to convert gravimetric soil moisture to volumetric soil moisture (Jackson et al. 1999; Mohanty et al. 2002). The relationship between field points measured sample with SAR backscattering shown in Figure 21 and Figure 22 for 02nd and 12th July 1997 data. The details about field condition during the SGP97 mission were given in Appendix B.

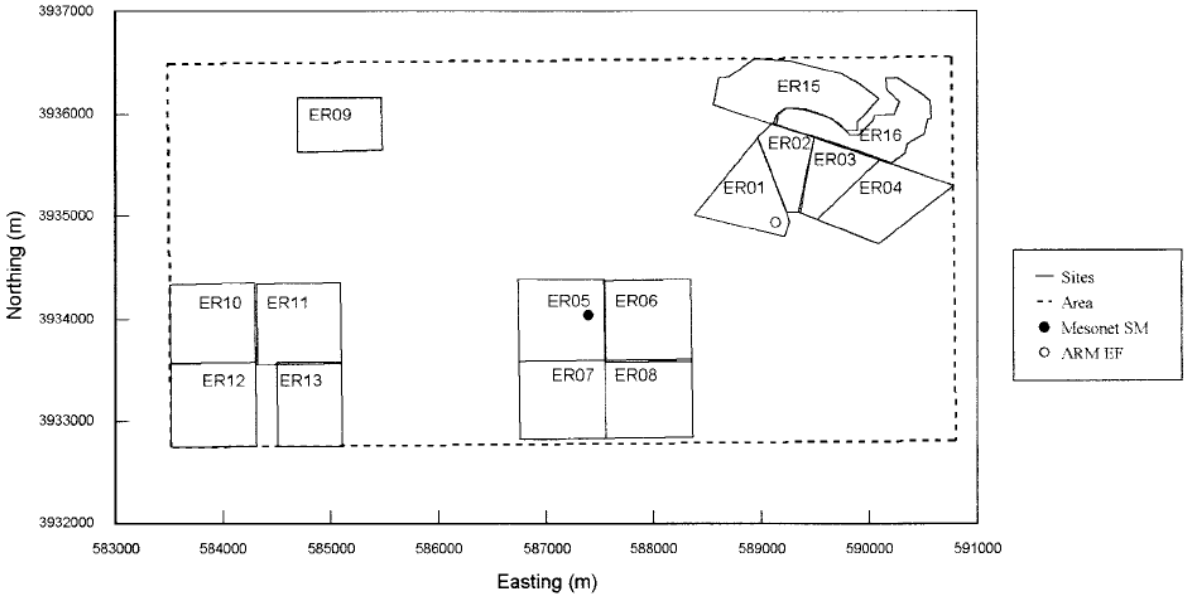

Figure 18: Test sites in the El Reno (ER) area. Coordinates are UTM.

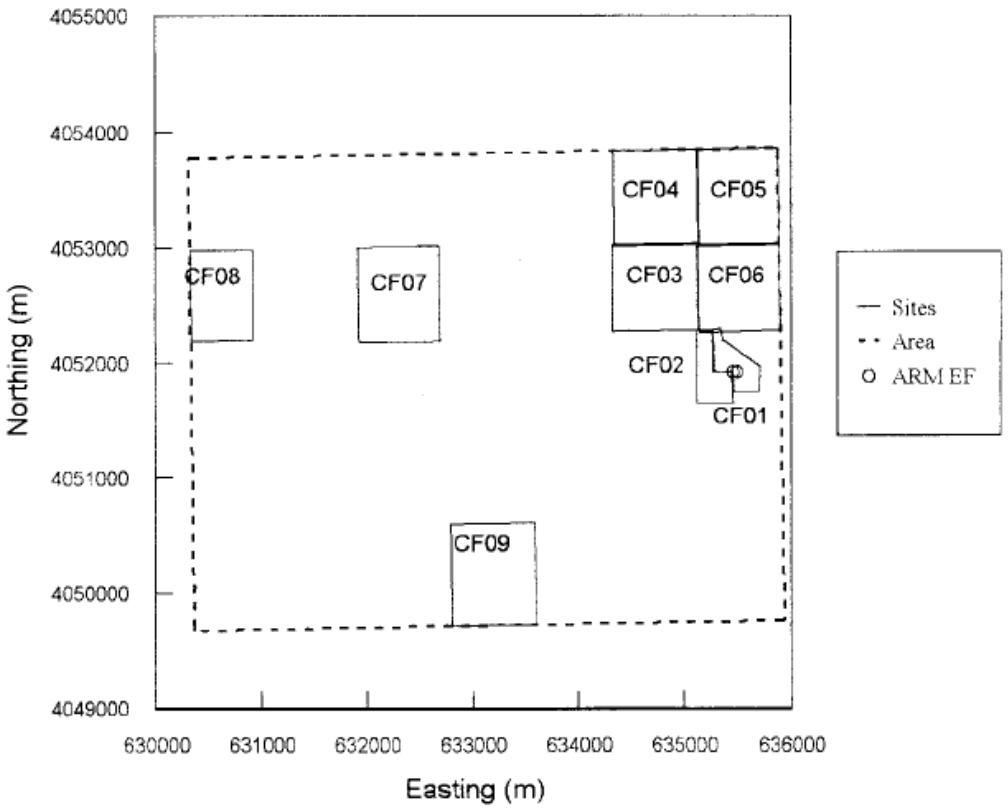

Figure 19: Test sites in the Central Facility (CF) area. Coordinates are UTM.

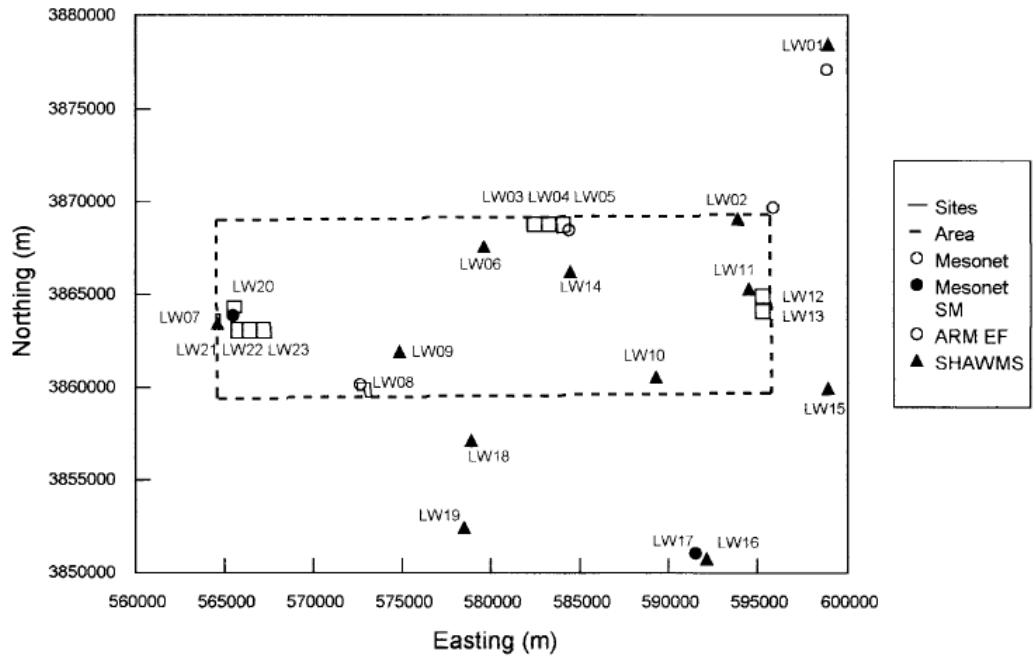

Figure 20: Test sites in the Little Washita (LW) area. Coordinates are UTM.

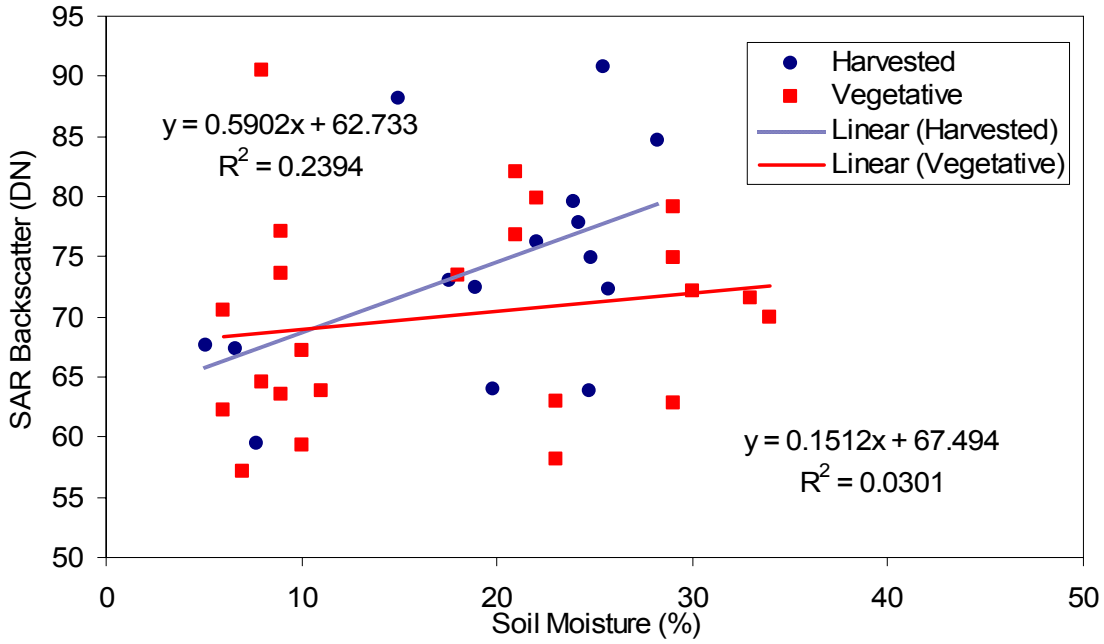

Figure 21: SAR backscattering and L-Band SM for vegetated and harvested area (July 02 data)

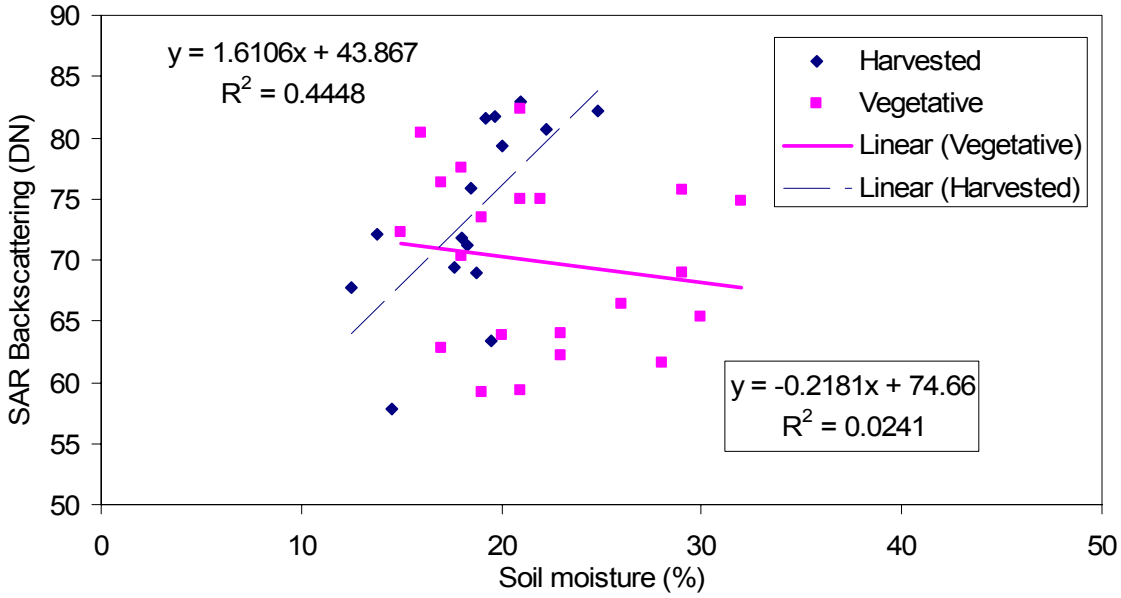

Figure 22: SAR backscattering and L-Band SM for vegetated and harvested area (July 12 data)

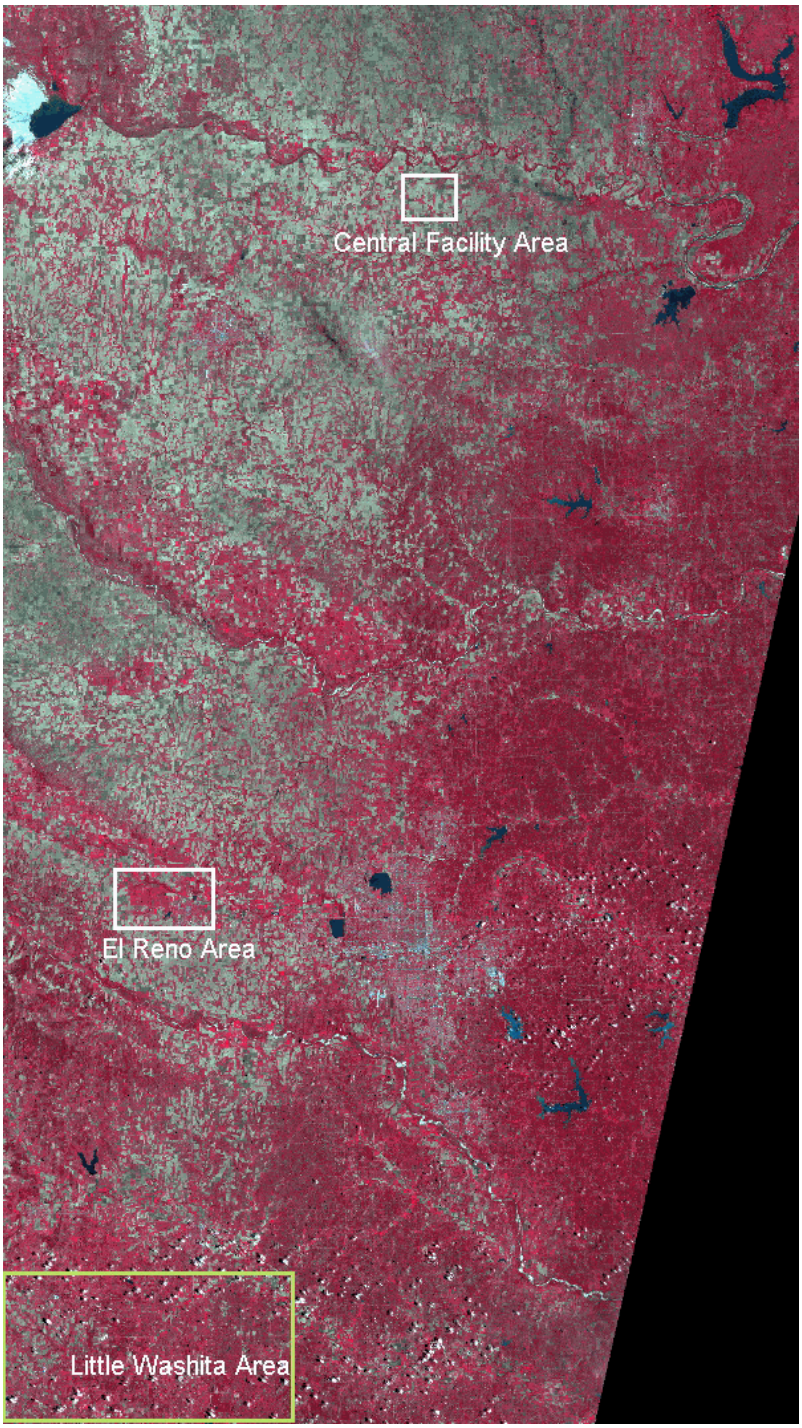

Figure 23: Landsat Thematic Mapper false color composite image of study area (SGP'97 website)

5.2.2 Truth Soil moisture Data

The soil moisture data retrieved from ESTAR instruments during the SGP97 experiment were used to train the neural network and fuzzy logic models in this study. The details about soil moisture retrieval algorithms from ESTAR can be found in (Jackson et al. 1999). The soil moisture data retrieved from ESTAR has a resolution of 800m x 800m. Two different soil moisture formats were tested as an input to the algorithm.

1. Quantitative values (in percentage) in their original resolution (800m)
2. Three qualitative classes based on the water content: dry soil (0-10%), slightly wet soil (11-20%), and wet soil (+21%).

The general relationship between SAR backscattering values in SCANSAR mode and the percentage soil moisture are shown in Figure 24 (a). The Figure 24 (b) shows relationship of SAR backscattering values and the deviation of soil moisture from means values of each class.

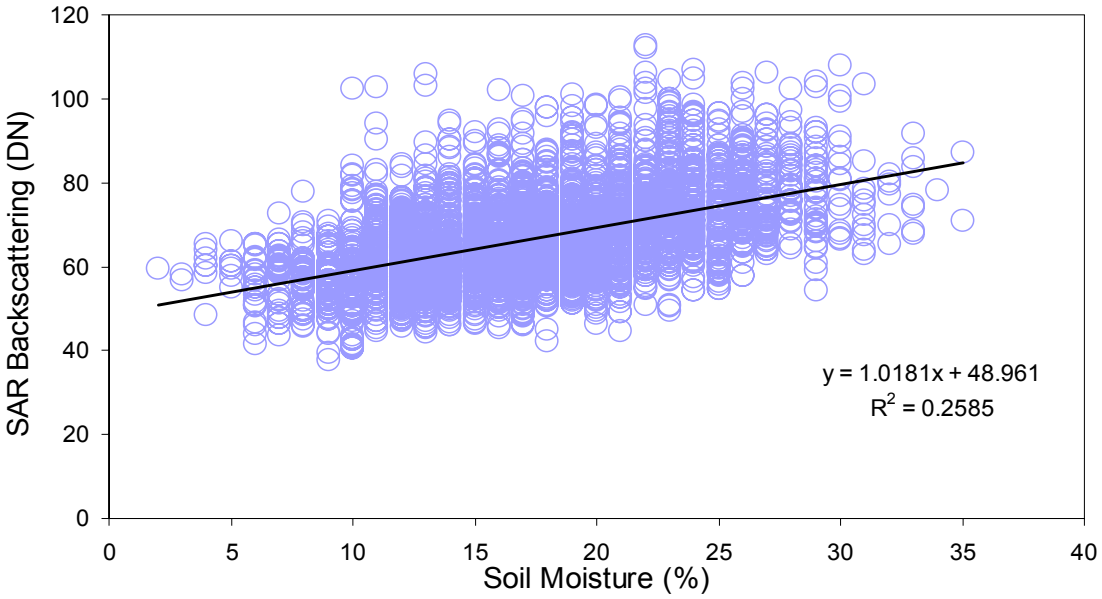

(a) SAR backscattering and soil moisture (percentage)

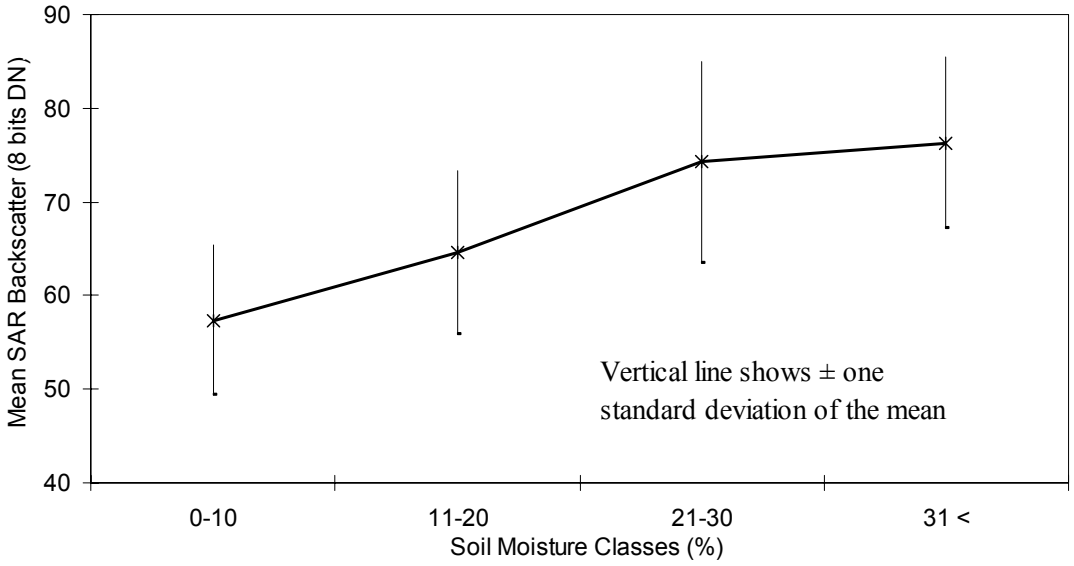

(b) SAR backscattering and the deviation from means of soil moisture in each class

Figure 24: Relationship of SAR backscattering values with truth soil moisture data

5.3 Vegetation and Ancillary Data

In addition to active microwave data, NDVI, vegetation optical depth, soil texture, and SAR textural images are used as inputs to the neural network and fuzzy logic model. The details of these input parameters are discussed in following sub-sections.

5.3.1 NDVI

The NDVI data used was obtained from one Landsat TM image acquired on July 25, 1997, and calculated by Jackson et al. (1999). These NDVI values were originally calculated at 30 meter resolution, but were aggregated to 800 meter resolution to match the soil moisture resolution.

5.3.2 Vegetation optical depth

To calculate vegetation optical depth, the vegetation *b* parameter for each crop type was considered based on studies made by Jackson and Schmugge (1991). The vegetation water content has been measured on the field during SGP'97 mission and correlated with NDVI values. (See equations 3.4 and 3.5).

Table 4: Parameter used for ESTAR soil moisture estimation for different land cover categories

Land-cover Category	Vegetation parameter, b	Vegetation water content (kg/m2)	Surface roughness, h
Alfalfa	0.085	1.0	0.1
Bare	0.000	0.0	0.2
Corn	0.119	1.0	0.2
Forage	0.095	Eq. (3.4)	0.1
Legume	0.085	0.5	0.1
Pasture	0.095	Eq. (3.4)	0.1
Trees	X	X	0.1
Shrub	0.095	Eq. (3.4)	0.1
Urban	X	X	X
Water	X	X	X
Wheat	0.000	0.0	0.1
Summer corn	0.119	0.5	0.1
Summer legume	0.085	0.5	0.1
Unclassified	X	X	X

5.3.3 Soil Texture

Soil texture data was obtained from the SGP ’97 mission. These soil texture data used in this mission was calculated by a combination of sources. One of these sources was a product from the state soil geographic database (STATSGO) of the USDA Natural Resources Conservation Service (NRCS), which provide soil texture classification on a 1 km grid. In addition to this source, soil texture samples and published data at the study site were used to produce a more general value for soil texture classification in terms of sand or clay percent content. Once those values were acquired, a re-sampling was made to generate 800 meter resolution grid.

Table 5: Details of soil texture data used as input parameter

Image DN value	Class	Percent Sand	Percent Clay
0	No Data	X	X
1	Sand	95	5
3	Sandy Loam	60	10
4	Silt Loam	20	15
6	Loam	35	20
8	Silty Clay Loam	10	35
9	Clay Loam	35	30
11	Silty Clay	10	45
12	Clay	20	60
14	Water	X	X

5.3.4 Land-cover data

Land-cover classification data at 25m x 25m resolution derived from multiple Landsat TM is used in this study. This data is used to understand the effect of sub-pixel variability on the overall accuracy of soil moisture retrieval.

5.4 Active Microwave Data from RADARSAT-1 Satellite

The Radarsat-1 satellite was launched on November 4, 1995 by the Canadian Space Agency (CSA). It circles the Earth with an orbital altitude of 798 kilometers at an inclination of 98.6 degrees to the equatorial plane circles (Figure 25). RADARSAT-1 has a sun-synchronous orbit, always overpasses a particular location at the same local mean time, and covers the earth 14 times a day. Radarsat-1 covers most of Canada every three days and the artic every single day, depending on the swath selected. Because this satellite has in almost continuous sunlight, it is able to rely on solar rather than battery power. Radarsat-1 carries a C-band SAR capable of offering a wide variety of beam

selections operated in multiple modes with resolutions ranging from 10 to 100 meters. The unique ability of Radarsat-1 to shape and steer its beam from an incidence angle of 10 to 60 degrees, in swaths of 35 to 500 kilometers, differs from other SAR satellites. The data from Radarsat-1 can be downloaded in real time or stored on the onboard tape recorder until the satellite is within range of a receiving station.

With its unique C-band channel, the effective penetration depth of RADARSAT-1 beam is shallower than 5 cm for very wet soil and deeper than 5 cm for dry soil (Ulaby et al. 1986b). The Radarsat-1 transmits and receives the signal in horizontal polarization (HH). The satellite has seven beam modes, each with their own typical incidence angle range and resolution and swath. The Standard beam and ScanSAR modes are found to be the most useful compared to the other modes. Further, the frequency of the revisit to the same location allows researchers to monitor the dynamics of soil moisture change and to improve the accuracy of soil moisture models (Engman and Chauhan 1995). The potential of application of Radarsat-1 satellite for large-scale soil moisture monitoring has been investigated by different researchers (Boisvert et al. 1995a; Boisvert et al. 1995b; Glenn and Carr 2003; Wickel et al. 2001).

Table 6: Characteristics of RADARSAT-1 beam mode **(**Courtesy: Canadian Space Agency**)**

Mode	Nominal Resolution (m)	No. of Positions / Beams	Swath Width (km)	Incidence Angles (degrees)
Fine	8	15	45	37 - 47
Standard	30	7	100	20 - 49
Wide	30	3	150	20 - 45
ScanSAR Narrow	50	2	300	20 - 49
ScanSAR Wide	100	2	500	20 - 49
Extended High	18 - 27	3	75	52 - 58
Extended Low	30	1	170	22-Oct

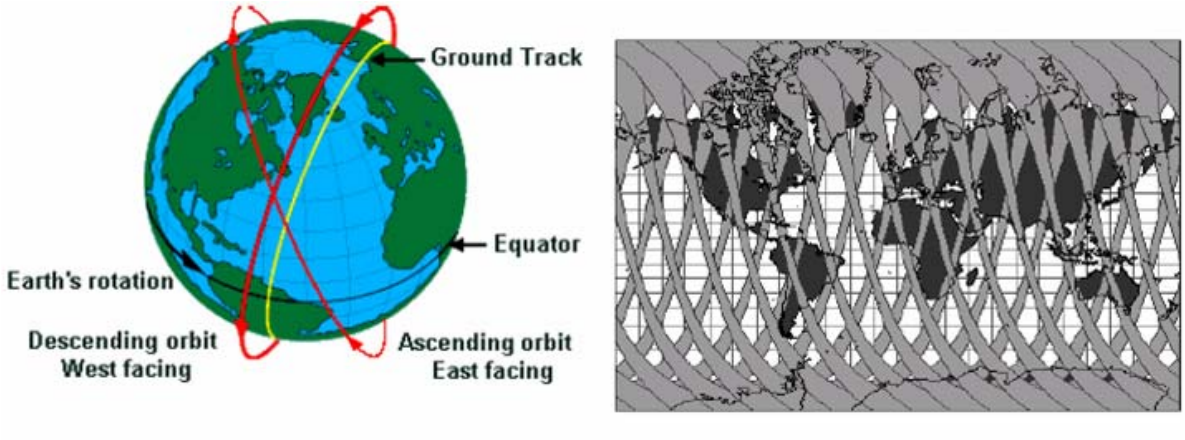

Figure 25: Path of Radarsat-1 satellite (Courtesy: Canadian Space Agency)

Table 7: Main characteristics of used RADARSAT-1 scenes

Parameter	Scene-1	Scene-2
Date and time	July 02, 1997; 12:27:11	July 12, 1997; 12:36:29
Pass	Descending	Descending
Beam Mode	(B) W2 (31-39), S5 (36-42), S6 (41-46)	(A) W1 (20-31) W2 (31-39)
Product type	ScanSar Narrow	ScanSar Narrow
Incidence angle	31 – 46	20 – 39
Resolution	25 m	25 m
Scene centre	36°06'N 96°38'W	36°08'N 96°58'W

5.4.1 Data Acquisition

Two RADARSAT-1 images acquired on July 2nd and July 12th, 1997 by SCANSAR Narrow Mode have been used in this study. The characteristics of these images are presented in Table 2. The two raw data have been received from the official distributor

(RADARSAT International), in CEOS standard format. Each Radarsat image contains five supporting data files:

1. the SAR leader file containing data acquisition and pre-processing information
2. the SAR trailer file with a descriptor record
3. the volume directory file, containing information about the data product
4. the null volume directory file with the null volume descriptor record
5. the label file giving a summary the image files

5.4.2 Data Pre-processing

PCI Geomatica software has been used to convert RADARSAT data into calibrated radar backscatter (σ°) in dB (Decibel) using CDSAR, SARINCD and SARSIGM commands. The module CDSAR is used to read data from CD, and converted to a PCI file format. Further, CDSAR module creates four separate segments, such as: the geo-reference segment, orbit segment, SAR scaling offset segment and SAR scaling gain segment. Second module SARINCD is used to create an additional array segment of incidence angles to use with the SAR gain-scaling table. Finally, SARSIGM module is used to generate a calibrated radar backscatter image using the orbit information, scaling and angle segments information. SARSIGM model uses the following equation to calculate calibrated radar backscatter:

$$\sigma_{ij} = \beta_{ij} + 10 * \log_{10}\left(Sin\ (I_i)\right) \tag{5.1}$$

$$\beta_{ij} = 10 * \log_{10}\left(\frac{DN^2 + A_0}{A_j}\right) \tag{5.2}$$

Where, σ_{ij} is the output backscatter coefficient for scanline i, pixel j

β_{ij} is the radar brightness coefficient for scanline i, pixel j

I_j is the expanded incidence angle table value for column j.

A_0 is the gain offset from the first member of A0SEG (the gain offset segment).

A_j is the expanded gain scaling table value for column j.

DN is the input image value for scanline i, pixel j

5.4.3 Image Registration

The soil moisture and vegetation data acquired from NASA website was imported to PCI Geomatica format (*.pix). The module GCP works has been used to georeference the Radarsat images with the soil moisture and NDVI images. The georeferencing process has been done by selecting standard ground control points. The care should be taken by maintaining the root mean square error (rmse) smaller than one pixel. Two windows (A and B) covered by all available data (Radarsat, soil moisture, vegetation, land-use data) were selected and subseted from the main image for further analysis (Figure 26). This step produces a total of 4 sub-images (2 for each date). The two areas A and B are close to Central Facility and Little Washita regions respectively. The study area A covers 26.4 km x 96 km = 2534.4 km^2 and B covers, 31.2 km x 103.2 km = 3220.0 km^2.

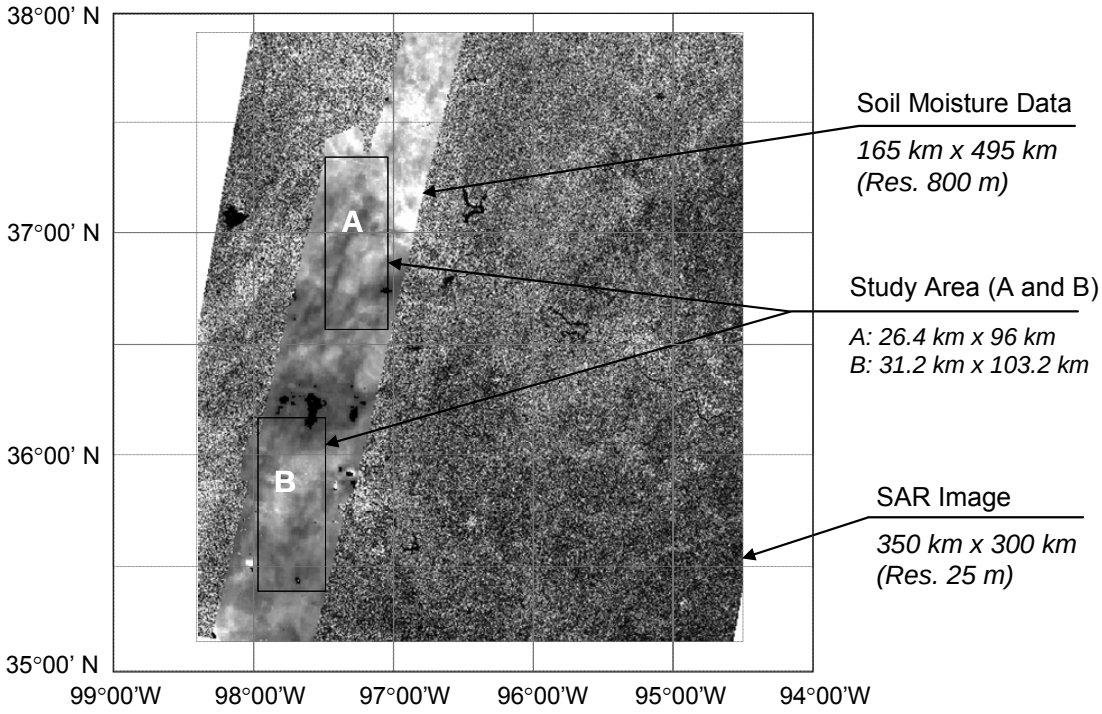

Figure 26: Details of study area with reference to soil moisture and SAR images

The high resolution 25m x 25m SAR data has been aggregated to 800m x 800m of moisture data. The aggregation process eliminated the effects of speckle, a form of noise which degrades the quality of an image. The mean, mode and median filtering algorithms have been tested for aggregation. A very high correlation between the outputs of these three aggregation methods were found, hence we selected the mean method for both images.

5.5 Textural Analysis SAR data

Texture measurements are used as important input information in image analysis. They have been widely studied in addition to spectral features to discriminate between different land cover categories (Ghedira and Bernier 2004; Kurvonen and Hallikainen 1999; Low

et al. 1999; Soares et al. 1997; Ulaby et al. 1986a). The use of textural measures as input to neural network classifiers has been shown to improve significantly the classification accuracy (Augustejin et al. 1995; Ghinelli and Bennett 1997; Haralick 1979; Kanellopoulos and Wilkinson 1997).

Texture information represents the pixel gray level variability measured over an image segment. The addition of this information into the classification process improves significantly the land cover identification accuracy since a single class usually occupies a large region of neighboring pixels. Haralick (1979) defined eight textural measures that can be derived directly from the Grey Level Co-occurrence Matrix (GLCM), but many of them are highly correlated.

There are two general types of textural analysis: Statistical and Structural. The textures derived from remote sensing images are not uniform because of its uncertainty and effect of other random factors. The structural approach is more suitable for analyzing textures where much regularity in the placement of texture elements. However, the features generated from the statistical approach, characterize only the stochastic properties of the spatial distribution of grey levels in an image. They have been proved to be more powerful and useful than the structural features. The most popular textural measurement approaches are based on GLCM (Henderson and Lewis 1998).

The GLCM elements measure the relative frequencies of occurrence of grey level combinations among pairs of pixels within a pre-specified spatial relationship. The GLCM approximates the joint probability distribution of a pair of pixels. Most of the texture measurements are computed from GLCM directly. GLCM is a second order statistical measure of image variation by giving the joint probability of occurrence of

grey levels of two pixels separated spatially in a fixed way. $P = [p_d(i, j)]$, where $p_d(i, j)$ is the probability that the grey level j follows (co-occurs with) the grey level i at a pixel separation, say, d = (dx, dy).

Example: $d = (0,1)$

	→ y			
	0	0	0	1
↓	0	0	1	1
x	0	1	1	2
	1	1	2	2

Image

	→ j		
	0	1	2
0	3	3	0
↓ 1	0	3	2
i 2	0	0	1

No. of Coocurrences

The co-occurrence matrix generates high value for smooth texture, if d is small compared to texture spatial variation. And, if texture is large compared to d, the p_d values are spread more uniformly. The p_d values don't directly provide a single feature for texture discrimination (Soares et al. 1997; Ulaby et al. 1986a).

The equations shown in Table 8 defines different textural features by considering $p_d(i, j)$ is the $(i, j)^{th}$ entry in a normalized GLCM. A detailed discussion about GLCM theory and computation can be found at (Baraldi and Parmiggiani 1995; Haralick 1979; Ulaby et al. 1986a). In the present research, eight texture measures, described in Table 8, extracted from the July 12^{th} and 2^{nd} image have been computed. To reduce the quantity of data to be used in the classification process, correlation coefficients were computed for all the textural measures (Table 9). Based on these correlations, three independent (the least correlated) textural measures; mean, standard deviation and homogeneity were selected for soil moisture classification. The derived images of textural measures; mean, standard deviation and homogeneity are shown in Figure 27.

Table 8: GLCM based features

Sr. No.	GLCM features	Formula	Description
1	Mean	$\mu_i = \sum_{i,j=0}^{N-1} i \cdot P(i,j)$	* Average gray level of matrix.
2	Standard deviation (Variance)	$V_i = \sum_{i,j=0}^{N-1} P(i,j) \cdot (i-\mu_i)^2$	* Measure of heterogeneity.
3	Homogeneity (Inverse Difference Moment)	$H = \sum_{i,j=0}^{N-1} \frac{P(i,j)}{1+(i-j)^2}$	* High when GLCM concentrates along the diagonal
4	Contrast	$C = \sum_{i,j}^{N-1} (i-j)^2 * P(i,j)$	* Measures variability of grey value differences as coarseness of texture * opposite of Homogeneity
5	Dissimilarity	$D = \sum_{i,j=0}^{N-1} P(i,j) * \lvert i-j \rvert$	* Similar to Contrast but high when the local region has a high contrast
6	Entropy	$E = -\sum_{i,j}^{N-1} P(i,j) * \ln(P(i,j))$	* Measure the disorder of an image
7	Energy (Uniformity or Angular Second Moment)	$U = \sum_{i,j}^{N-1} P(i,j)^2$	* Measure the textural uniformity
8	Correlation	$C_r = \sum_{i,j}^{N-1} \frac{(i-\mu_i)(j-\mu_j)}{V_i * V_j} * P(i,j)$	* Measures the linear dependency of grey levels of neighboring pixels

Table 9: Relationship between SAR Textural images using Correlation Coefficients

	Homoge-neity	Contrast	Dis-similarity	Mean	Std-Deviation	Entropy	AS-Moment	Cor-relation
Homogeneity	1	-0.6475	-0.8485	**0.3031**	**-0.0527**	-0.9495	0.8704	0.5441
Contrast	0.6475	1	0.9478	0.3085	0.4128	0.7000	-0.4807	-0.5648
Dissimilarity	0.8485	0.9478	1	0.0890	0.3024	0.8685	-0.6666	-0.6118
Mean	**0.3031**	0.3085	0.0890	1	**0.1944**	-0.2517	0.3244	-0.1517
St Deviation	**0.0527**	0.4128	0.3024	**0.1944**	1	0.2981	-0.0959	0.5091
Entropy	0.9495	0.7000	0.8685	0.2517	0.2981	1	-0.8592	-0.3724
AS Moment	0.8704	0.4807	0.6666	0.3244	0.0959	0.8592	1	0.3375
Correlation	0.5441	0.5648	0.6118	0.1517	0.5091	0.3724	0.3375	1

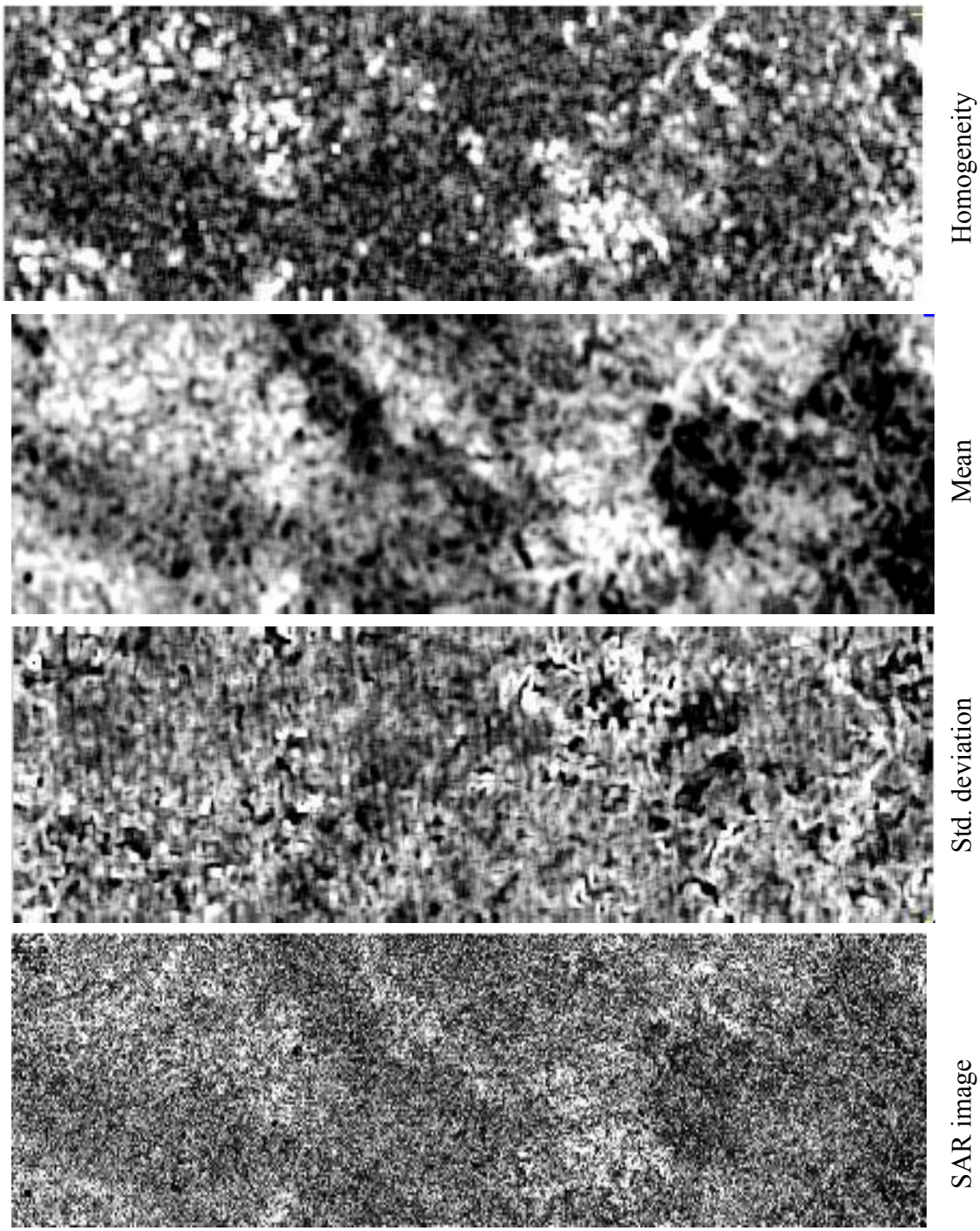

Figure 27: Textural images generated from SAR image.

6 Methodology and Algorithm Development

6.1 Introduction

The general theory of active microwave remote sensing discussed in chapter 2 is the basis of the methodology used for retrieving soil moisture from active microwave data. The most important applications of satellite derived soil moisture are agriculture and hydrological modeling. This chapter will concentrate more on the capabilities and limitations of neural network and fuzzy logic techniques on soil moisture retrievals. In addition to these techniques, a simple multivariable linear model is proposed and some preliminary results of soil moisture mapping are discussed. The results from these models were statistically evaluated and compared.

6.2 Neural Network Algorithm

A multi-layer perception network (MLP) trained by Back-error Propagation (BP) learning algorithm is used in this research. The basic feature of MLP is that the input layer is not directly connected to the output layer. The artificial neurons arranged in adjacent layers are fully interconnected (Figure 15). A short-hand notation M-H-N is used in this chapter to describe the network architecture with M inputs, H nodes in the hidden layer, and N outputs. The perceptron NN is organized into layers where each node transforms the inputs received from the nodes of the previous layer. The input to one node is the weighted sum of the outputs of the previous layer nodes. This sum is then passed through an activation function to produce the input for the next layer. The activation

functions are usually a sigmoid or hyperbolic tangent, which are non-linear with an asymptotic behavior (Rumelhart et al. 1986).

6.2.1 Neural Network Architecture

An ideal neural network should have a combination of greater prediction accuracy, reliability, training and processing time. Those three performance criteria depend on the training parameters and selected size of the network and complexity, which are function of the number of hidden layers and the number of nodes in each layer. The number of input nodes and output nodes are directly linked to the application itself. However the optimization of the number of the hidden nodes and number of hidden layers in a MLP network requires in-depth attention. Unfortunately, there is no single approach available to determine these two variables.

Lippman (1987) has suggested that the number of hidden nodes must be at least equal to the number of input nodes to ensure the convergence of MLP network. In addition, at least one hidden layer is needed for a neural network to be able to solve non-linear problem. If a neural network with two hidden layer is used, the number of nodes must be two to three times of the number of nodes in the input layer. Nevertheless, the presence of tow or more hidden layers in MLP may increase the computational processing time. Trial-and-error is the best method to optimize the number of hidden layers and nodes, and to reach the convergence of MLP. Thus, to obtain the best neural network architecture, many networks with different numbers of nodes in the hidden layers were tested, and then the optimal network configuration was selected for further analysis.

Generally, to achieve accurate classification results, the network should be expanded in terms of the number of nodes (Kanellopoulos and Wilkinson 1997). In general, complex

networks are able to achieve accurate classification of training pixels compared to simple networks. However, the problem with complex networks is that they may have a high risk of overtraining. In the this study, we present different steps of network architecture optimization, its size and complexity, amount of training data, the learning algorithm, and training processes.

To optimize the internal neural network parameters, the same network was trained 25 times with different architectural configurations. The results showed that the standard deviation of the accuracy of 25 runs was very low when two hidden layers and equal number of nodes in each layer. Further, the increase of the number of nodes in each hidden layers did not improve the overall accuracy. The results indicate that the classification accuracy increases when the number of hidden nodes is equal in each of the two hidden layers (Figure 30).

When a single hidden layer is used, the number of nodes should be greater than the number of input data layers to get reliable results (Figure 31). Further, as shown in Figure 32, the standard deviation of 25 successive runs is stable when the number of hidden nodes in single layer is less than 22. This showed that no improvement is found by increasing the number of nodes to more than 6 times of the number of input nodes.

The effect of the number of training pixels has also been evaluated. The larger size of training data provides the network with a greater range of experience requires for more successful generalizations. Often, the increase in number of training pixels increases the training time, so it is necessary to find out the optimum size of the training set. Further, the training data must represent the entire range of values associated with a particular class (Atkinson and Tatnall 1997). After several successive runs of the same network, we

found that by increasing the number of training pixels, it is able to achieve a slightly higher accuracy on testing pixels, as shown in Figure 28. However, once the size of training data reached to maturity, no significant increases in accuracy were observed. The difference between training and testing accuracy was reduced by increase in training pixels is due to fact that larger training data improves the generalization of network with wide range of experience. Furthermore, the larger size of training data has less variation in the accuracy of classification during multiple runs of same network (Figure 29).

Based on this optimization process, we have observed no apparent advantage for multi-hidden-layer networks over single-hidden-layer networks for our data. Thus, we used a single hidden layer network structure to predict the soil moisture in our study. Network architecture 3:10:3 and 3:10:1 were used in the next processing steps. The [3:10:1] architecture was used when network was trained directly by normalized values of soil moisture. However, [3:10:3] architecture was used when network was trained using three soil moisture classes in output layer.

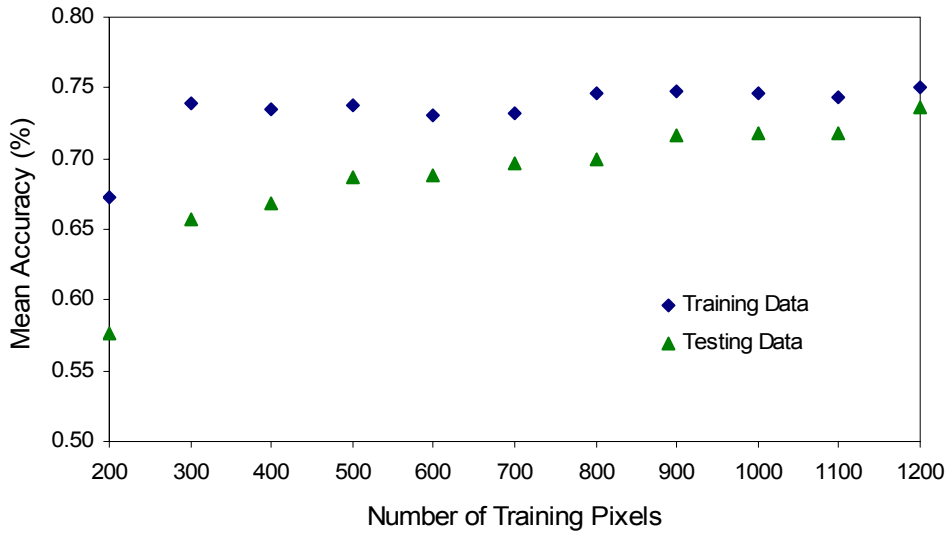

Figure 28: Effect of number of training pixel on classification accuracy

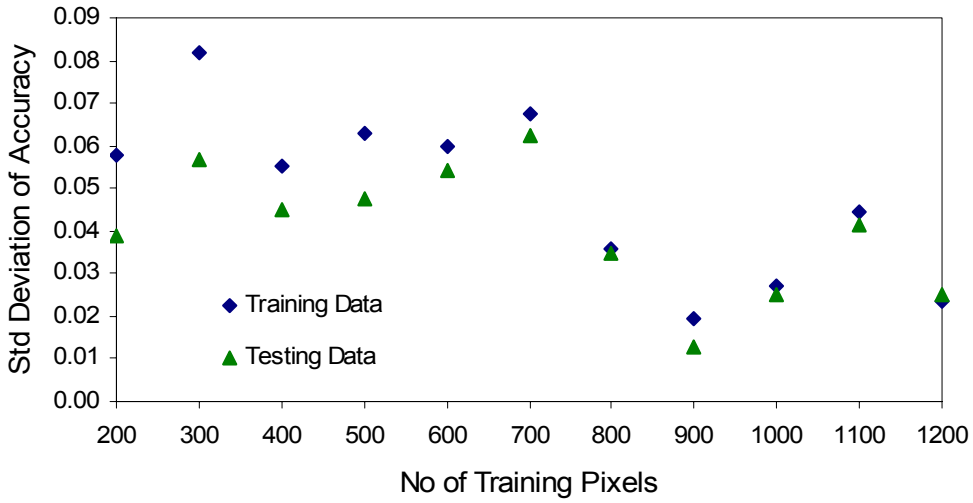

Figure 29: Effect of training pixels on variance of the accuracy for 25 runs of model

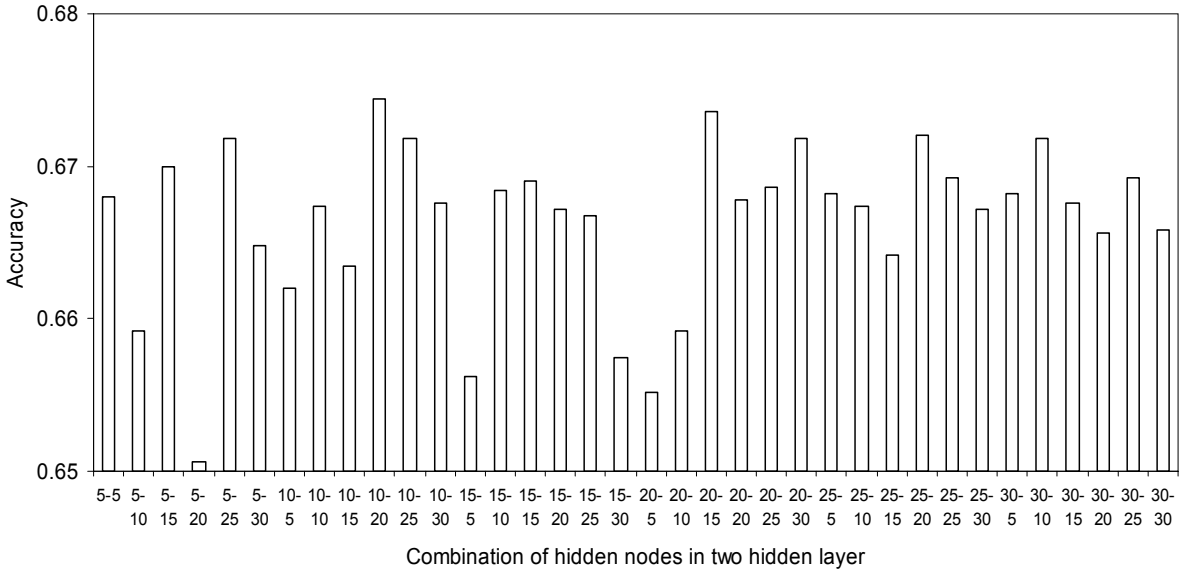

Figure 30: Accuracy of test data with combination of hidden nodes in two hidden layers

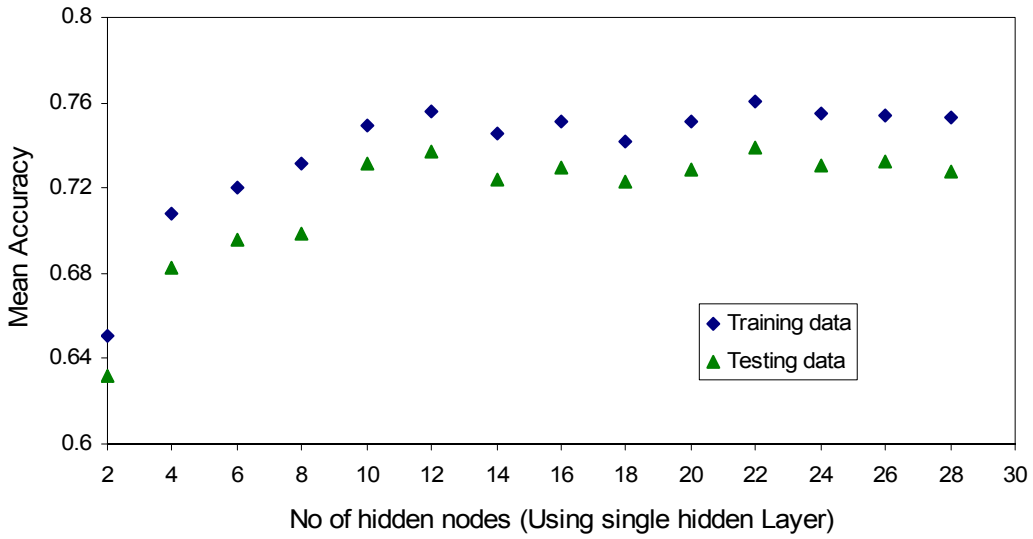

Figure 31: Accuracy of data with combination of hidden nodes in single hidden layer

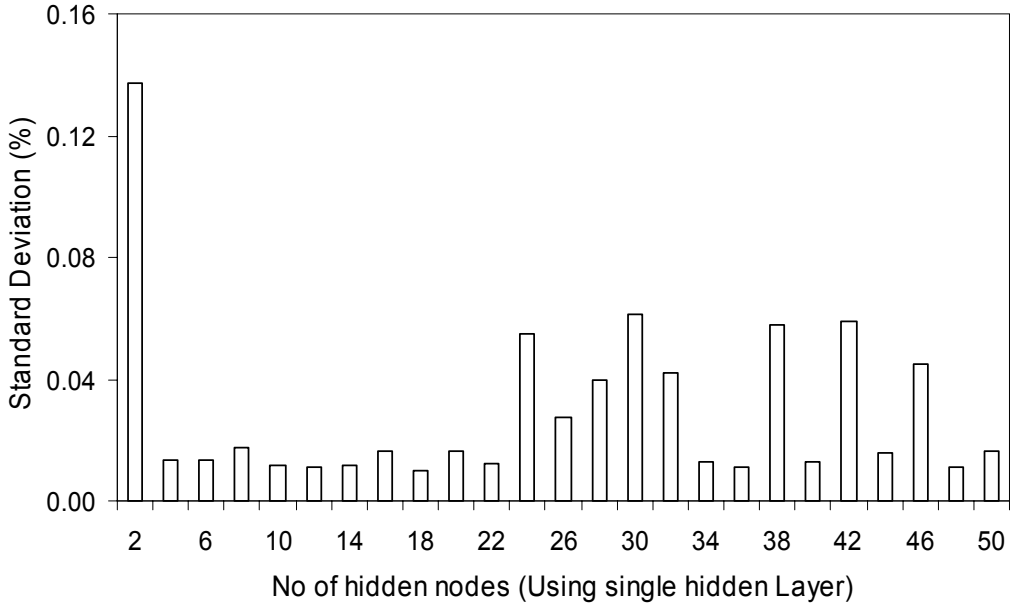

Figure 32: Standard deviation of accuracy of test data with variation in nodes in the hidden layer

6.2.2 Neural Network Training

To start the training process, all weights should be initialized to a random floating numbers between -1 to +1. In addition, it is necessary to initialize the extra input node called bias input in both input and hidden layers to a numerical value of one. This bias input serves as the threshold value for the network activation function; and its value remains at 1 during the entire learning process. At a j^{th} node in the s^{th} layer, a weighted sum is calculated as follows:

$$T_j^s = \sum_l w_{ji}^s * x_j^{s-1} \tag{6.1}$$

where w_{ji}^s = connection weight between the i^{th} neuron in $(s-1)^{th}$ layer and the j^{th} neuron in the s^{th} layer.

x_j^{s-1} = output state of the jth neuron in the (s-1)th layer.

This sum is then passed through an activation function to produce the node's output. The most widely used activation function is the sigmoid function (Lippman 1987) which is given as:

$$h_j^s = \frac{1}{1 + e^{-T_j^s}} \tag{6.2}$$

The NN uses the available data sets (SAR data, SAR textural data, vegetation data, and soil texture) as input vector to produce the output vector (soil moisture class or percentage values). First, the training data is presented to the input layer and propagated through the hidden layer to the output layer. The training stage consists of adjusting the connection weights (randomly initialized) in order to decrease the difference between the network output and the desired outputs (truth data). Second, the network outputs are compared with the desired output vector (training class). The training process will stop if there is no difference between the network output and the desired output. Otherwise, the network error is minimized by changing the weights using the gradient descent algorithm and fed backwards to adjust the network connections. This iterative process shown in (Figure 33) continues until the mean square error reaches a preset threshold or when the validation criteria are reached. The connection weights are then stored and the trained network may now be used as a classifier for soil moisture retrieval.

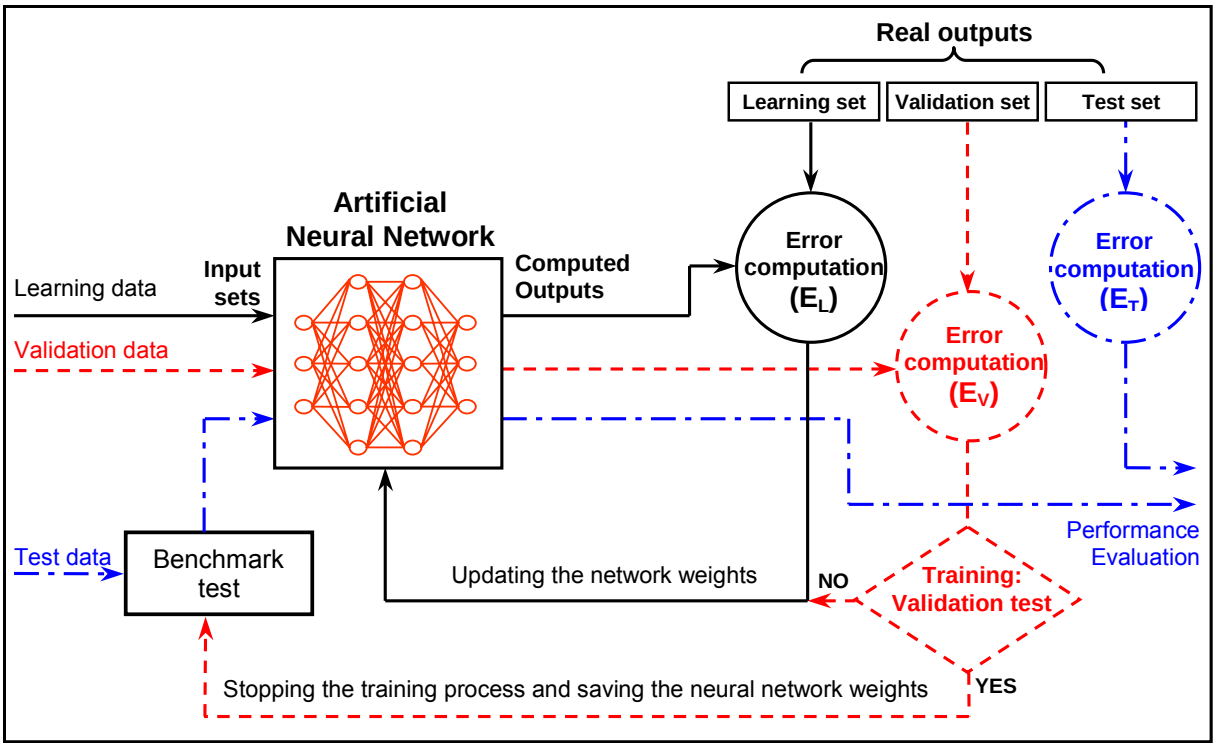

Figure 33: Role of each training data set in the training process (Ghedira and Bernier, 2004)

Over-fitting is one of the major concerns in the process of neural network training. Over-fitting is take place when the error on the training data is driven to a very small value but when new data is presented to the network the error is large. This is due to fact that, the neural network's generalization ability is compromised and the classification space becomes narrowly defined around the training data. Normally, the error computed on the validation set decreases during the initial phase of training. However, when the network begins to overfit the learning data, the validation error will begin to increase slowly for the following iterations. Then, the training process must be stopped, and the neural network weights corresponding to the minimum validation error must be identified and maintained for the next steps (Ghedira and Bernier 2004).

The proper selection of training data and internal parameters is a crucial step in achieving best results. At every training step (also called an epoch) the neural network estimates the direction in which each bias and link weight can be changed to reach convergence. A learning rate is user-defined to estimates the link weights and node biases. The higher learning rate (max. of 1.0) trains the neural network faster. At lower learning rate, network will train slower, but increase the chances to get a better accuracy. Momentum constant is a positive integer used for changing the link weights considering the previous weights to suggest the new weights even in the absence of error. Momentum constant is used to minimize the chances of the network becoming stuck in local minima of the error surface curve. Momentum constant is usually kept higher (0.5 to 0.9) to compensate for lower learning rate and to speed-up the training. The network training terminates at network achieved the performance goal or reached the desired number of epoch. Performance goal is the minimum network error set by the user to stop the network training process. The details of neural network parameters used in this study are given in Table 10.

Table 10: Neural network training parameters

Performance goal	0.001
Maximum number of epochs to train	4000
Maximum validation failures	200
Learning rate	0.01
Ratio to increase learning rate	1.05
Ratio to decrease learning rate	0.80
Maximum performance increase	1.04
Momentum constant	0.90

Training samples should adequately represent all classes. Out of the 120x33=3960 pixels in the image, 1000 pixels were randomly selected for training (500), validation (200) and testing (300). The data selection process is illustrated in Figure 34. At the output layer, one output neuron was assigned for each soil moisture class. Training data was used for computing and updating the network weights and validation data was used for stopping the training by monitoring the validation error during the training process. Testing data was not used during the training process, and was only used to test the neural network performance. The network architecture used in this project was based on the optimized configuration discussed in previous section (§ 6.2.2). The methodology flowchart used in the retrieval of the soil moisture is illustrated in Figure 35.

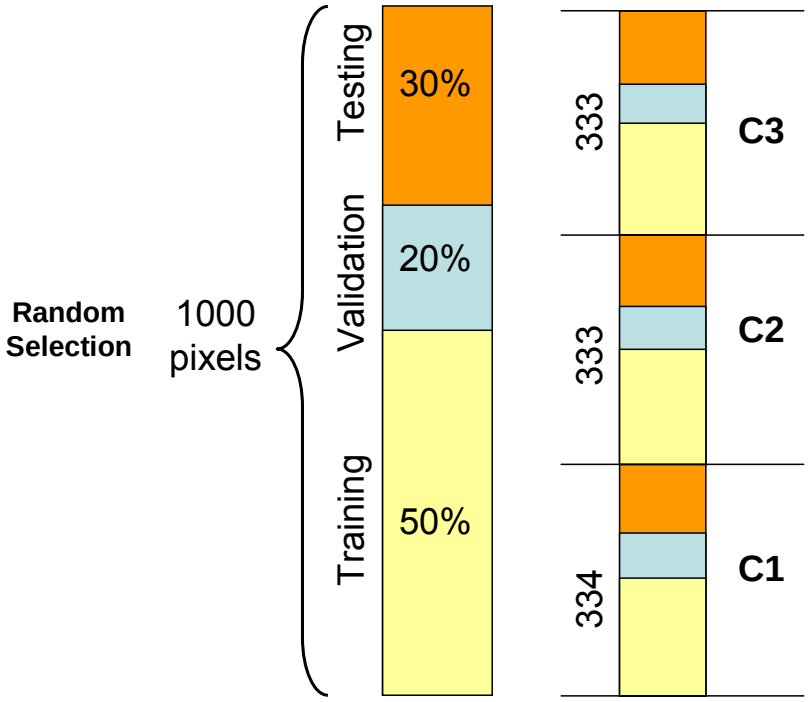

Figure 34: Data selection methodology for model development

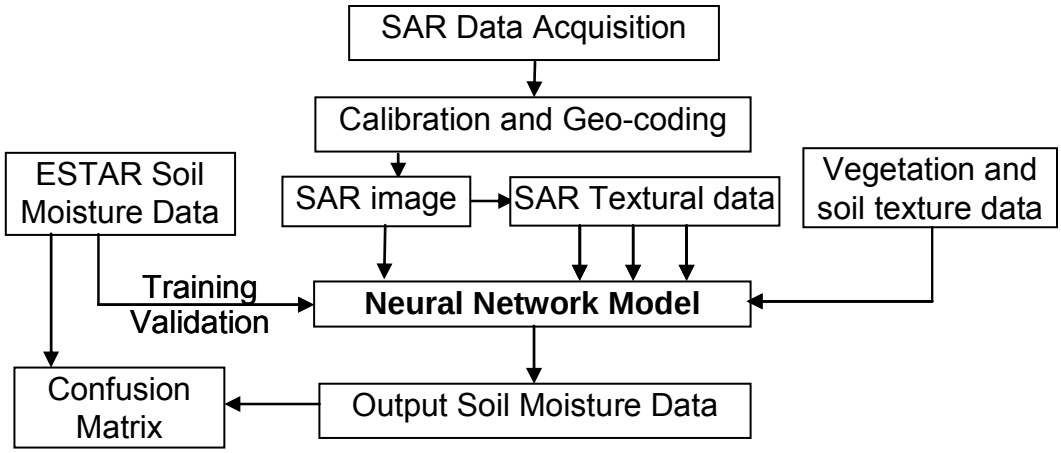

Figure 35: Methodology applied in soil moisture estimation

The trained network was evaluated with the testing data and the output of the network was then assessed for its accuracy. For this, the output of the network was compared with the actual ground truth data and the percentage of the testing vectors that were correctly classified was calculated. For the network that was designed to classify the data into three soil moisture classes, the confusion matrix was used to determine accuracy and kappa coefficient were calculated. For the network designed to predict the soil moisture in percentage values, the root mean square error (RMSE) and correlation coefficient of the truth and predicted soil moisture data was calculated.

6.2.3 Effect of Threshold Limit

The neural network outputs calculated for various threshold limit values have a great impact on the overall classification. One output neuron was assigned for each soil moisture class. For each pixel presented in the input layer, a high value (one) was assigned to neurons that correspond to the pixel's assigned class, and a low value (zero) was assigned to the remaining neurons. In this study, four output nodes are assigned in the output layer, corresponding to three soil moisture classes and a nil class, as

determined earlier. A winner-and-take scheme is used to code the output class. This is to avoid any unclassified class result during the classification process. This scheme basically can be described as below:

The OUTPUT array has an index value from 1 to 4, thus

0UTPUT[i] = 1 for the desired class and

0UTPUT[i] = 0 elsewhere

where i = 1….. 4

Example of this scheme is as below:

Class 1, 0UTPUT[i] = 1000, for i = 1..4

Class 2, 0UTPUT[i] = 0100, for i = 1..4

Class 3, 0UTPUT[i] = 0010, for i = 1..4

Class 4, 0UTPUT[i] = 0000, for i = 1..4

However, during the classification, a continuous range from 0 to 1 will be computed for each output neuron. To prevent the network from forcing the classification of all pixels, we introduced a threshold value between 0 and 1 to decide if a class would be assigned to the input pixel, or if that pixel would be considered unclassified. Thus, a pixel is considered unclassified if all output values are lower than this threshold; otherwise the pixel is assigned the class corresponding to the neuron with the highest value (Ghedira et al. 2004).

The optimal threshold value cannot be identified with certainty without measuring its effects on the overall accuracy of the neural network classification. In this project, we tested the threshold values from 0.4 to 0.7. The effect of the decision threshold on the overall accuracy is illustrated in Figure 36 and Figure 37. The threshold tests show that

the increase of the threshold value affects the overall classification significantly. Furthermore, the increase of the threshold decision value above 0.4 results in a simultaneous decrease of the percentage of correctly and incorrectly classified pixels, and an increase in the percentage of unclassified pixels. Thus, an increase in the threshold limit leads to more nil pixels in soil moisture classification, but increases the likelihood that the classified pixels have been correctly classified.

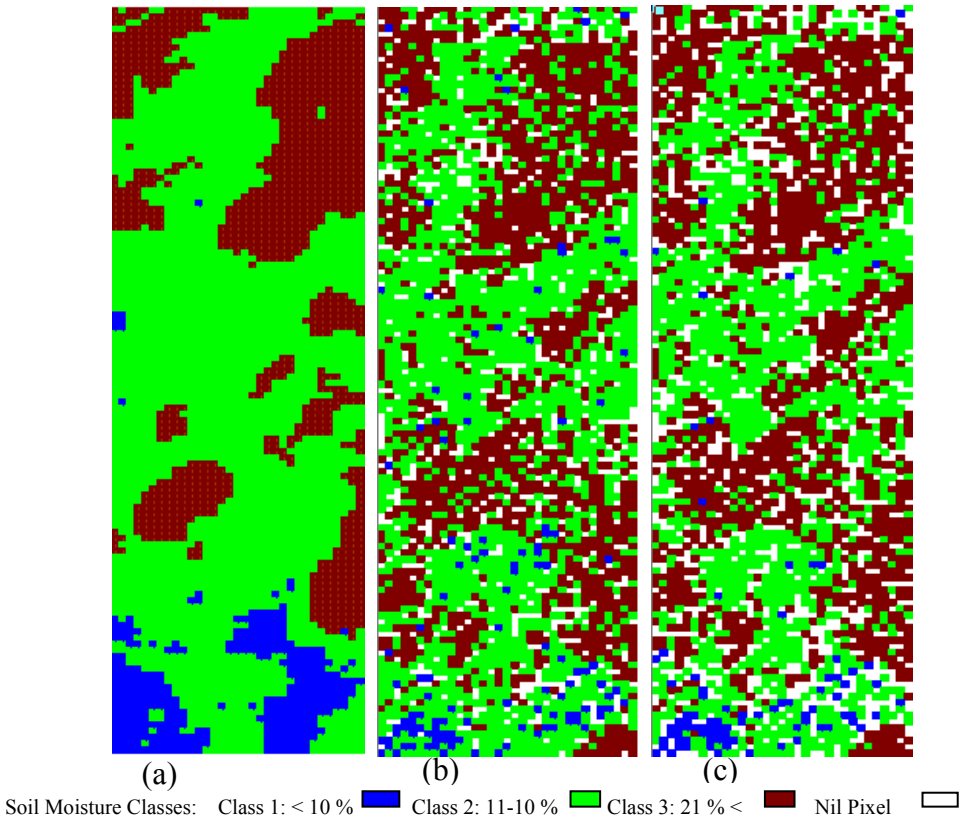

Figure 36: Effect of threshold limit on soil moisture maps (Area A, July 12 data)

(a) ESTAR soil moisture map,
(b) Neural Network output of soil moisture with threshold limit 0.5
(c) Neural Network output of soil moisture with threshold limit 0.6.

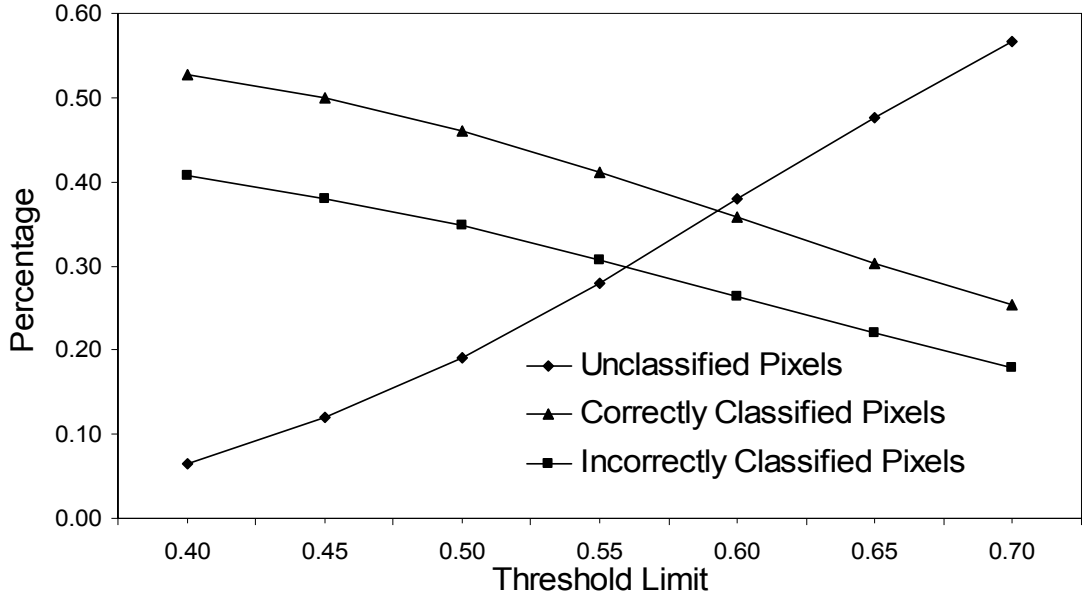

Figure 37: Effect of threshold limits on pixel classification

6.2.4 Neural Network output

The optimum configuration of NN model was run for several times with combination of different input parameters. The RMSE and correlation coefficient of the independent testing data applied to trained neural network has given in Table 11. The RMSE error was 4.847 percent of soil moisture values obtained when SAR backscatter is only input parameter applied to neural network. The retrieval accuracy improves by independent additions of NDVI and soil texture in terms of percent of sand to 3.940 and 4.344 percent of soil moisture respectively. The better retrieval accuracy in terms RMSE and correlation coefficient was obtained with combined NDVI and soil texture values have been applied.

Table 11: RMSE and correlation values for input variable used in neural network model

Data Input	Root means square error (RMSE)	Correlation coefficient, R
SAR	4.847	0.620
SAR+NDVI	3.940	0.716
SAR+PS	4.344	0.660
SAR+NDVI+PS	3.396	0.767

6.3 Fuzzy Logic Algorithm

Subtractive clustering is a fast and robust method for estimating the number and location of cluster centers present in a collection of data points. Clustering is processing which deals with the task of partitioning a set of patterns into a number of homogeneous classes (clusters) with respect to a suitable similarity measure. Patterns belonging to any one of the clusters are similar, and the patterns of different clusters are as dissimilar as possible. In classical cluster analysis, the boundary of different clusters is crisp such that one pattern is assigned to exactly one cluster. In that case, where data distribution is not good, cluster boundary may not be precisely defined. Hence, a data point could belong to two or more clusters with different degrees of membership. Clustering technique is a used for structure identification based on input–output data. In this study, fuzzy subtractive clustering-based system identification and a Sugeno-type fuzzy inference system was the basis of our approach to predict soil moisture from SAR, vegetation and soil type data. The procedures used to define the modeling process are as following:

1. Select factors to be involved in the process and choose the levels of these factors.
2. Conduct the experiments randomly at all possible factor-level combinations.

3. Construct the fuzzy model using a subtractive clustering-based system identification algorithm and a Sugeno-type fuzzy inference system.
4. Search through clustering parameters to obtain a model with minimum error.

The Least Square Estimation algorithm used for the overall optimization of the regression parameters for a given set of clusters. The optimization of the fuzzy model depends mainly on finding the optimum range of the clustering parameters such as squash factor (s_f), cluster radius (r_a), acceptance ratio, and rejection ratio (η). The models which result in an acceptable error are selected for further validation with the testing set.

The *genfis2* algorithm provided by MATLAB® software uses a subtractive clustering method to generate Fuzzy Inference System (FIS). The *genfis2* function uses the *subclust* function to estimate an antecedent membership function and set of rules. Further, the *subclust* function uses the linear least-square method to determine each rule's consequent equation, and returns FIS structure that contains a set of fuzzy rules. The *subclust* function assumes each data point is a potential cluster center and calculates a measure of the likelihood that each data point will define the cluster center, based on the density of surrounding data points (MATLAB Toolbox, 2004).

The subtractive clustering approach is used to identify cluster centers using r_a parameter. This value is the maximum distance between any two points within the same cluster, yet less than the distance between any two points from different clusters where each point belongs. Cluster center selection criteria are based on acceptance and rejection ratios. Acceptance ratios can be determined by fractions of the potential first cluster center over another potential cluster center data that has been accepted. The rejection ratio is the

condition required to reject a data point. A data point will be rejected as a cluster center if it is below the rejection ratio obtained from fractions of the potential first cluster center. The acceptance ratio is selected as 0.5 for the first cluster center and rejection ratio (η) between 0.15-0.5 to derive other cluster centers. Detailed descriptions of steps followed during the subtractive clustering are given below:

1. Compute the initial potential value for each data point (x_i)

$$P_i = \sum_{j=1}^{n} e^{-\alpha \|x_i - x_j\|^2} \tag{6.3}$$

Where, $\alpha = \frac{4}{r_a^2}$

$\| x_i - x_j \|$ is the Euclidean distance and r_a is a positive constant representing a normalized neighborhood data radius. Any point falling outside this circle region will have little influence on the potential point. The point with the highest potential value is selected as the first cluster center. This tentatively defines the first cluster center.

2. A point is qualified as the first cluster center if its potential value ($P^{(1)}$) is equal to the maximum of initial potential value ($P^{(1)^*}$)

$$P^{(1)^*} = \max_i \left(P^{(1)}(x_i) \right) \tag{6.4}$$

3. Define a specific threshold δ to make decision to either continue or stop the cluster center search. This process continues until current maximum potential remains greater than δ.

δ = (rejection ratio) × (potential value of the first cluster center)

where the rejection ratio (η) used in this work is 0.15-0.5, and $P^{(1)^*}$ is the potential value of the first cluster center.

4. Remove the previous cluster center for further consideration.

5. Revise the potential value of the remaining points according to the following equation.

$$P_i = P_i - P_k^* * e^{-\beta \|x_i - x_k^*\|^2} \tag{6.5}$$

where $\beta = \frac{4}{r_b^2}$

x_k^* is the point of the k^{th} cluster center, P_k^* is its potential value, and r_b is a positive constant. Thus, the potential value of each data point is revised by subtracting an amount of potential from each data point as a function of its distance from the first cluster center. Therefore, data point near the first cluster center will have greatly reduced potential, and will unlikely be selected as the future cluster center. The constant r_b typically selected as $r_b = s_f * r_a$ is the radius defining the neighborhood which will have measurable reductions in potential. The squash factor (s_f) is a positive constant greater than 1.

6. For the point having the maximum potential value, calculate the acceptance ratio. If this value is greater than the predefined constant (0.5), the point is accepted as the next cluster center. Otherwise, compute the rejection ratio. If the rejection ratio is greater than the predefined threshold (η = 0.15-0.5), this point is accepted.

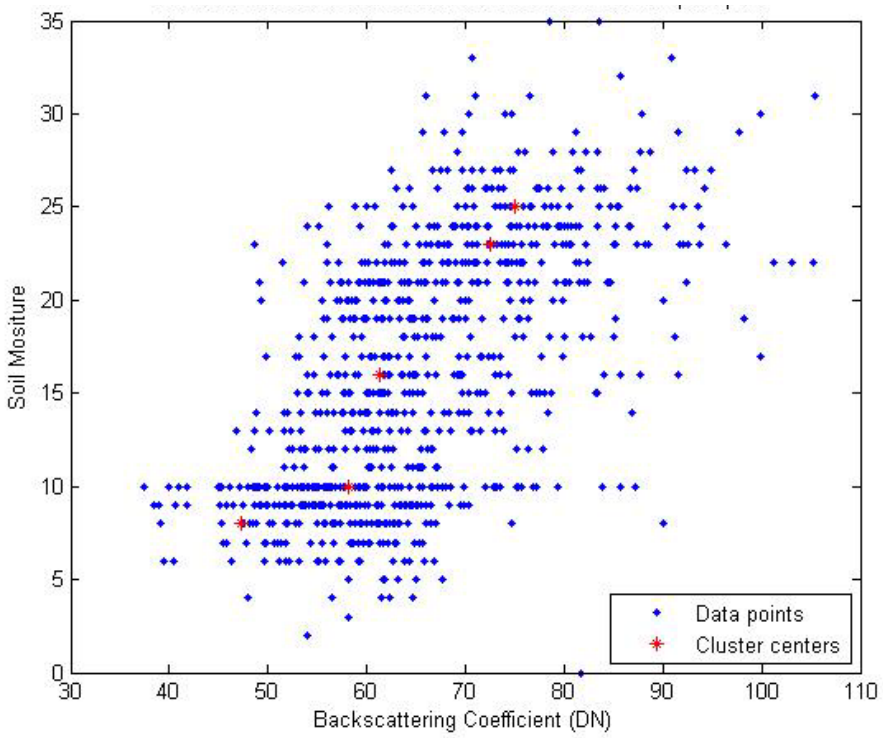

Figure 38: Data and clusters in selected two dimensions of the input space (SM and Backscatter)

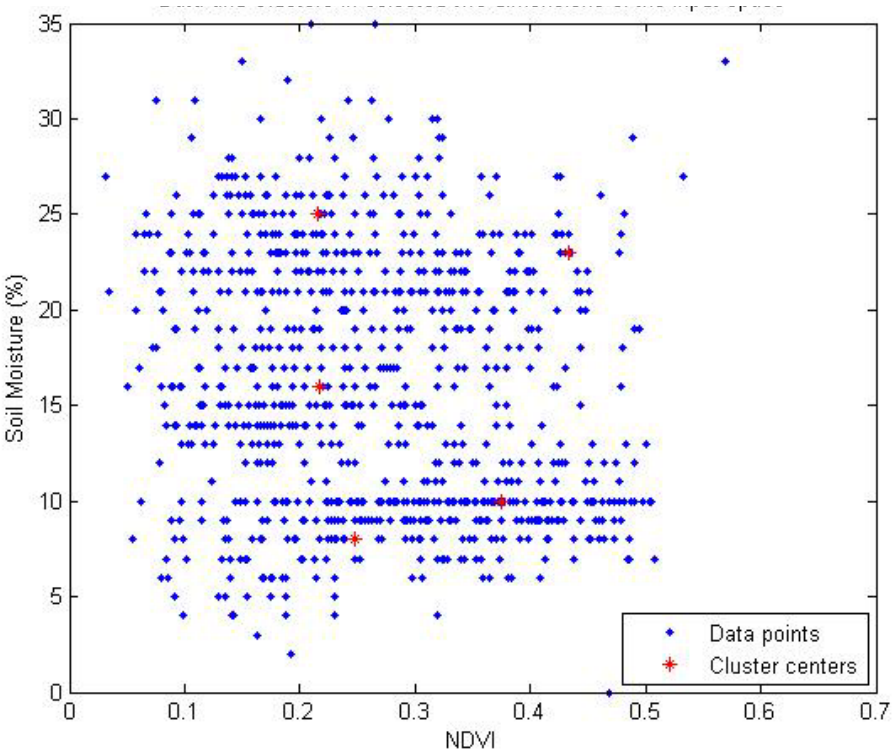

Figure 39: Data and clusters in selected two dimensions of the input space (SM and NDVI)

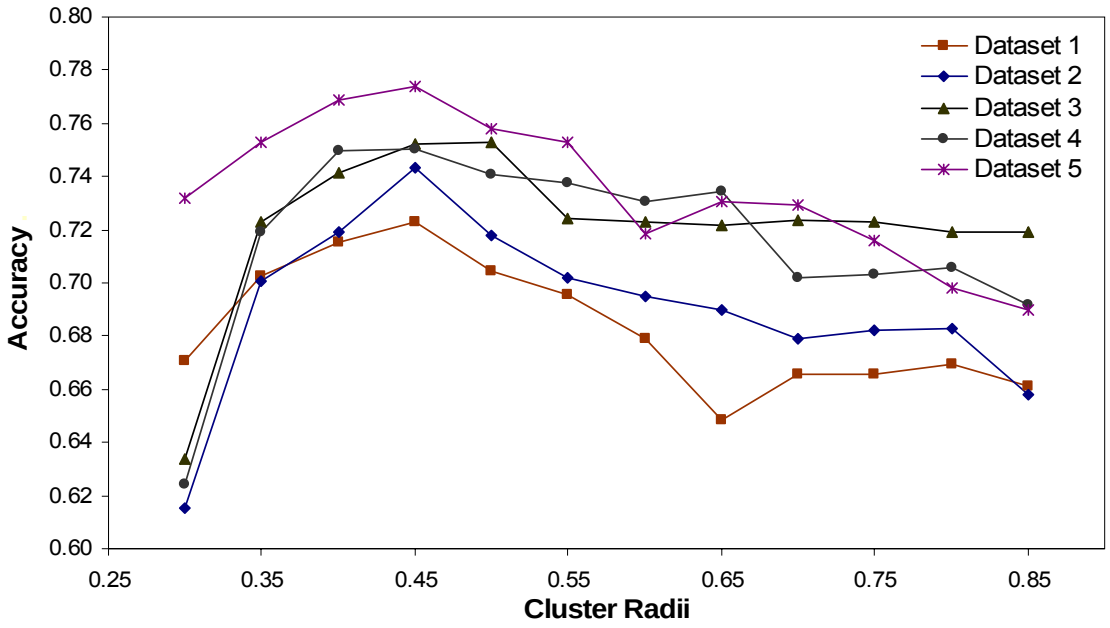

Figure 40: Effect of cluster radii on retrieval accuracy for different datasets

This procedure is repeated to generate the cluster centers until the maximum potential value in the current iteration is equal to or less than the threshold δ. This process iterates until all the data are within a radius of the cluster center. A typical cluster centers for soil moisture with SAR backscatter and NDVI are shown in Figure 38 and Figure 39 respectively. The radius used for marking is a value that ranges between 0 and 1. Small radius values generally result in finding a few large clusters. The cluster centers are varied based on training patterns that depend on different rejection ratios. In this study, the fuzzy model was run several times for various radius values with different datasets to find the optimum cluster radius value. Based on several runs the optimum cluster radius was found about 0.45, shown in Figure 40. This optimum cluster radius values was used for further soil moisture estimation with different set of input parameters. Figure 41 shown the data input and output applied to Sugeno fuzzy model.

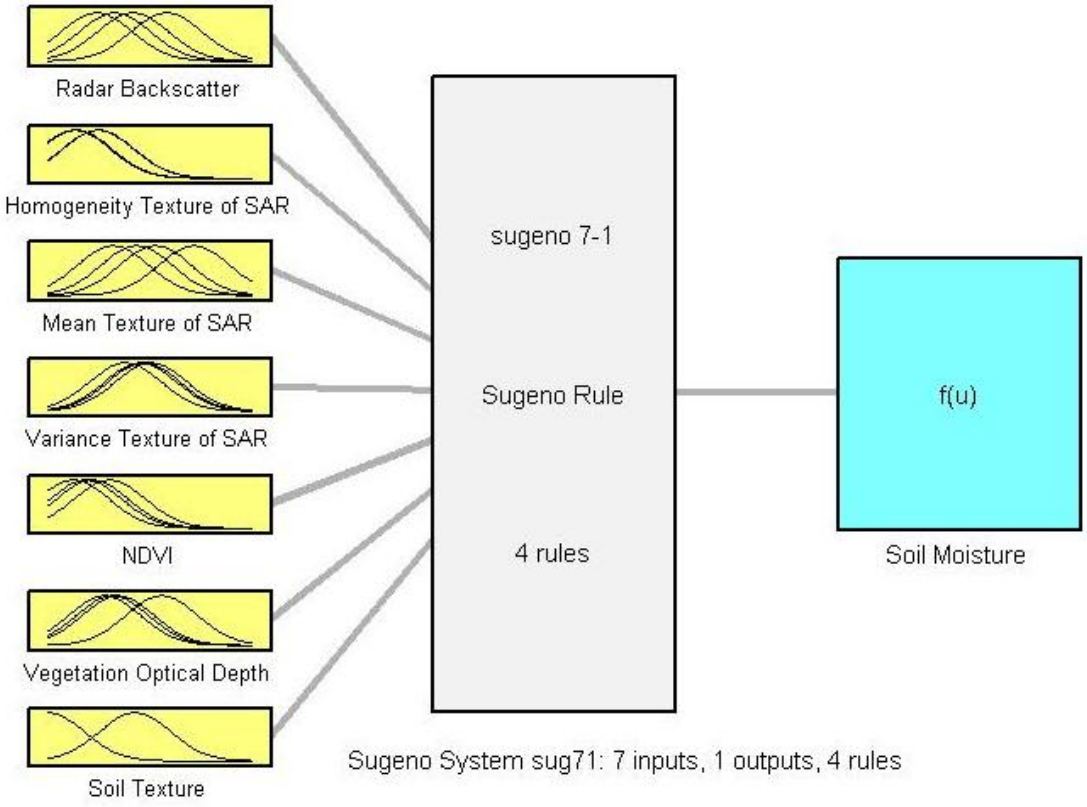

Figure 41: Sugeno Rule used for prediction of soil moisture

Table 12: RMSE and correlation values for input variable used in fuzzy logic model

Data Input	**Root means square error (RMSE)**	**Correlation coefficient, R**
SAR	4.506	0.645
SAR+NDVI	4.075	0.693
SAR+PS	3.955	0.684
SAR+NDVI+PS	3.454	0.759

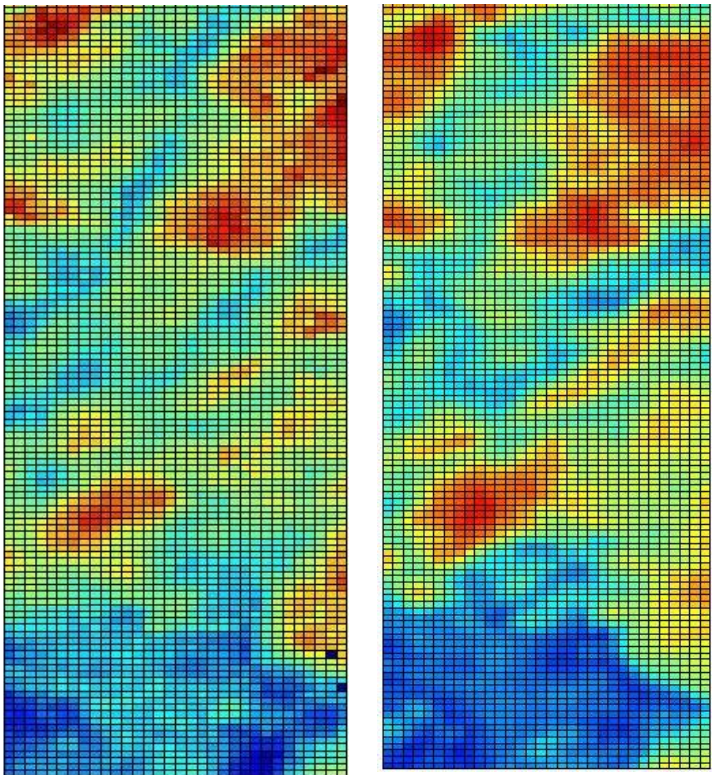

Truth (left) and predicted (right) Soil moisture map for area A

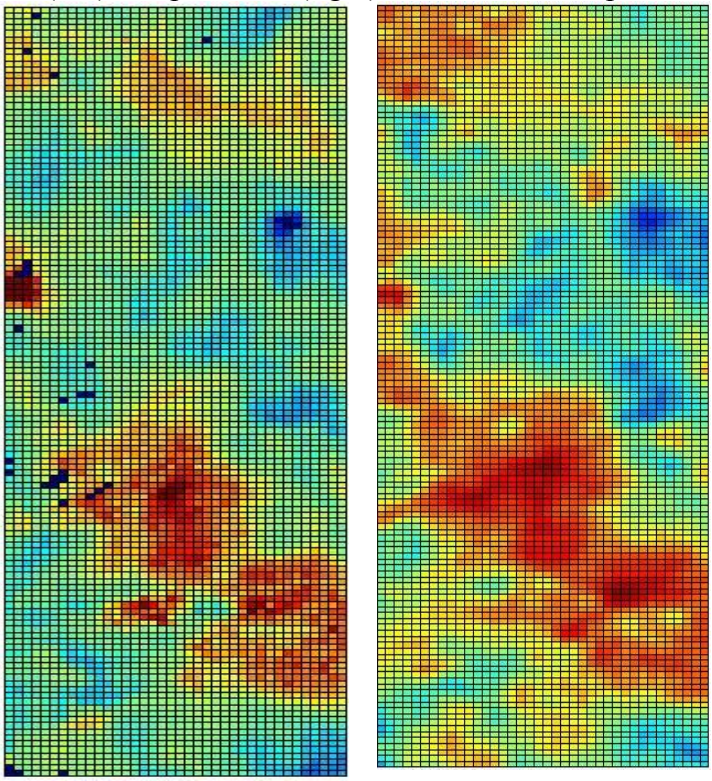

Truth (left) and predicted (right) Soil moisture map for area B

Figure 42: Soil moisture map using fuzzy logic method (July 12, 1997)

6.4 Multiple Regression Analysis

Multiple linear regressions are extensions of simple linear regression treating more than one independent variable to form a relative predictive model of the independent variables by creating beta weights. Multiple regression can establish a set of independent variables having a fraction of the variance in a dependent variable at a significant level (through a significance test of R^2). Curvilinear effects can be explored by adding independent variables as a power term in the model. Interaction effects can be tested by adding the cross-product terms of independent variables. The effect of addition of an independent variable to the model can be tested based on two R^2's values as a test of significance. Hierarchical regression can be used to compare the variance in the dependent due to one or a set of new independent variables over others. The estimates of b coefficients can be used to construct a prediction equation on a variable for further analysis (Gilfilian and Page 1986 ; Khoshgoftaar et al. 1995).

The stepwise regression method is used to generate the multivariable model. The data fitting in stepwise regression is tested by multiple correlations and an overall test of significance. Multiple correlations are actually values of r^2 for the observed values versus predicted values. The test of significance is done by:

- a standardized regression coefficient (*b* if all variables are standardized)
- *t* value, and
- *p* value associated with that *t* value.

The standardized coefficient equates the value of *r* between the variable of interest and the residuals from the regression. The general multivariable model is expressed as:

$$y = \beta_0 + \beta_1 x_1 + \beta_2 x_2 + \beta_3 x_3 + \beta_4 x_4 + \beta_5 x_5 + \beta_6 x_6 + \beta_7 x_7 + \ldots\ldots\ldots + c \qquad (6.6)$$

The ß's are the regression coefficients; these express the amount to which the dependent variable *y* changes with the change in 1 unit of the corresponding independent variable. The β_0 is the constant intercept of the regression line at the y axis, which represents the amount of the dependent *y* when all the independent variables are 0. The standardized versions of the *b* coefficients are expressed as the beta weights. The ratio of the beta coefficients determines the relative predictive power of the associated independent variables. The values of b coefficients and the constant are used to generate a prediction equation. The multiple correlations R^2, associated with regression model, is the percent of variance in the dependent variable explained collectively by all of the independent variables (Khoshgoftaar et al. 1995).

The basic procedures in stepwise regression analysis involve (A) identifying an initial model, (B) iteratively altering the initial model by adding or dropping an independent variable in agreement with the "significant test criteria", and (C) terminating the search when stepping is no longer possible given the significant test criteria, or when a specified maximum number of steps has been reached (Khoshgoftaar et al. 1995). Three techniques are used in stepwise regression analysis:

1. Forward Selection: In this method an independent variable is selected which is responsible for higher variation in the dependent variable. If the second variable selected has a higher residual variation then its regression coefficients are recalculated. This process, continue until no variables "significantly" explain residual variation.

2. Backward Selection: In this method select all variables in the model, and drop the least "significant", one at a time, until only "significant" variables are left.

3. Mixture Selection: The forward selection is used. However, variables which become no longer "significant" are dropped after introduction of new variables.

The significance test is performed using the *p*-values to compare the effect of different variables on regression analysis. It is necessary to run a stepwise procedure a number of times using random selection of data to find meaningful patterns.

In this study, we used stepwise regression analysis choosing soil moisture as dependent variables and vegetation and soil parameters as independent variables (NDVI, vegetation optical depth, soil texture, SAR textural images).

$$M_v = c + \beta_1 * \sigma_0 + \beta_2 * NDVI + \beta_3 * PS \quad (6.7)$$

The model coefficients have been estimated based on several runs (100) of stepwise regression analysis with different datasets:

$$M_v\,(\%) = 0.313\ (\mathrm{DN}) + (4.471 * \mathrm{NDVI}) - 8.50 * \mathrm{PS} \quad (6.8)$$

where M_v is volumetric soil moisture, DN is SAR backscattering, and PS is the percent of sand. Further, an effort has been made to estimate the values of these variables based on different input parameters. The following results are obtained:

Table 13: RMSE and correlation values for input variable used in regression model

Data Input	**Root means square error (RMSE)**	**Correlation coefficient, R**
SAR	7.436	0.591
SAR+NDVI	5.421	0.653
SAR+PS	5.631	0.634
SAR+NDVI+PS	4.482	0.719

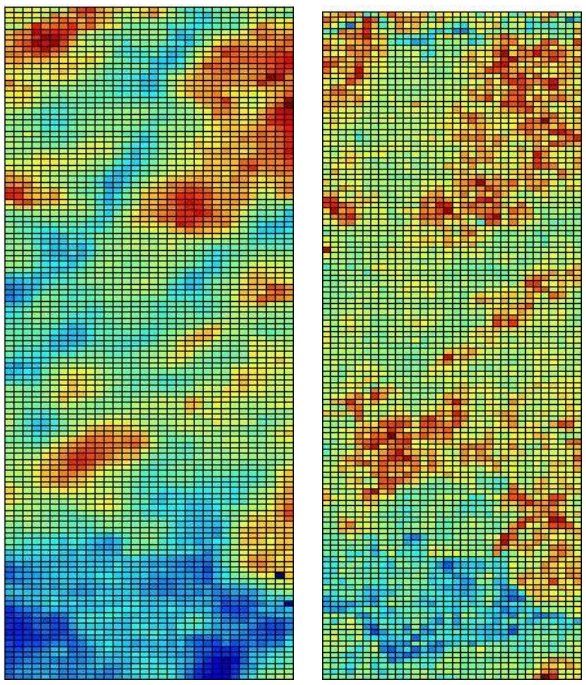

Truth (left) and predicted (right) Soil moisture map for area A

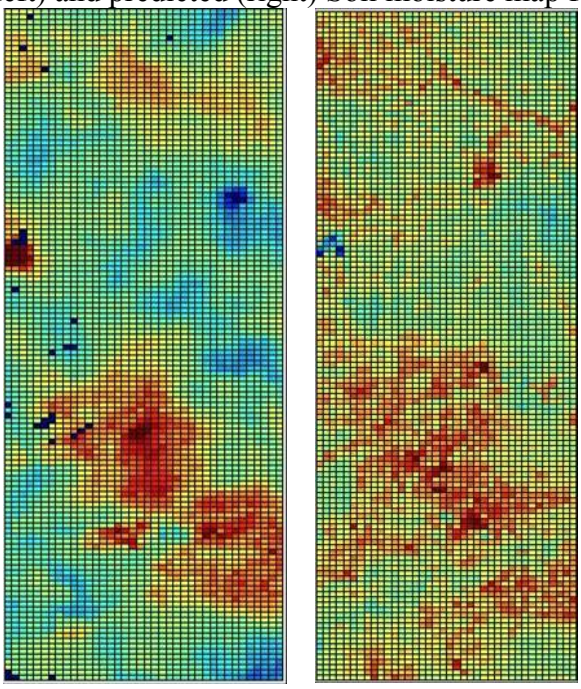

Truth (left) and predicted (right) Soil moisture map for area B

Figure 43: Soil moisture map using the multiple regression method (July 12, 1997)

6.5 Assessment and Validation

The output from neural network, fuzzy logic, multiple regression models are assessed categorically and quantitatively. The categorical assessments have been carried out using confusion matrix and kappa analysis. The quantitative analysis used to understand the value based output from models and significant difference in each model performance. The models developed in this study have validated using statistical features such as coefficient correlation as well as root mean square error (RMSE).

6.5.1 Categorical Assessment

The confusion matrix, also known as an error matrix, is a thematic display tool used to compare accuracies of different classes or groups in the same region (Congalton 1991; Foody 2002; Richards 1996). The confusion matrix not only refines the estimates, but also enhances the value of the classification of the areal extent of classes in the region. The confusion matrix has become a necessary element in accuracy assessments of various land cover classification systems (Foody 2002; Smits et al. 1999). The confusion matrix illustrates descriptive and analytical analysis. The descriptive analysis includes an estimation of the producer's accuracy and user's accuracy, overall accuracy, and individual class accuracy. The producer's accuracy is also called an error of omission, and is based on reference data. However, user's accuracy, known as error of commission, is based on total number of pixel classified in specific class. The analytical analysis of the confusion matrix includes normalization of matrix, calculation of kappa coefficients, etc., and is discussed in subsequent sections. Analytical analysis is useful in comparing the output of different classification methods (Congalton 1991; Janssen and Wel 1994).

The confusion matrix is a symmetrical array of numbers of classified and observed pixels. The diagonal values are the number of correctly classified pixels. The overall accuracy is determined by dividing the sum of diagonal values by the total number of pixels in the confusion matrix. Accuracy assessment was carried out using confusion matrices to evaluate the performance of the final classification. For each input combination, a confusion matrix was generated to compare between the real soil moisture values and those predicted by neural network. The matrix in Table 14 shows the soil moisture classification when only SAR data is used as an input to NN model. Further, the addition of NDVI and vegetation optical depth to the NN model improves the classification accuracy shown in Table 15. Using only SAR data as input to the neural network gave an overall accuracy of 64%. However, the addition of the vegetation optical depth and NDVI, improves the accuracy by 6% (up to 70%). The z statistics for difference in these two confusion matrices is found 1.147, which presumes that there is a significant difference with 87.3% confidence. This illustrates the importance of the vegetation data in the discrimination between soil moisture classes.

The normalized or standardized confusion matrix is a new way to define confusion matrices by eliminating the influence of number of pixel variation in each class (Congalton 1991; Stehman 1997a; Stehman 1997b). The normalized confusion matrix uses all the information in the confusion matrix to estimate cell probabilities. The normalized confusion matrix is calculated by proportional iteration of the confusion matrix to fitting, such that the sum of row and column of matrix should be one. It permits us to directly compare main-diagonal and the off-diagonal values of confusion matrices

obtained by different classification algorithms, irrespective of initial sample size chosen in each class.

In this study the normalized confusion matrix was used to assess the classification accuracy of the different soil moisture classes. The normalized confusion matrix illustrated in Table 16 shows the classification results when only SAR backscattering values are used, and Table 17 shows the confusion matrix obtained when NDVI and vegetation optical depth are used in addition to the SAR backscattering value. The major confusion was found between the immediate soil moisture classes. Further, the pixels from higher soil moisture categories obtained better classification accuracy suggesting better correlation between SAR data and soil moisture.

True class	Classify as				User Accuracy
	C1	C2	C3	Total	
C1	**41**	30	6	77	53.25
C2	19	**86**	17	122	70.49
C3	4	32	**65**	101	64.36
Total	64	148	88	300	
Producer Accuracy	64.46	58.11	73.86		
				Overall accuracy	**64.00**

Table 14: Confusion matrix using SAR for 200 test pixels

True class	Classify as				User Accuracy
	C1	C2	C3	Total	
C1	**49**	24	4	77	63.64
C2	8	**96**	18	122	78.70
C3	2	33	**66**	101	65.35
Total	59	153	88	300	
Producer Accuracy	83.05	62.75	75.00		
				Overall accuracy	**70.33**

Table 15: Confusion matrix using SAR, NDVI and optical depth for 200 test pixels

True class	Classify as			
	C1	C2	C3	Total
C1	**0.68**	0.24	0.08	1.00
C2	0.26	**0.55**	0.19	1.00
C3	0.06	0.21	**0.73**	1.00
Total	1.00	1.00	1.00	

Table 16: Normalized Confusion matrix using SAR for 200 test pixels

True class	Classify as			
	C1	C2	C3	Total
C1	0.81	0.14	0.04	1.00
C2	0.15	0.64	0.21	1.00
C3	0.04	0.21	0.75	1.00
Total	1.00	1.00	1.00	

Table 17: Normalized Confusion matrix using SAR, NDVI and optical depth for 200 test pixels

(Soil moisture Class: C1 = ≤10 %; C2 = 11-20%; C3 = 21+)

To understand the significance difference between these models output Kappa analysis has been performed. Kappa analysis is a discrete multivariate technique commonly used in confusion matrix accuracy assessment (Congalton 1991; Fitzgerald and Lees 1994; Foody 2002; Smits et al. 1999; Stehman 1996; Stehman 1997a; Stehman 1997b). The Kappa coefficient is a measure of the agreement or accuracy. The Kappa coefficient, also known as KHAT statistic, was presented by Congalton in 1991, by following equation:

$$\hat{K} = \frac{N\sum_{i=1}^{r} x_{ii} - \sum_{i=1}^{r}\left(x_{i+} * x_{+i}\right)}{N^2 - \sum\left(x_{i+} * x_{+i}\right)} \qquad (5.1)$$

Where, r is the number of rows in the matrix, x_{ii} is the number of observation in the row i, and column i, x_{i+} and x_{+j} are the marginal total of row i and column j respectively, and N is the total number of observations in the matrix.

The Kappa statistic and its variance were calculated to measure the significance differences between confusion matrices. They are also used to compare different matrices resulting from different classifiers or to find out if the addition of new input has a significant effect on the classification accuracy. A kappa coefficient is equal to 1 when there is complete agreement between the truth data and the classified data. The variance of the confusion matrix can be estimated by a delta model, as fallows (Smits et al. 1999):

$$\widehat{\sigma}^2 = \frac{1}{N}\left[\frac{\theta_1(1-\theta_1)}{(1-\theta_2)^2} + \frac{2(1-\theta_1)(2\theta_1\theta_2-\theta_3)}{(1-\theta_2)^3} + \frac{(1-\theta_1)^2(\theta_4-4\theta_2)^2}{(1-\theta_2)^4}\right] \quad (5.2)$$

where,

$$\theta_1 = \sum_{i=1}\frac{x_{ii}}{N},$$

$$\theta_2 = \sum_{i=1}\frac{x_{i+} * x_{+i}}{N^2},$$

$$\theta_3 = \sum_{i=1}\frac{x_{ii}(x_{i+}+x_{+i})}{N^2}, \text{ and}$$

$$\theta_4 = \sum_{i=1,j=1}\frac{x_{ij}(x_{j+}+x_{+i})^2}{N^3}$$

The significant difference between the two confusion matrices is given by Z statistic test (Smits et al. 1999):

$$Z \approx \frac{\widehat{K}_1 - \widehat{K}_2}{\sqrt{\widehat{\sigma}_1^2 + \widehat{\sigma}_2^2}} \quad (5.3)$$

The Z-test has been used to determine if there is a significant difference between two confusion matrices. In addition to the quantitative evaluation, a qualitative evaluation has

been done by classifying the SAR data in to soil moisture maps and compared it to the existing soil moisture maps visually.

The Kappa statistics and measures of variance derived from the classification error matrices were examined to determine if the results of the classification methods were statistically different from one another at a 95% confidence interval. Table 18 shows Z-test of classification to determine significant differences among classification methods. The results from all the possible pairings of the classification methods examined, showed that there is no significant difference at a 95% confidence level (Z-Score<1.96).

Table 18: Z-test of classification results using a 95% confidence level (Z-Score<1.96)

Model Paring	**Z-score**
Neural Network – Fuzzy logic	0.709
Neural Network – Stepwise Regression	0.126
Multi-linear Regression – Fuzzy logic	0.815

6.5.2 Quantitative Assessment

Neural network, fuzzy logic, and multiple regression techniques were tested in this study. Figure 44 (a) and (b), shows the output calculated by neural network and fuzzy logic for the same training and testing data set. By comparing these two figures we observed that the neural network overestimates the soil moisture for small values (less than 10%) and underestimates when soil moisture is greater than 20%. The fuzzy logic estimation of soil moisture is more balanced, although the overall accuracy is approximately the same.

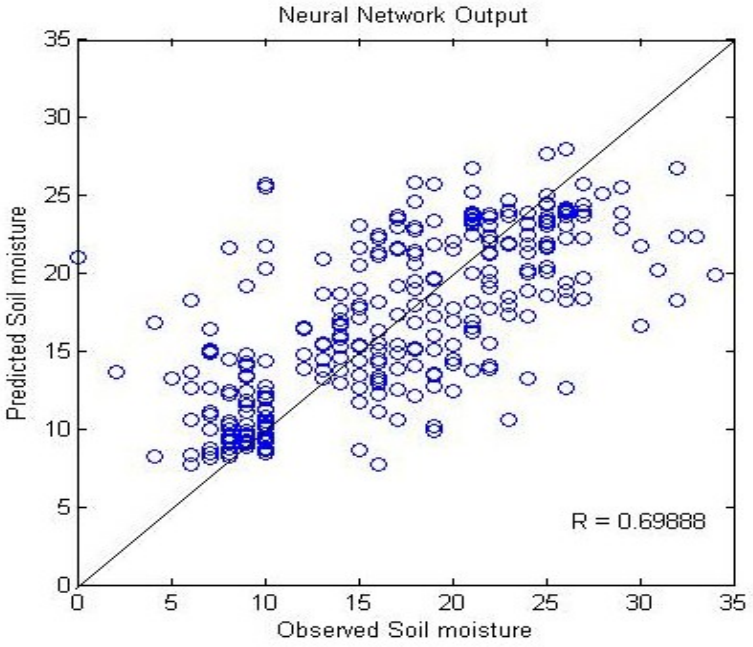

(a)

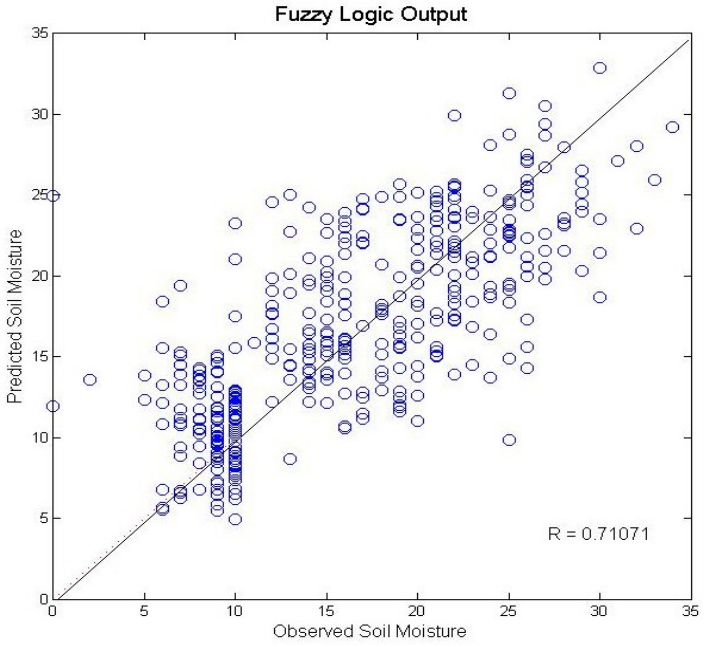

(b)

Figure 44: Comparison between neural network (a) and fuzzy logic (b) output

Through several successive runs of both techniques, we observed that the neural network model shows higher potential to estimate soil moisture (Figure 45). However, we

observed a high variation in soil moisture estimation accuracy. Using the same inputs, fuzzy logic outputs have very low variation in soil moisture estimation accuracy. Although the prediction made by neural network is higher than that of fuzzy logic in several runs of the model, we found that the prediction made by fuzzy logic is more stable in nature.

Significance difference denoted by α is the user-specified probability used to obtain the cut-off value from the F distribution. The commonly used value for the significance level is $\alpha = 0.05$ which means that the hypothesis of an adequate model will only be rejected in 5% of tests for which the model really is adequate. ANOVA model is used to test for significant differences of results obtained from neural network, fuzzy logic and multiple regression analysis. In this study, ANOVA model was tested with significant level ($p < 0.05$), and results obtained was shown in Table 19.

Table 19: ANOVA test for RMSE for 100 models runs of NN and FL output

Anova: Single Factor

SUMMARY

Groups	*Count*	*Sum*	*Average*	*Variance*
Column 1, NN	100	363.3174	3.633174	0.055693
Column 2, FL	100	365.4694	3.654694	0.036668
Column 3, MR	100	450.4006	4.504006	0.331558

ANOVA

Source of Variation	*SS*	*df*	*MS*	*F*	*P-value*	*F crit*
Between Groups	49.33805	2	24.66902	174.5783	7.4E-51	3.026153
Within Groups	41.968	297	0.141306			
Total	91.30605	299				

It should be noted that because both tests are subject to estimation error, the resulting hypothesis test could be generally less powerful than a test of one method against the actual soil moisture data. It seems reasonable to support this hypothesis as we tested enough trials (100) using both the technique. ANOVA testing of these methods, as well as coefficient correlation obtained from predicted and truth soil moisture data, indicated that the fuzzy logic was the most successful ($p < 0.005$) method in retrieving soil moisture.

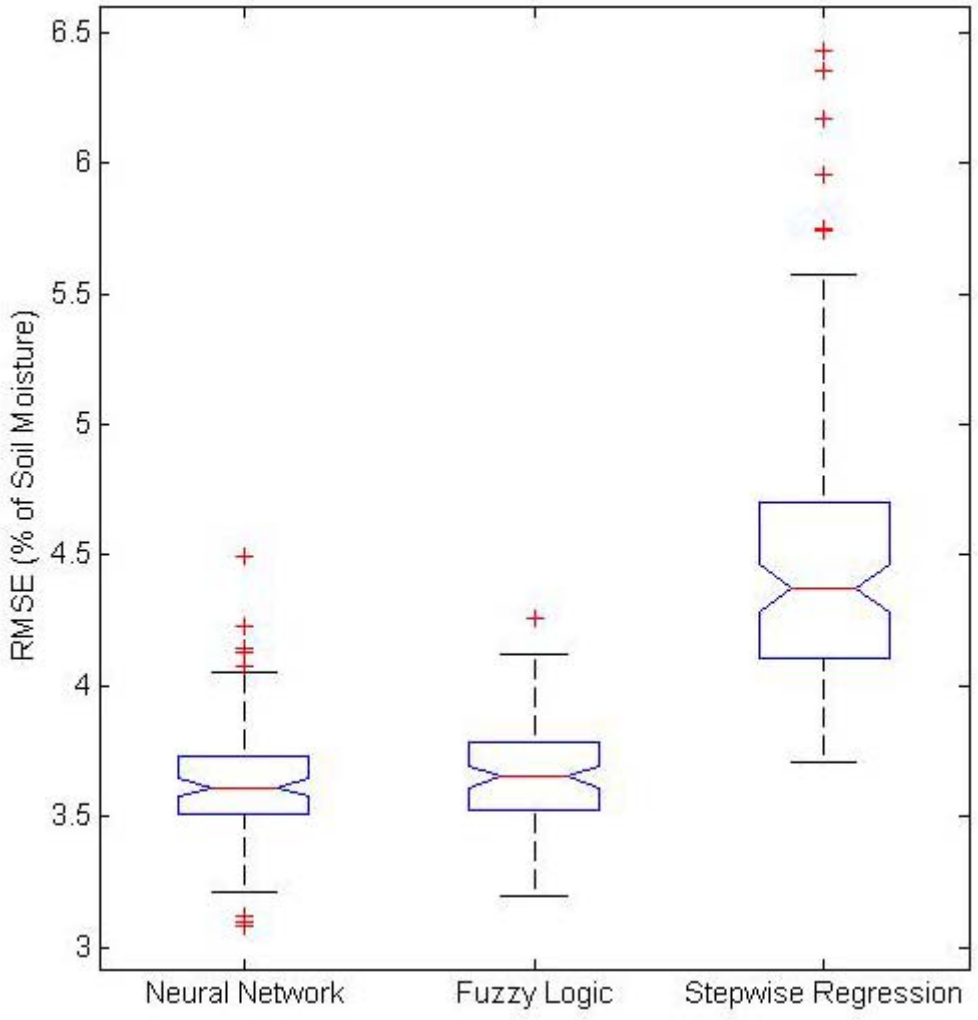

Figure 45: BOX plot shows RMSE for 100 models runs of NN, FL and MR output

6.5.3 Model Validation

Model validation is one of the most important steps in the modeling. Correlation coefficient and root mean square error (RMSE) have been used to neural network, fuzzy logic, and multiple regression models. Since, a R^2 value alone does not assure the fitting observed and predicated data, RMSE has also been used in the model validation. The soil moisture data predicted with three models: neural network, fuzzy logic, and multiple regression models have been validated using two independent data sets: truth soil moisture data from ESTAR and in-situ soil moisture measurements. The three models were trained using 500 independent pixels from study area A of July 12 image and tested for both images (July 02 and July 12). The testing data selected from area A of 12 July, was independent and no pixels were picked from training data.

The RMSE and correlation coefficient values for the predicted versus observed soil moisture data are presented in Table 20 for the three tested models. These results show that, for region A, the neural network model has the lowest RMSE. However, for other study area and day, fuzzy logic performance is better than neural network. The performance by multiple regression analysis is not as good as neural network and fuzzy logic, but showed to be consistent for both images and study areas.

Table 20: Model validation using RMSE and correlation coefficient (in bracket)

Models	Independent Training and testing data	Independent testing data		
	A – 12th July	B – 12th July	A – 02nd July	B – 02nd July
Neural Network	3.672 (0.700)	6.493 (0.458)	7.967 (0.414)	8.294 (0.397)
Fuzzy Logic	3.735 (0.715)	3.853 (0.504)	5.763 (0.493)	6.195 (0.448)
Regression	4.063 (0.674)	4.822 (0.483)	6.696 (0.523)	5.834 (0.405)

Since, there is no significant difference in model predictions, the predicted soil moisture values from fuzzy logic model was selected to reduce the computation for validation. Model predicted soil moisture values were compared with in-situ soil moisture measurements and ESTAR soil moisture data (Figure 46 and Figure 47). The RMSE of predicted and in situ soil moisture, in terms of soil moisture percentage, were 7.94 and 6.54 for 2nd and 12th July data respectively. These data also plotted against NDVI values (Figure 48 and Figure 49) shows higher error observed in field site having higher NDVI values.

The RMSE error observed with field point measured soil moisture was higher than that observed with L-band based soil moisture data. This is due to fact that, in remote sensing images, one pixel represents a mixture of class covers, within-class variability or complex land cover patterns. With this magnitude of heterogeneity typically observed in surface soil moisture fields, and uncertainty associated with gridded point-scale observations to space-borne sensors footprint scales makes difficult to correlate the soil moisture values (Crow et al. 2005; Famiglietti et al. 1999; Jacobs et al. 2004).

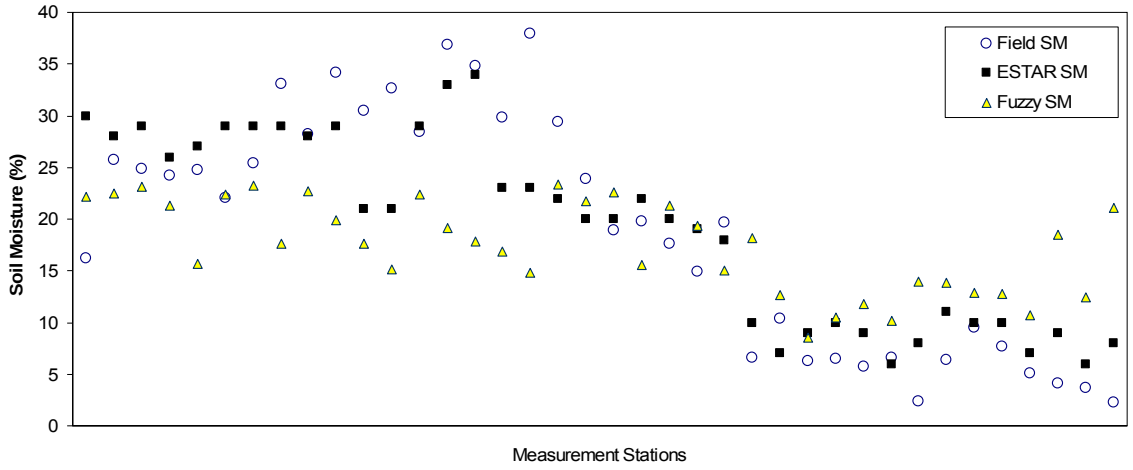

Figure 46: Comparison of soil moisture retrieval from fuzzy model with truth values (July 02 data)

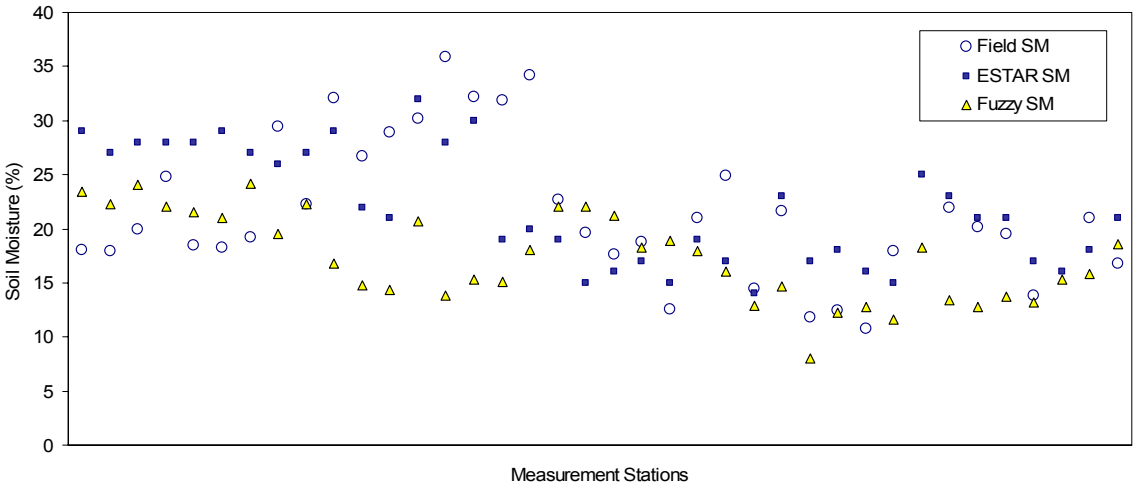

Figure 47 Comparison of soil moisture retrieval from fuzzy model with truth values (July 12 data)

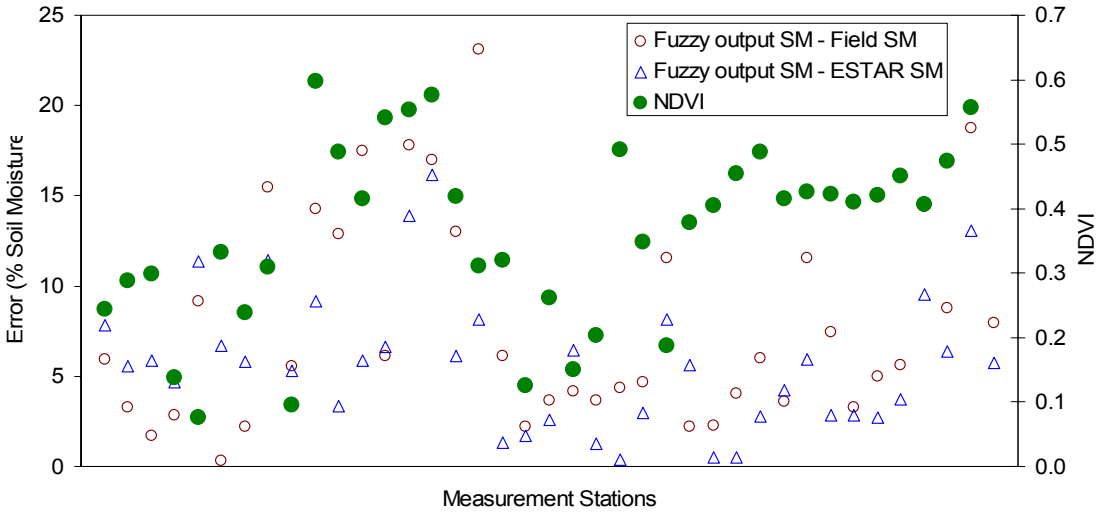

Figure 48 Comparison of soil moisture retrieval error and its relationship with NDVI (July 02 data)

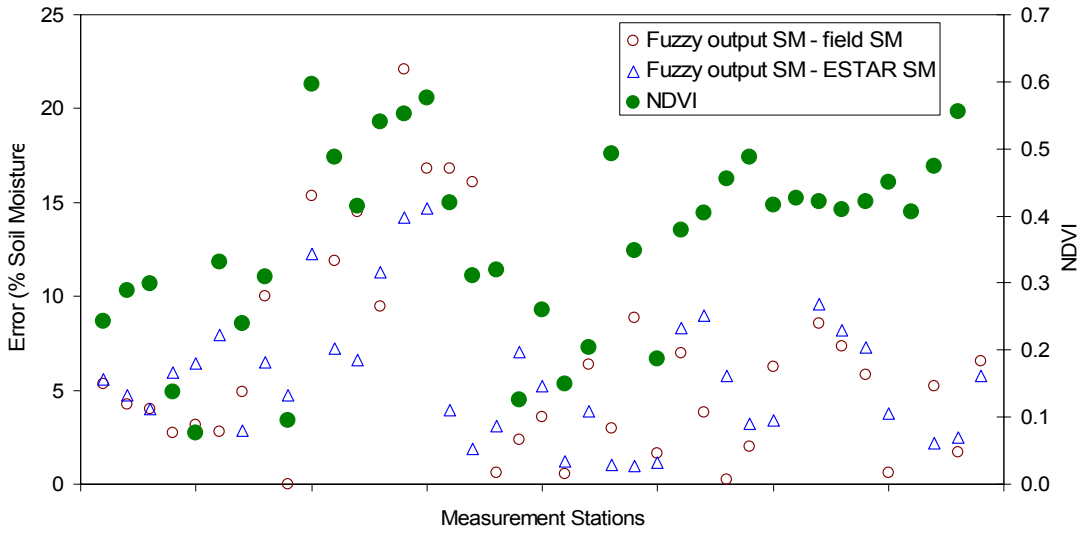

Figure 49 Comparison of soil moisture retrieval error and its relationship with NDVI (July 12 data)

7 Effect of Vegetation on Soil Moisture Retrieval

7.1 Introduction

The backscattering signal from vegetated areas depends mainly on soil moisture content and the vegetation overlying the soil surface. The volume scattering which is related to the structure and the density of vegetation dominates backscattering from vegetated areas. The structure of vegetation refers to geometry, density, canopy height, vegetation water contents, and vegetation volume fraction of canopies. Due to lack of such parameters over large areas NDVI which is directly or indirectly calculated to most of these parameters, can be considered as a good representation of vegetation. In this chapter, the effect of NDVI on soil moisture retrieval will be discussed. Further, the surface heterogeneity is expected to have a major effect on soil moisture retrieval.

7.2 Effect of Normalized Difference Vegetation Index (NDVI)

NDVI is an indication of the green vegetation density because leaf pigments absorb most incident radiation in the red band and reflect or transmit the incident radiation in the near-infrared band. The presence of a vegetation cover reduces microwave sensitivity to variations in the underlying surface soil moisture. The amount of biomass and geometrical structural properties, individually or in combination, has an impact on the overall passive microwave emission measured above the canopy. Thus it is important to have a sufficient understanding in the impact of NDVI on surface soil moisture retrieval from active microwave data.

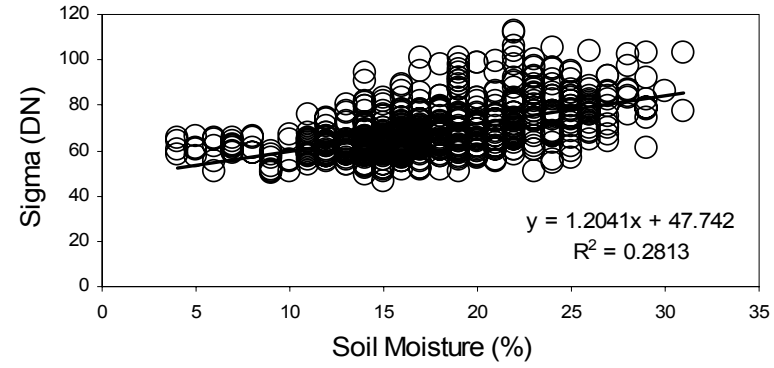

NDVI < 0.15

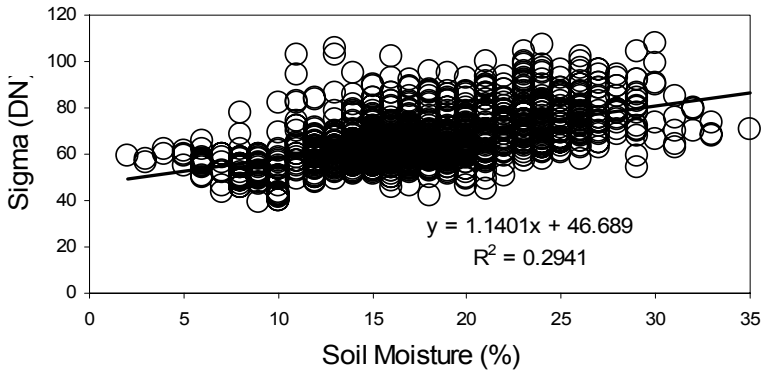

NDVI 0.15 – 0.25

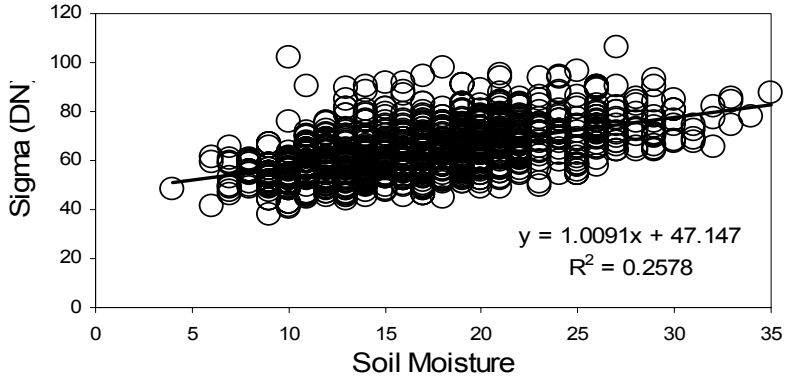

NDVI 0.25 – 0.35

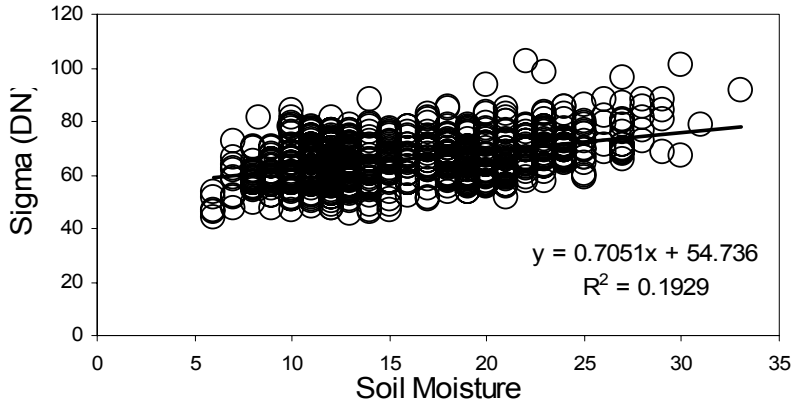

NDVI > 0.25

Figure 50: Effect of NDVI classes on SAR backscattering and soil moisture relationship

The correlation between SAR backscattering and surface soil moisture for the study area is given in Figure 50. The correlation between backscattering and soil moisture is reduced at higher NDVI values (>0.25). As shown in Figure 50, the slope of trend line is decreasing (tend to horizontal) at higher NDVI, showing a reduction in sensitivity of backscatter to soil moisture.

In this study, NDVI was also been used as extra input to the neural network model. The neural network output was assessed to improve our understanding the effect of NDVI on soil moisture retrieval. In the qualitative assessment, predicted soil moisture pixels were compared with truth soil moisture pixels. The classification accuracy has been evaluated for different NDVI classes (Figure 51). The pixels with high NDVI were classified as healthy vegetation; the lower NDVI class was considered non-vegetated areas. This comparison showed that pixels with low NDVI have better correlation than the pixels with high NDVI.

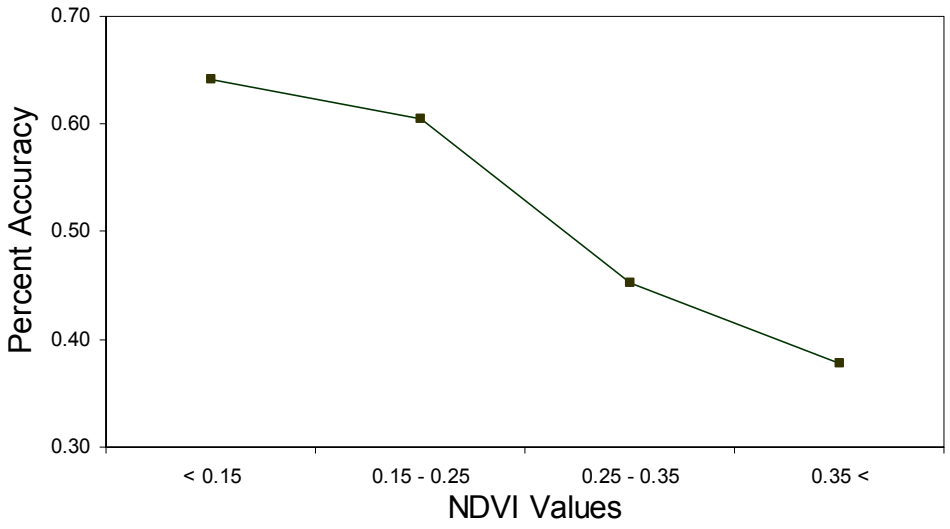

Figure 51: Effect of NDVI class on soil moisture classification accuracy

The effect of NDVI as additional input has been tested with respect to NDVI values. The use of NDVI and soil texture as additional input improves the RMSE of the pixels from highly vegetated areas (Figure 52). The RMSE error was reduced by 1.0 to 1.5 % of soil moisture from pixels having higher NDVI. Further, the addition of input does not result in improvement in pixels having lower NDVI. This might be due to limitation of the microwave sensor to retrieve the accurate soil moisture from lower NDVI area.

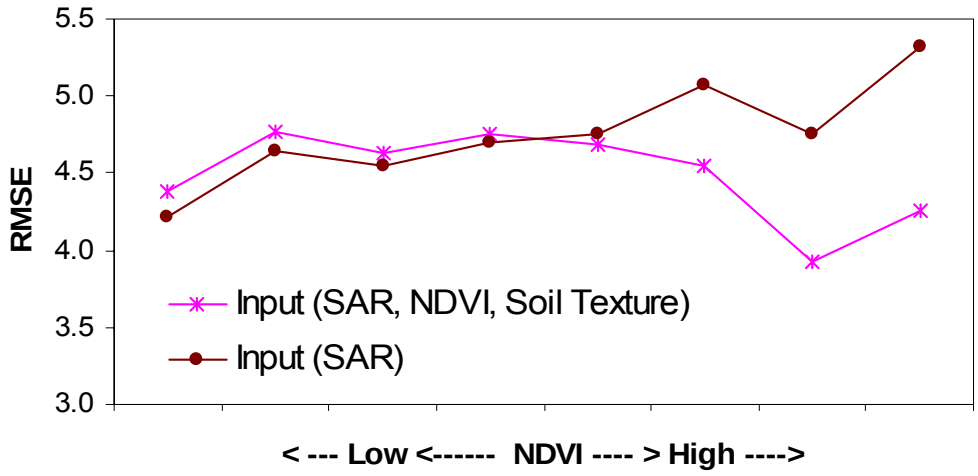

Figure 52: Effect of NDVI and soil texture as an input on accuracy of soil moisture retrieval

The absolute difference between predicted soil moisture from the fuzzy logic model and the field soil moisture was compared with respect to NDVI, as illustrated in Figure 53 and Figure 54 for 2nd and 12th July data respectively. These figures showed a positive correlation between NDVI and soil moisture retrieval error. The vegetation effects moving from the light to heavy regime was associated with an increase in absolute RMS retrieval errors. The higher error was observed in the field site having reproductive and

vegetative area. The details of the vegetation condition at the sites during the SGP mission are given in Appendix B.

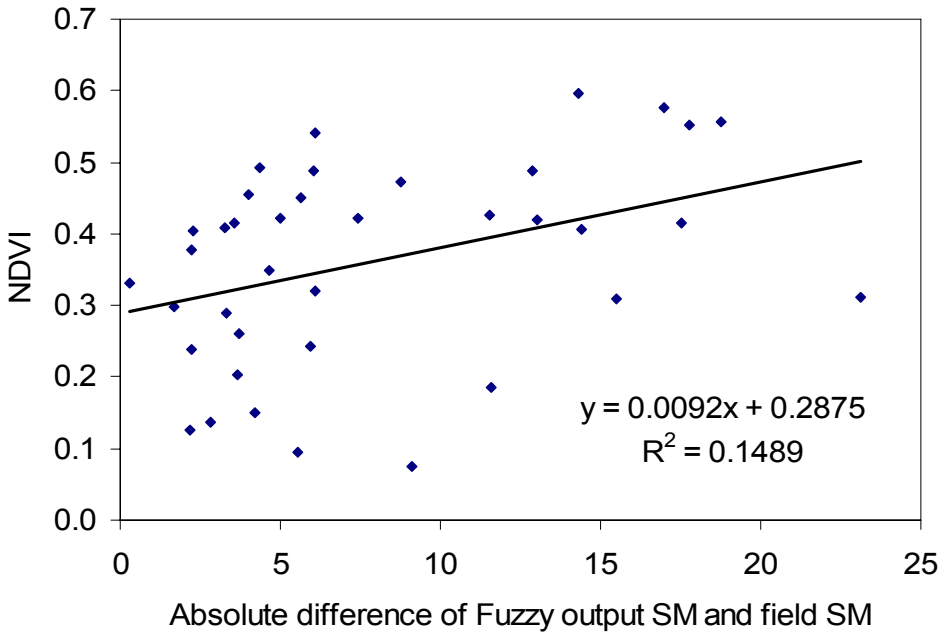

Figure 53 Correlation between NDVI and soil moisture retrieval error (July 02, 1997 data)

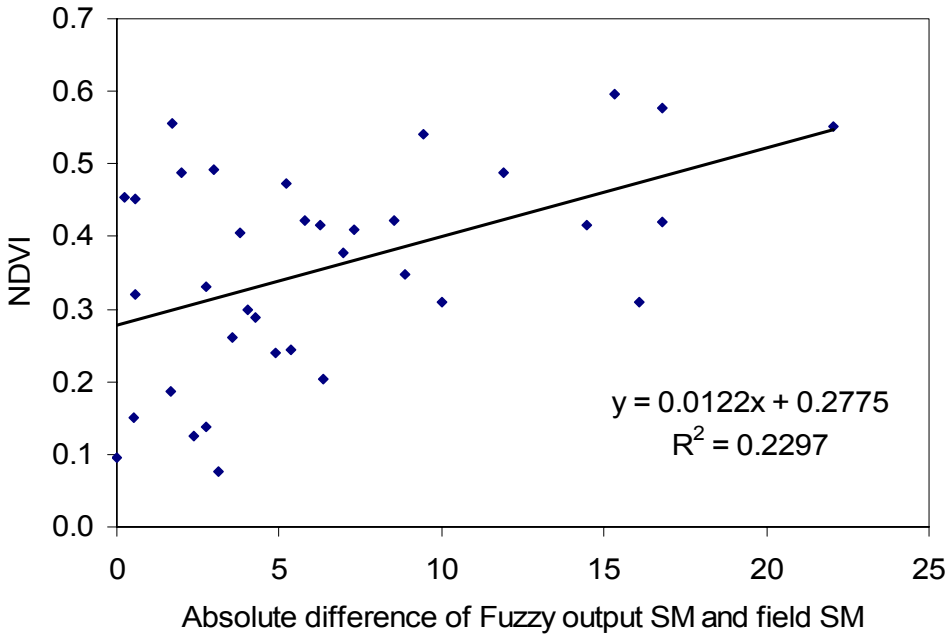

Figure 54 Correlation between NDVI and soil moisture retrieval error (July 12, 1997 data)

At the complete stage the typical grass in Oklahoma region grows upto 50-60 cm height. The vegetation species found in study area are: alfalfa, pasture/rangeland, wheat and summer legume. The plants have average height at maturity level varying from 50 to 100 cm. An increase in plant's height directly affects the NDVI values of vegetation. Figure 55 illustrate the relation between the plant heights at site location and the absolute difference between soil moisture measured on field and predicted soil moisture from the fuzzy logic model.

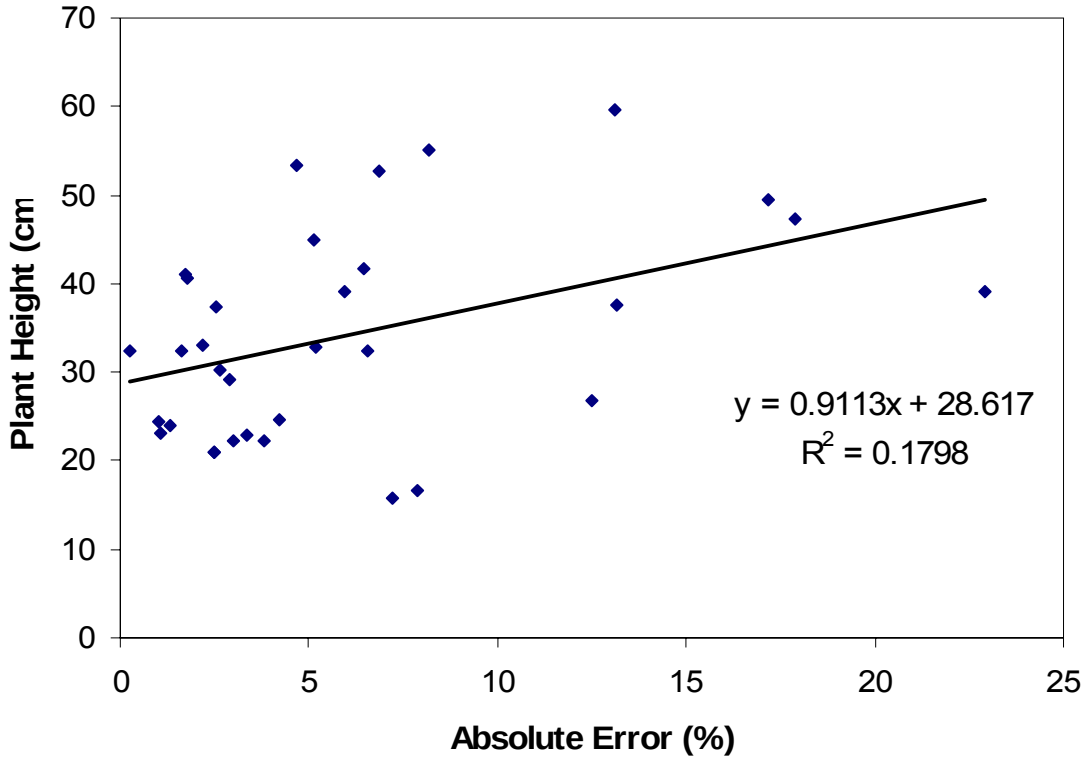

Figure 55: Effect of plant height on absolute error in soil moisture retrieval

7.3 Effect of Vegetation Optical Depth

The optical depth is a vegetation parameter that quantifies the effect of vegetation on microwave emission from a surface or body and depends upon vegetation water content. NDVI and vegetation optical depth respond differently to microwave sensors. NDVI responds to differences in the reflectance of visible (red) and near infrared wave bands, and is influenced by several canopy properties, including leaf water content, but color as well. However, vegetation optical depth responds primarily to the vegetation water content, as a function of the vegetation dielectric properties. Therefore, knowledge of the vegetation optical depth is crucial for the retrieval of accurate soil moisture values.

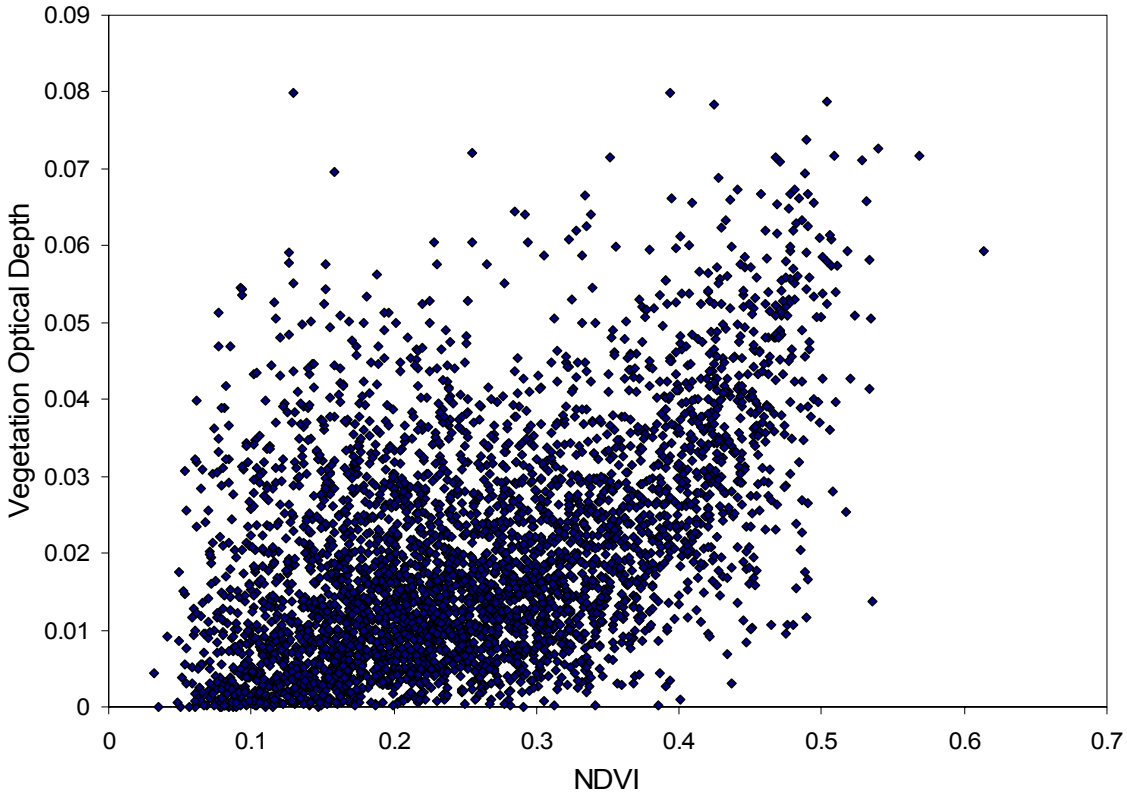

Figure 56: Relationship between NDVI and vegetation optical depth for the study area

Vegetation cover introduces errors into the estimated soil moisture obtained by remote sensing because of the attenuation effect of the vegetation. At the higher optical depth more error is introduced, hence the less accuracy observed in the soil moisture prediction. In this research, we tested the vegetation optical depth information as additional input to the neural network model. The results illustrated in Figure 57 show that the classification of pixels with high vegetation optical depth values was less accurate (by 25%) than pixels with low vegetation optical depth values. This indicates that confusion in pixel classification increases when the vegetation optical depth increases. Further, an addition of optical depth as input parameter applied to the neural network improved the correlation coefficient by 3-5%. However, if both NDVI and optical depth are used as input parameter, we did not observe a significant improvement to the one with NDVI only. Therefore NDVI was selected as vegetation input in the next steps. Since, the NDVI is easier to obtain.

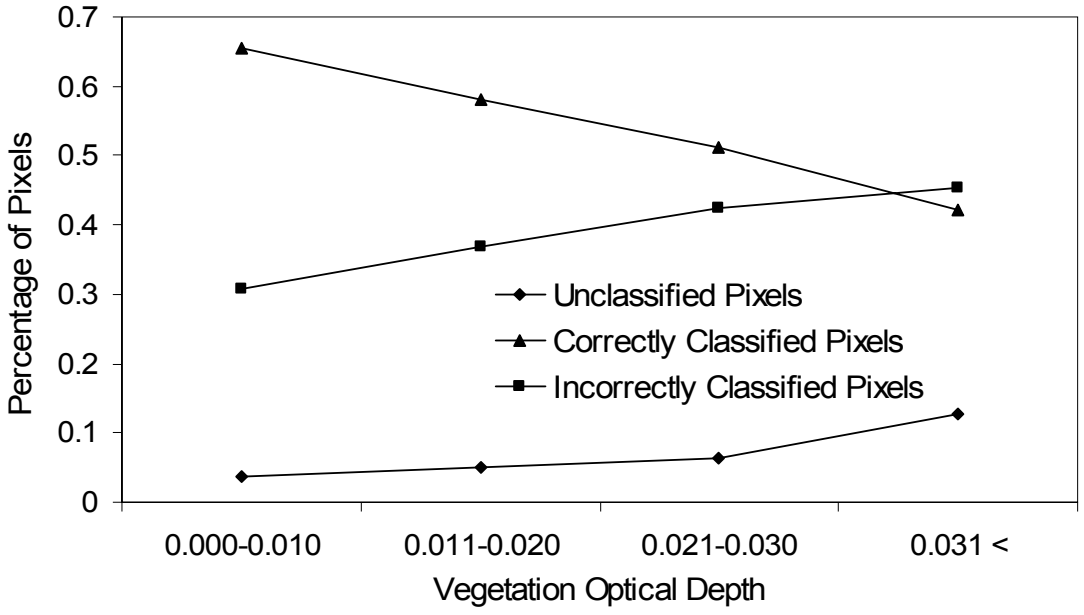

Figure 57: Effect of vegetation optical depth class on classification accuracy

7.4 Effect of Sub-pixel Variability of Land Cover

The presence of a mixture of land cover, and soil texture within-class variability makes the retrieval of soil moisture difficult. Mapping large scale soil moisture using remote sensing averages the within-pixel variability by masking the underlying heterogeneity observed at the land surface. The magnitude of heterogeneity observed in surface soil moisture retrieval has emerged as a major challenge in validating remote sensing mapping. Hence, it is necessary to understand the impact of this sub-pixel variability on retrieval accuracy. This section highlights the impact of spatial heterogeneity in land surface conditions on soil moisture retrieval from microwave data.

The effect of heterogeneity of land cover vegetation on the overall accuracy of soil moisture retrieval was tested. The retrieved soil moisture can be affected by the surface area parameters, such as, topography, soil texture, and vegetation cover. Therefore, the calculated soil moisture will be affected by the heterogeneity of those parameters within a single pixel. As stated before in this study, vegetation cover and SAR images were originally in 25m x 25m resolution. Because soil moisture image resolution is coarse (800m x 800m), those values were aggregated to the same resolution of soil moisture image. This aggregation process decreases the sensitivity of the SAR to soil moisture, which are related to land and backscattering characteristics.

In our study area, the land was covered by rangeland, pasture, winter wheat, corn, and alfalfa. Both soil moisture and aggregated SAR data have a resolution of 800m x 800m containing total of 1024 (32x32) 25 m resolution pixels. A pixel is considered homogeneous if most of its 1024 sub-pixels are of single vegetation class; otherwise the pixel is considered heterogeneous. Pixel heterogeneity has been classified in three

categories, H1, H2 and H3, which are a function of sub-pixel variability within 800 m resolution pixel (Figure 58).

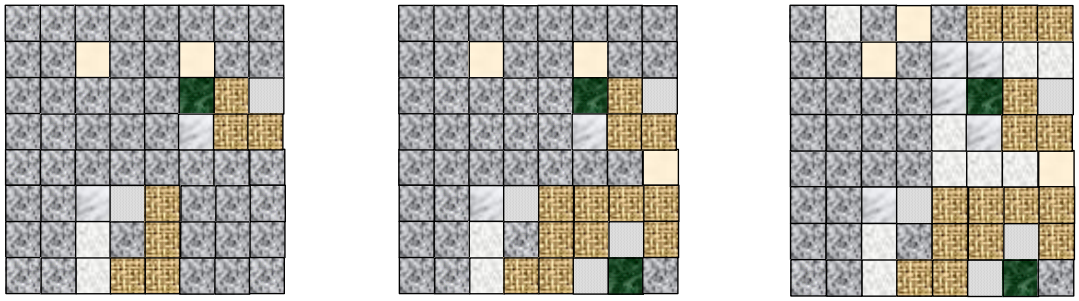

H1: $P_i \geq 75\%$ (a)

H2: $75\% > P_i \geq 50\%$ (b)

H3: $50\% > P_i \geq 25\%$ (c)

Figure 58: Example of heterogeneity classes

The H1 category is assigned to pixels having more 75% of sub-pixels of a single vegetation specie (see Figure 58-a). Similarly, H2 class contains the sub-pixels ranging from 50% to 75%, and H3 class contains sub-pixels ranging from 25% to 50%, shown in Figure 58-b and Figure 58-c. If any vegetation class represents less than 25% of sub-pixels, that pixel is considered heterogeneous. The results showed that homogeneous pixel (H1 category) have better accuracy in soil moisture classification. The effect of heterogeneity of pixels for all categories in soil moisture estimation is illustrated in Table 22. Based on the results, we noted that the retrieval of soil moisture from a heterogeneous land surface is difficult. It requires an understanding of the distribution of small pixels with different species of vegetation.

Table 21: Average values of NDVI for different land cover in study area

Land-cover type	NDVI (average)
Alfalfa	0.1284
Forage	0.4090
Pasture/Rangeland	0.2918
Wheat	0.1384
summer Legume	0.1831

Table 22: Effect of heterogeneity of pixel on accuracy of classification

Type of Land	"Mode" class			0.75			0.5			0.25		
	Total Pixel	CC*	%	Total Pixel	CC	%	Total Pixel	CC	%	Total Pixel	CC	%
Forage	159	71	45%	3	2	67%	42	17	40%	150	66	44%
Pasture/Rangeland	1939	963	50%	77	49	64%	744	396	53%	1924	958	50%
Wheat	1396	784	56%	140	81	58%	718	424	59%	1386	778	56%
summer Legume	199	128	64%	10	7	70%	83	57	69%	198	127	64%
Total pixel	3960	2089	53%	232	141	61%	1623	911	56%	3909	2066	53%

*CC = correctly classified pixels

7.5 Sub-pixels Variability of SAR backscatter and NDVI

The presence of spatial heterogeneity in land surface (soil wetness, soil texture, vegetation cover) over the coarse spatial resolutions, introduces a range of complexities in the retrieval and validation of active microwave-based estimates of soil moisture. Numerical models generally assumes that sub-grid variability is averaged with equal areal weighting, while the satellite product is obtained through averaging by some combination of nonlinear antenna gain functions (Crow et al. 2001). The physical connection between soil moisture estimates at the pixel scale and local values within the pixel weakens strongly as the sensor resolution decreases (Bindlish and Barros 2002).

The reduction in sensitivity of SAR backscatter to soil moisture is influenced by the presence of highly vegetated areas as well as the type of land cover. Sub-pixel variability in SAR backscatter and NDVI (available in 25m x 25m resolution) within 800 m resolution of soil moisture pixel was evaluated. The variability of sub-pixels in SAR images increases with the increasing of NDVI average values (between 0.1 and 0.3), and saturates as NDVI average continue to increase (Figure 59). A positive correlation has also been observed in sub-pixel variability in SAR backscattering and NDVI (Figure 60) for both areas A and B (Table 24).

Table 23: Correlation coefficient for SAR variability and NDVI values

Date / Site	Area A	Area B
July 2nd 1997 data	0.2590	0.1902
July 12th 1997 data	0.0595	0.1092

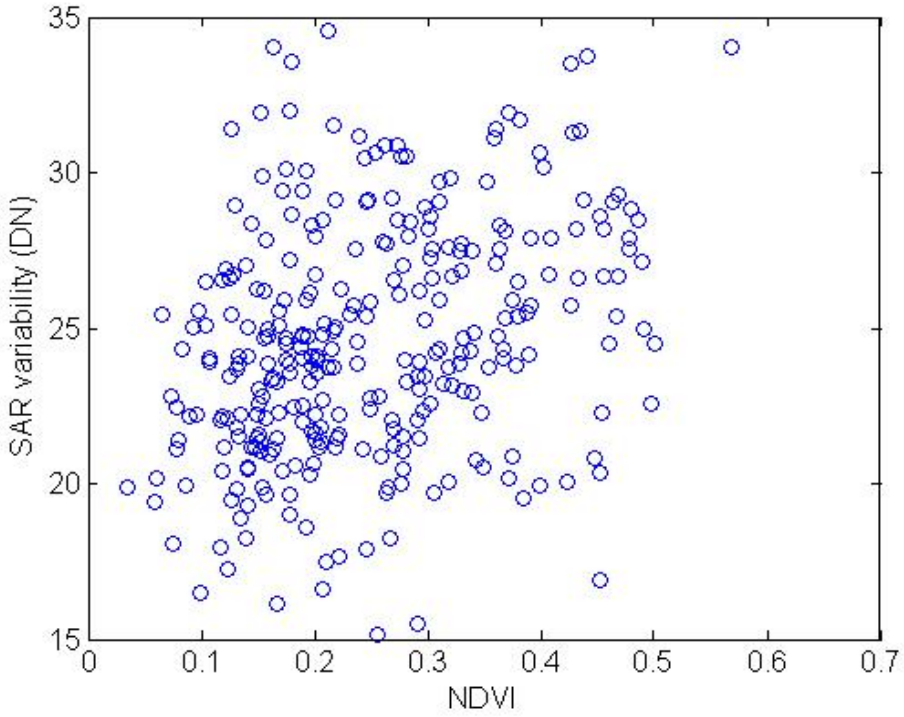

Figure 59: SAR variability as function of NDVI values (Area A on July 2nd 1997)

Table 24: Correlation coefficient for SAR variability and NDVI variability

Date / Site	Area A	Area B
July 2nd 1997 data	0.2653	0.1421
July 12th 1997 data	0.1825	0.2173

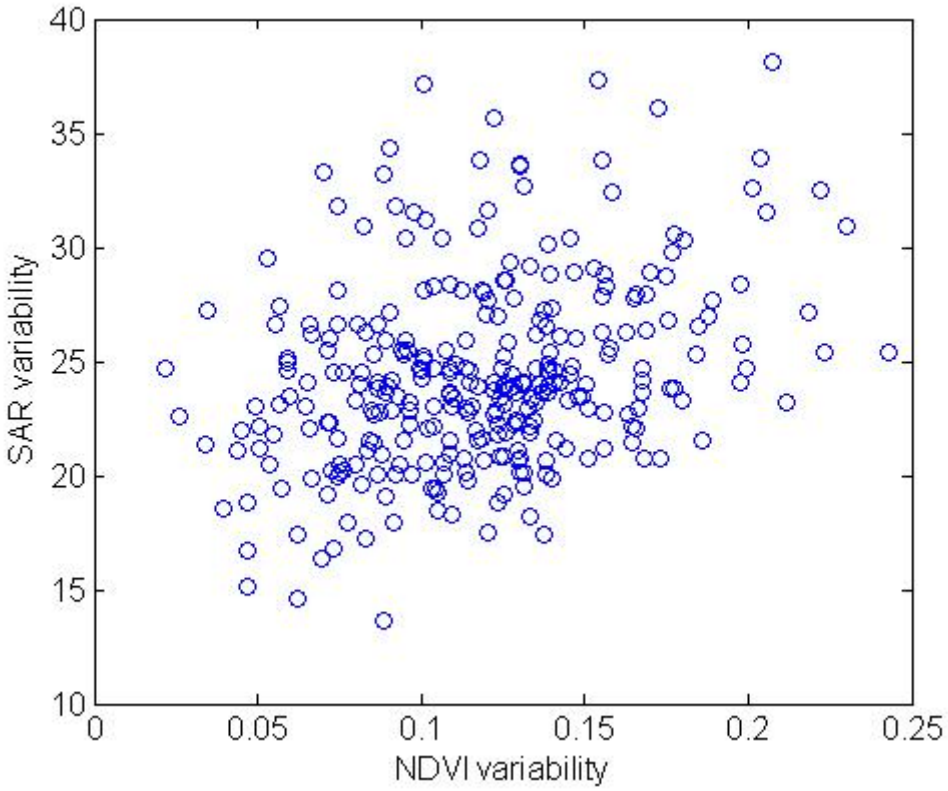

Figure 60: SAR variability as function of NDVI variability (Area A on July 2nd 1997)

8 Conclusions

The results obtained in this study clearly show that active microwave remote sensing has significant capabilities in estimating soil moisture in faster and more reliable ways with sufficient accuracy. Soil moisture retrieval is highly influenced by soil texture and vegetation parameters, as well as the heterogeneity of surface land cover. The influence of such related parameters can be better understood by technique like neural network and fuzzy logic, where more than one input parameter can be automatically weighted and used to improve the model retrieving capabilities. These models were studied for various input parameters such as SAR textural data, vegetation optical depth, NDVI, soil texture and surface roughness which, shown to have certain effects on the soil moisture retrieval process.

To reduce the speckle noise in SAR images, various textural images have been generated based on GLCM and used as an input (§5.5). The overall effect of textural images on soil moisture accuracy was not significant compared to the effect of vegetation data to the models. Therefore, textural data has not been used in further analysis. The effect of vegetation data, in the form of NDVI and vegetation optical depth were data tested and evaluated. When NDVI were used the soil moisture estimation become more accurate, but no significant improvement has been observed by adding optical depth to an already existing NDVI in the neural network input layer. Therefore the vegetation optical depth was not used as input to the neural network for the further analysis. This can be explained by the indirect relationship between NDVI and vegetation optical depth. As explained in chapter 2, the vegetation optical depth is a function of vegetation water

content and vegetation *b* parameter, where vegetation water content is estimated as a function of NDVI.

Two forms of soil moisture data have been used for training the model: quantitative and qualitative. In terms of qualitative data, we classified data in three soil moisture classes based on the water content: dry soil (0-10%), slightly wet soil (11-20%), and wet soil (+21%). In terms of quantitative data, the original values in percentage of soil moisture were used to train the neural network. The neural network output was analyzed for different threshold limits. The threshold limit determined the likelihood that the classified pixel was correctly classified. A higher threshold limit gives a higher confidence to a specific pixel to be correctly classified. The quantitative data were used to train and test the neural network and fuzzy logic, and the multi-linear regression model.

In the first part of this research, soil moisture was predicted by the neural network in 3 qualitative classes with an accuracy of 64% when only SAR data were used. However, by adding the textural measures and vegetation parameter such as NDVI and vegetation optical depth as additional inputs, the average classification accuracy was improved up to 70-75%. The correlation between SAR backscattering and soil moisture is better for high soil moisture content, which validates the studies by Wang *et al.* (2004) which stipulated that the dominance of soil moisture on backscattering is higher in wet soil than dry soil. The modeling results showed also that areas with low NDVI values obtain better classification accuracy which can be explained by the decrease of vegetation contribution to the backscatter. The addition of vegetation data to SAR is important to improve the accuracy of dry soil moisture pixels, where the dominance of vegetation water content can be higher than soil water content.

A fuzzy modeling algorithm establishes the relationship between the basic input and output parameters in soil moisture retrieval. A subtractive clustering-based fuzzy identification method and a Sugeno type fuzzy inference system have been used to retrieve of soil moisture from SAR data. The fuzzy model has been applied to various potential input parameters such as SAR textural data, vegetation optical depth, NDVI, soil texture and surface roughness. Based on several runs of the model we identified SAR, NDVI and soil texture, which influence the retrieval process significantly. The RMSE errors in soil moisture retrieval were minimized through an exhaustive search of clustering parameters. The accuracy of the fuzzy model depends on the number of the rules applied as well as to the clustering parameters. However, the results can be varied by changing these parameters. The fuzzy model obtained is capable of retrieving soil moisture for a given set of inputs. The model output is verified using different sets of inputs taken from area A and B from two different images (2^{nd} and 12^{th} July data). The results obtained using different sets of inputs are in a good agreement with truth soil moisture data.

A multiple linear regression model has also been developed to establish the relationship between soil moisture and SAR, NDVI, and soil texture data. The stepwise regression method was used to derive this relationship. The stepwise procedure was run a number of times using random selection of data to find the best input subset. An analysis of variance was performed using the *p*-values (95%) to compare and measure the effect of different variables on regression analysis as well as their level of significance.

Results obtained from these three models from the same datasets were compared. No significance difference (Z-score < 1.96) was found between these results. The RMSE, in

terms of soil moisture percentage of the output data for neural network and fuzzy logic and multi-linear regression model were 3.672, 3.735, and 4.063 respectively. The predicted soil moisture data from fuzzy logic model were also compared with field point measurements of soil moisture. The observed RMSE in terms of soil moisture percentage were 7.94 and 6.54 for 2nd and 12th July data respectively.

The neural network model has shown a high potential to estimate soil moisture from SAR data. However, a high variation in soil moisture estimation accuracy was produced by neural network model. Fuzzy logic was also been tested and evaluated to predict the soil moisture using the same input data and resulted in very low variation in soil moisture estimation accuracy compared to neural network. The prediction made by neural network is higher than fuzzy logic in several runs of the model, but we found that the prediction made by fuzzy logic is more stable in nature.

One of the principle motivations of this project is to contribute to the ongoing research undertaken by the NASA's Hydrosphere Sate Mission (HYDROS) research team exclusively dedicated for soil moisture retrieval from both active and passive microwave sensors. HYDROS, a new microwave satellite project expected to be launched in December 2009, will deliver the first global views of the Earth's soil moisture content with a resolution of 1 km. The new HYDROS system will open a new era in the capabilities to predict costly natural hazards such as extreme rain, floods, and droughts. Furthermore, high resolution soil moisture data have important applications in the agricultural field, where crop growth and production is highly dependant on available surface soil moisture. A high resolution soil moisture map can be a valuable scene of

information by helping irrigation scheduling and by providing an estimate of optimum amount of water required in agriculture field.

Suggested Future Work

- Addition of accurate estimation of the distribution of soil moisture to the advanced hydrologic prediction system (AHPS) will improve its flood forecasting accuracy and flash flood warning capabilities.
- The contribution of remote sensing derived soil moisture into the AHPS operated by NWS/NOAA can be also evaluated through practical experience.
- Determine the attenuation/addition factor for different type of vegetation to improve the relationship between soil moisture and SAR backscattering.
- Temporal assessment of SAR backscattering and soil moisture relationship to determine the effect of precipitation.

Appendix A: IEM Model

$$\sigma_{pp}^{0}(\theta) = \frac{k^2}{2} e^{-2k^2h^2\cos^2\theta} * \sum_{n=1}^{\infty} h^{2n} \frac{\left|\mathrm{I}_{pp}^{n}\right|^2}{n!} W^{(n)}(-2k_x, 0)$$

Where, $\mathrm{I}_{pp}^{n} = (2k\cos\theta)^n f_{pp} * e^{-k^2h^2\cos^2\theta} + \frac{(k\cos\theta)^n}{2} F_{pp}$

$$f_{vv} = \frac{2R_{\parallel}}{\cos\theta} \qquad f_{hh} = -\frac{2R_{\perp}}{\cos\theta}$$

$$F_{vv} = \frac{2\sin^2\theta}{\cos\theta}\left[\left(1 - \frac{\varepsilon\cos^2\theta}{\varepsilon - \sin^2\theta}\right)(1 - R_{\parallel})^2 + \left(1 - \frac{1}{\varepsilon}\right)(1 + R_{\parallel})^2\right]$$

$$F_{hh} = \frac{2\sin^2\theta}{\cos\theta}\left[4R_{\perp} - \left(1 - \frac{1}{\varepsilon}\right)(1 + R_{\perp})^2\right]$$

$$W^n(k_x, k_y) = \frac{1}{2\pi}\iint \rho^n(\tau_x, \tau_y)^{e - j(k_x\tau_x, k_y\tau_y)} d\tau_x d\tau_y$$

$$h^2\rho(\tau_x, \tau_x) = \left\langle Z(x,y) * Z(x+\tau_x, y+\tau_y) \right\rangle$$

Where, *pp* = *hh* or *vv*,

k = wave number of medium 1,

$k_s = k \sin\theta$,

h = rms surface height,

θ = incidence angle,

ε = dielectric constant of the surface,

$R_{\parallel}$ = Fresnel reflection coefficient for vertical polarization,

$R_{\perp}$ = Fresnel reflection coefficient for horizontal polarization,

$W^n(k_x, k_y)$ = Fourier Transform of the nth power of the surface correlation coefficient,

$Z(x,y)$ = surface function, a stationary random process with zero mean, and

<> denotes the ensemble average operator.

Appendix B: Sampling location and Vegetation type and growth stage

Location	Longitude	Latitude	Vegetation type	Growth stage
CF01	-97.485758	36.606104	Grass	Reproductive
CF02	-97.487701	36.605754	Wheat	Harvested
CF03	-97.494440	36.612380	Wheat	Harvested
CF04	-97.494240	36.619440	Wheat	Harvested
CF05	-97.485386	36.619388	Wheat	Harvested
CF06	-97.485466	36.612270	Wheat	Harvested
CF07	-97.521392	36.612241	Wheat	Tilled
CF08	-97.539972	36.612346	Pasture	Vegetative
CF09	-97.511890	36.590298	Wheat	Harvested, burnt
ER01	-98.018460	35.558820	Pasture	Vegetative
ER02	-98.015883	35.561400	Pasture	Vegetative
ER03	-98.011460	35.560240	Pasture	Reproductive
ER04	-98.005640	35.558400	Grass	Mature
ER05	-98.039478	35.548229	Grass	Reproductive
ER06	-98.030582	35.548114	Grass	Reproductive
ER07	-98.039478	35.541190	Grass	Vegetative
ER08	-98.030638	35.541188	Grass	Reproductive
ER09	-98.061944	35.565404	Grass	Reproductive
ER10	-98.075214	35.548213	Wheat	Harvested
ER11	-98.066354	35.548152	Wheat	Harvested
ER12	-98.075214	35.541039	Wheat	Harvested
ER13	-98.065158	35.541033	Wheat	Tilled
ER14	-97.916670	35.883333	Pasture	Vegetative
ER15	-98.014395	35.566555	Wheat	Harvested
ER16	-98.007056	35.565040	Grass	Reproductive
LW01	-97.915500	35.046000	Wheat	Harvested
LW02	-97.972330	34.961500	Pasture	Vegetative
LW03	-98.079954	34.960409	Pasture	Vegetative
LW04	-98.088956	34.960543	Grass	Reproductive
LW05	-98.097736	34.960563	Grass	Reproductive
LW06	-98.128110	34.949083	Grass	Reproductive
LW07	-98.292298	34.916027	Grass	Grazed
LW08	-98.203171	34.880800	Wheat	Harvested
LW09	-98.180870	34.898439	Pasture	Vegetative
LW10	-98.023050	34.885381	Grass	Grazed
LW11	-97.965580	34.927694	Grass	Reproductive
LW12	-97.957390	34.924728	Grass	Reproductive
LW13	-97.957526	34.917427	Pasture	Grazed
LW14	-98.075280	34.936575	Grass	Harvested
LW15	-97.917100	34.878983	Grass, Bushes	Mature
LW16	-97.993240	34.796647	Pasture	Mature
LW17	-98.000000	34.800000	Pasture	Vegetative
LW18	-98.137030	34.855233	Grass	Reproductive
LW19	-98.141670	34.813333	Pasture	Vegetative
LW20	-98.282750	34.921487	Wheat	Tilled
LW21	-98.280962	34.910326	Wheat	Tilled
LW22	-98.273594	34.910234	Wheat	Harvested
LW23	-98.265088	34.910204	Wheat	Harvested

Appendix C: Vegetation Plant Height, Water Content and Biomass at SGP sites

(Values are the Mean for Each Field Sub-sample)

		Green Standing			Brown Standing			Surface Residue		
	Plant	Wet	Dry	Water	Wet	Dry	Water	Wet	Dry	Water
	height	biomass	biomass	content	biomass	biomass	content	biomass	biomass	content
Field	(cm)	(g m^{-2})	(g m^{-2})	(%)	(g m^{-2})	(g m^{-2})	(%)	(g m^{-2})	(g m^{-2})	(%)
CF01	18.0	213.3	81.5	61.0	15.0	11.0	25.8	55.3	38.4	32.6
CF02	22.3	97.0	35.1	63.8	0.0	0.0	0.0	0.3	0.1	26.7
CF03	24.5	131.5	36.9	72.3	119.5	104.6	11.8	39.5	32.6	12.5
CF04	22.3	22.1	6.5	69.2	185.8	178.2	4.0	321.7	297.5	7.8
CF05	37.4	0.0	0.0	0.0	241.7	236.9	2.0	318.4	305.9	4.0
CF06	41.0	120.1	31.0	49.1	149.1	135.8	6.0	104.3	86.5	11.8
CF07	40.6	0.0	0.0	0.0	0.0	0.0	0.0	0.0	0.0	0.0
CF08	26.8	466.0	202.4	56.2	82.4	72.0	12.2	311.2	251.0	18.2
CF09	32.4	11.2	3.4	46.7	308.4	295.4	4.3	582.9	466.6	17.8
ER01	59.7	1403.1	460.1	66.7	133.4	97.2	25.8	967.1	509.9	46.6
ER02	53.3	1093.0	401.1	63.3	71.5	57.8	12.8	933.3	595.2	36.1
ER03	52.7	923.7	314.1	65.6	161.3	77.3	31.4	54.3	23.0	38.0
ER04	55.0	1458.3	397.8	72.5	8.1	4.3	28.1	1371.6	599.9	55.4
ER05	39.1	678.7	281.1	58.1	22.8	16.2	9.6	193.2	130.6	29.5
ER06	37.7	660.8	290.2	56.4	20.5	13.0	35.0	432.6	286.3	33.5
ER07	47.2	956.3	357.3	62.1	36.1	26.3	21.9	532.7	416.6	21.8
ER08	49.4	616.0	219.1	63.7	81.3	66.7	16.5	614.0	462.8	27.4
ER09	32.4	241.3	111.1	54.3	45.7	30.3	32.5	81.7	53.1	35.4
ER10	24.0	1.2	0.2	83.3	269.6	260.2	3.4	404.5	355.2	38.0
ER11	22.9	23.8	5.6	73.8	180.4	167.4	7.5	330.7	148.2	34.3
ER12	24.6	1.3	0.0	32.5	255.3	242.1	5.2	554.3	502.7	9.1
ER13	41.6	0.0	0.0	0.0	0.0	0.0	0.0	0.0	0.0	0.0
ER14	15.1	881.8	231.8	71.6	24.7	16.8	47.3	264.8	215.2	18.2
ER15	23.2	46.1	16.2	67.0	245.4	236.8	3.4	244.2	218.5	9.9
ER16	29.1	662.7	179.0	72.7	100.0	65.4	40.1	171.9	92.2	46.3
LW01	21.0	184.0	112.8	30.0	164.2	136.2	12.9	118.3	101.3	12.7
LW02	30.2	350.2	161.0	53.3	184.1	158.1	18.5	159.7	141.2	13.6
LW03	33.0	375.7	168.0	55.5	147.6	108.8	25.4	231.8	148.3	33.4
LW04	32.3	310.5	126.2	60.9	38.3	26.8	10.1	114.5	86.3	19.4
LW05	32.8	502.9	170.2	64.3	9.8	7.6	25.1	220.8	187.5	16.9
LW06	16.6	111.7	40.6	61.5	22.0	18.1	11.2	17.7	12.2	10.3
LW07	24.2	711.8	280.9	60.4	6.1	3.6	43.8	136.7	111.9	18.0
LW08	26.2	0.0	0.0	0.0	240.7	234.1	2.7	388.3	360.3	6.0
LW09	34.8	525.1	221.8	57.4	79.6	65.8	35.1	210.3	172.4	22.4
LW10	25.0	386.3	146.8	60.3	12.3	9.8	17.9	33.3	26.6	22.2
LW11	39.2	939.5	245.8	73.2	68.9	43.9	42.9	494.3	319.5	34.9
LW12	44.9	344.0	139.8	59.0	173.0	136.7	21.6	246.7	180.6	26.9
LW13	20.9	450.2	147.1	66.1	11.9	7.6	35.6	57.3	44.0	23.1
LW14	15.8	225.9	95.6	57.7	9.5	6.7	29.3	265.5	215.6	25.7
LW15	20.5	269.6	129.8	52.6	9.6	8.0	36.1	127.8	114.2	12.0
LW16	14.0	122.7	53.1	57.4	2.2	1.2	15.2	73.3	47.4	36.0
LW17	41.0	540.8	234.0	56.7	53.0	35.4	32.8	186.3	163.5	12.1
LW18	57.4	316.7	173.0	45.0	71.0	58.9	16.3	173.3	137.2	17.2
LW19	22.5	427.1	158.6	61.2	15.9	11.2	27.5	91.3	76.4	17.3
LW20	46.5	0.0	0.0	0.0	0.0	0.0	0.0	0.0	0.0	0.0
LW21	77.9	0.0	0.0	0.0	0.0	0.0	0.0	0.0	0.0	0.0
LW22	26.6	23.5	5.2	77.8	211.3	200.5	5.1	248.1	233.8	5.6
LW23	33.8	0.0	0.0	0.0	254.7	241.5	5.1	326.4	306.0	7.0

Appendix D: Leaf Area Index measured at SGP97 sites

Field	Leaf area index*	Photosynthetically Active Radiation			
		fR_C (%)	fT_C (%)	fR_S (%)	fAPAR (%)
CF01	1.49	6.94	56.17	5.76	42.65
CF02	2.32	6.67	36.44	3.74	60.63
CF03	1.29	7.56	49.82	5.11	47.73
CF04	0.70	7.29	67.56	6.93	32.08
CF05	1.24	7.01	50.19	5.15	47.95
CF06	0.94	7.20	70.29	6.80	29.31
CF07	0.00	10.62	100.00	10.62	0.00
CF08	2.57	6.49	39.84	4.09	57.75
CF09	1.03	6.87	63.19	6.48	36.42
ER01	4.66	4.67	8.11	0.83	88.05
ER02	3.78	4.71	20.91	2.15	76.52
ER03	4.45	4.66	9.86	1.01	86.49
ER04	4.41	4.91	5.33	0.55	90.30
ER05	2.37	5.35	40.39	4.15	58.40
ER06	3.19	5.61	16.27	1.67	79.78
ER07	4.43	5.74	16.03	1.65	79.87
ER08	3.60	5.81	14.28	1.46	81.37
ER09	2.72	6.99	27.46	2.82	68.37
ER10	0.65	8.12	66.28	6.80	32.40
ER11	0.58	6.48	56.61	5.81	42.72
ER12	1.11	6.56	63.97	6.56	36.04
ER13	0.00	10.84	100.00	10.84	0.00
ER14	1.90	5.85	62.41	6.41	38.15
ER15	1.44	7.55	35.39	3.63	60.70
ER16	3.95	8.50	12.47	1.28	80.30
LW01	0.13	6.53	75.73	7.77	39.82
LW02	2.21	6.18	54.02	5.54	45.34
LW03	1.79	5.55	70.57	7.24	31.12
LW04	1.97	5.40	56.34	5.78	44.05
LW05	1.76	6.81	32.17	3.30	64.33
LW06	0.90	7.07	81.11	8.32	20.14
LW07	2.21	5.58	37.58	3.86	60.70
LW08	1.55	6.67	55.60	5.70	43.43
LW09	2.77	6.13	40.44	4.15	57.58
LW10	1.36	5.92	39.03	4.01	59.05
LW11	3.57	5.81	11.83	1.22	83.58
LW12	3.40	6.77	20.47	2.10	74.86
LW13	1.43	6.07	71.40	7.33	29.86
LW14	1.00	5.80	52.12	5.35	47.43
LW15	1.30	6.51	59.46	6.10	40.13
LW16	0.55	7.28	57.31	5.88	41.29
LW17	2.17	5.67	37.28	3.82	60.87
LW18	2.24	7.46	22.93	2.35	71.97
LW19	1.28	6.09	47.99	4.92	50.84
LW20	0.00	9.85	100.00	9.85	0.00
LW21	0.00	0.00	100.00	0.00	0.00
LW22	0.72	7.40	60.48	6.20	38.32
LW23	1.13	7.43	55.22	5.67	43.01

Appendix E: Optimization of NN architecture for nodes in single hidden layer

1. Overall accuracy for 25 runs of NN model when Number of nodes varied in single hidden layer

No of Nodes	Training	Validation	Testing
2	0.6505	0.6361	0.6317
4	0.7077	0.6888	0.6822
6	0.7206	0.6973	0.6956
8	0.7316	0.7065	0.6982
10	0.7490	0.7264	0.7315
12	0.7563	0.7329	0.7370
14	0.7460	0.7257	0.7241
16	0.7516	0.7249	0.7299
18	0.7417	0.7217	0.7234
20	0.7514	0.7236	0.7289
22	0.7604	0.7325	0.7393
24	0.7553	0.7285	0.7307
26	0.7543	0.7312	0.7322
28	0.7527	0.7232	0.7280
30	0.7667	0.7419	0.7474

*Average value of overall accuracy for 25 runs of NN model

2. Accuracy of training and testing data with different combination of nodes in two hidden layers

						Accuracy of Data		Accuracy for test data		
Sr No	Tr. Pixel	Input layer	Hidden layer 1	Hidden layer 2	output layer	Training	Test	Class 1	Class 2	Class 3
1	500	4	**5-5**	**5**	3	**0.671**	**0.67**	**0.673**	**0.687**	**0.644**
2	500	4	5-10	10	3	0.670	0.66	0.686	0.647	0.644
3	500	4	5-15	15	3	0.671	0.67	0.691	0.660	0.659
4	500	4	5-20	20	3	0.653	0.65	0.675	0.655	0.621
5	500	4	5-25	25	3	0.670	0.67	0.653	0.698	0.665
6	500	4	5-30	30	3	0.662	0.66	0.668	0.694	0.632
7	500	4	10-5	5	3	0.669	0.66	0.689	0.647	0.648
8	500	4	**10-10**	**10**	3	**0.672**	**0.67**	**0.668**	**0.678**	**0.656**
9	500	4	10-15	15	3	0.672	0.66	0.648	0.695	0.648
10	500	4	10-20	20	3	0.673	0.67	0.666	0.704	0.653
11	500	4	10-25	25	3	0.671	0.67	0.636	0.724	0.656
12	500	4	10-30	30	3	0.668	0.67	0.635	0.712	0.658
13	500	4	15-5	5	3	0.663	0.66	0.654	0.653	0.662
14	500	4	15-10	10	3	0.668	0.67	0.638	0.717	0.651
15	500	4	**15-15**	**15**	3	**0.668**	**0.67**	**0.649**	**0.701**	**0.658**
16	500	4	15-20	20	3	0.667	0.67	0.627	0.724	0.652
17	500	4	15-25	25	3	0.669	0.67	0.624	0.724	0.654
18	500	4	15-30	30	3	0.662	0.66	0.642	0.714	0.617
19	500	4	20-5	5	3	0.661	0.66	0.629	0.725	0.612
20	500	4	**20-10**	10	3	0.664	0.66	0.645	0.696	0.637
21	500	4	20-15	15	3	0.665	0.67	0.635	0.719	0.667
22	500	4	20-20	**20**	3	**0.671**	**0.67**	**0.651**	**0.696**	**0.657**
23	500	4	20-25	25	3	0.669	0.67	0.648	0.727	0.632
24	500	4	20-30	30	3	0.671	0.67	0.652	0.713	0.650
25	500	4	25-5	5	3	0.673	0.67	0.684	0.707	0.613
26	500	4	25-10	10	3	0.672	0.67	0.675	0.684	0.644
27	500	4	**25-15**	15	3	0.673	0.66	0.645	0.724	0.624
28	500	4	25-20	20	3	0.671	0.67	0.668	0.710	0.638
29	500	4	25-25	**25**	3	**0.674**	**0.67**	**0.652**	**0.716**	**0.640**
30	500	4	25-30	30	3	0.670	0.67	0.649	0.694	0.659
31	500	4	30-5	5	3	0.674	0.67	0.682	0.668	0.655
32	500	4	**30-10**	10	3	0.672	0.67	0.651	0.718	0.648
33	500	4	30-15	15	3	0.671	0.67	0.654	0.710	0.639
34	500	4	30-20	20	3	0.673	0.67	0.636	0.716	0.645
35	500	4	30-25	25	3	0.667	0.67	0.639	0.710	0.659
36	500	4	30-30	**30**	3	**0.671**	**0.67**	**0.650**	**0.714**	**0.634**

Conference Proceeding and Presentation

2006

1. Tarendra Lakhankar, Hosni Ghedira and Reza Khanbilvardi, (2006), "Effect Land-cover parameter on Soil Moisture Retrieval from Active Microwave Data", **In Preparation** to be submitted to *International journal of remote sensing*.
2. Tarendra Lakhankar, Hosni Ghedira and Reza Khanbilvardi, (2006) "Soil Moisture Retrieval from Radarsat Data: A Neuro-Fuzzy Approach". **Submitted** to proc. *IEEE International Geosciences and Remote Sensing Symposium*. **IGARSS'2006**, Denver, USA, July 31-August 4, 2006.
3. Tarendra Lakhankar, Hosni Ghedira Ami Azar and Reza Khanbilvardi, (2005), "Effect of Sub-pixel Variability of NDVI and Land-cover on Soil Moisture Retrieval from RADARSAT-1 Data", In proc. ***Microrad'06*** *(9th Specialist Meeting on Microwave Radiometry and Remote Sensing Applications)*, San Juan, Puerto Rico, 28 Feb-03 March 2006.
4. Tarendra Lakhankar, Hosni Ghedira and Reza Khanbilvardi, (2006) "Combine Neural Network and Fuzzy Logic for an Improved Soil Moisture Estimation". In proc. *Prospecting for Geospatial Information Integration,* ***ASPRS*** *Annual Conference*, Reno, Nevada, USA, May 1-5, 2006.
5. Tarendra Lakhankar, Hosni Ghedira and Reza Khanbilvardi, (2006) "Spatial Mapping of Soil Moisture using RADARSAT-1 Data". In proc. *Prospecting for Geospatial Information Integration,* ***ASPRS*** *Annual Conference*, Reno, Nevada, USA, May 1-5, 2006.
6. Tarendra Lakhankar, Hosni Ghedira and Reza Khanbilvardi, (2006) "Non-Parametric Tools for Soil Moisture Mapping Using Active Microwave Data", American Meteorological Society (**AMS**) Annual Meetings, Georgia, Atlanta, USA, 29 January- 2 February, 2006.
7. Tarendra Lakhankar, Hosni Ghedira and Reza Khanbilvardi, (2006) "Improving the Efficiency of Neural Network Retrieval of Soil Moisture from Active Microwave Data", American Meteorological Society (**AMS**) Annual Meetings, Georgia, Atlanta, USA, 29 January- 2 February, 2006.

2005

8. Hosni Ghedira, Tarendra Lakhankar (2005) "Neural Network application using Passive and Active Microwave Data for Soil Moisture Estimates", Submitted to the ***IEEE Geosciences and Remote Sensing Letters.***
9. Tarendra Lakhankar, Hosni Ghedira and Reza Khanbilvardi, (2005), "Vegetation Effect on Soil Moisture Retrieval from Active Microwave Data", In proc. *The 9th International Symposium on Physical Measurements and Signature in Remote Sensing (****ISPMSRS****)* Beijing. China, vol. 2. pp. 811-814, October 17-19, 2005.
10. Tarendra Lakhankar, Hosni Ghedira and Reza Khanbilvardi, (2005), "Effect of Sub-Pixel Variability of Land-Cover Data on Soil Moisture Retrieval using SAR data", Eos Trans. **AGU**, , Fall Meet. Suppl.

11. Hosni Ghedira, Juan Carlos Arevalo, Tarendra Lakhankar, and Reza Khanbilvardi, (2005), "An Adaptive Neural Network System for Improving the Filtration of Non-Snow Pixels from SSM/I Images", In proc. IEEE International Geosciences and Remote Sensing Symposium. **IGARSS'2005**, vol. 8, No 167, pp. 5459-5463, Seoul, South Korea, 25–29 July, 2005.
12. Hosni Ghedira and Tarendra Lakhankar (2005) "Capabilities and Limitation of Satellite Microwave Data in Soil Moisture Retrieval in Semi-Arid Regions" In. proc. Kuwait First International Remote Sensing Conference, 26-28, September 2005.
13. Hosni Ghedira, Juan Carlos Arevalo, Tarendra Lakhankar, and Reza Khanbilvardi, (2005), "Capabilities and Limitations of Neural Networks in Snow Cover Mapping from SSM/I Images", In proc. *The 9th International Symposium on Physical Measurements and Signature in Remote Sensing (**ISPMSRS**)* Beijing. China, vol. 1. pp. 211-214, October 17-19, 2005.
14. Tarendra Lakhankar, Hosni Ghedira and Reza Khanbilvardi, (2005), "Neural Network and Fuzzy Logic system for Soil Moisture Estimation using Remote Sensing Data", Einstein's in the City, 2005, New York, USA, April 11-12, 2005.
15. Tarendra Lakhankar, Hosni Ghedira, and Reza Khanbilvardi, (2005), "Neural Network and Fuzzy Logic Systems: Two Promising Tools for Soil Moisture Mapping Using Active Microwave Data", *6th Annual Science, Engineering and Mathematics Celebration* at Graduate Center of The City University of New York, New York, March 14, 2005.

2004

16. Hosni Ghedira, Tarendra Lakhankar, Nasim Jahan, and Reza Khanbilvardi, (2004) "Combination of Passive and Active Microwave Data for Soil Moisture Estimates", In proc. *IEEE International Geosciences and Remote Sensing Symposium*. **IGARSS'2004,** vol. 4, pp. 2783 - 2786, Anchorage, Alaska USA, 20-24 September, 2004.
17. Tarendra Lakhankar, Hosni Ghedira and Reza Khanbilvardi, (2004), "Neural Network application using Passive and Active Microwave Data for Soil Moisture Estimation" In proc. of NOAA Educational Partnership Program, Education & Science Forum 2004, City College of New York, October 21-23, 2004, pp. 254-259.
18. Tarendra Lakhankar, Hosni Ghedira and Reza Khanbilvardi, (2004), "Comparison between Neural Network and Fuzzy Logic system for Soil Moisture Estimation using Microwave Remote Sensing Data", Eos Trans. **AGU**, 85(46), Fall Meet. Suppl., H13C-0438.
19. Nasim Jahan, Tarendra Lakhankar, and Hosni Ghedira, (2004), "The Effect of Vegetation Optical Depth on Temporal Variation of Soil Moisture", Eos Trans. **AGU**, 85(46), Fall Meet. Suppl., H13D-0463.
20. Hosni Ghedira, Tarendra Lakhankar and Reza Khanbilvardi, (2004), "Integration of Multi-Source and Multi-Resolution Data for Soil Moisture Estimates", Eos. Trans. **AGU**, 85(17), H23A-07, American Geophysical Proceedings, Montreal, Canada May 17-21, 2004.
21. Tarendra Lakhankar, Hosni Ghedira, and Reza Khanbilvardi, (2004), "Application of Textural Analysis for Soil Moisture Estimation using RADARSAT Data", In proc. *Annual NOAA-CREST Research Symposium*, Hampton University, April 20-22, 2004.

References

Aires, F., Prigent, C., and Rossow, W. (2005). "Sensitivity of satellite microwave and infrared observations to soil moisture at a global scale: 2. Global statistical relationships." *Journal of Geophysical Research*, 110 (D11103).

Alhumaidi, S. M., Jones, L., Park, J.-D., and Ferguson, S. M. (1997). "A neural network algorithm for sea ice edge classification." *IEEE Transactions on Geoscience and Remote Sensing*, 35(4), 817-826.

Anderson, M. C., Neale, C. M. U., Li, F., Norman, J. M., Kustas, W. P., Jayanthi, H., and Chavez, J. (2004). "Upscaling ground observations of vegetation water content, canopy height, and leaf area index during SMEX02 using aircraft and Landsat imagery." *Remote Sensing of Environment*, 92(4), 447-464.

Atkinson, P. M., and Tatnall, A. R. L. (1997). "Neural networks in remote sensing." *International Journal of Remote Sensing*, 18(4), 699-709.

Atluri, V., Hung, C. C., and Coleman, T. L. "An artificial neural network for classifying and predicting soil moisture and temperature using Levenberg-Marquardt algorithm." *Southeastcon '99. Proceedings. IEEE*, 10-13.

Attema, E., and Ulaby, F. (1978). "Vegetation modeled as a water cloud." *Radio Science*, 13, 357-364.

Augustejin, M., Clemens, L., and Shaw, K. (1995). "Performance evaluation of texture measures for ground cover identification in satellite images by means of a neural network classifier." *IEEE Transactions on Geoscience and Remote Sensing*, 33(3), 616-626.

Baghdadi, N., Gaultier, S., and King, C. (2002). "Retrieving surface roughness and soil moisture from synthetic aperture radar (SAR) data using neural networks." *Canadian Journal of Remote Sensing*, 28(5), 701-711.

Baraldi, A., and Parmiggiani, F. (1995). "An investigation of textural characteristics associated with gray level co-occurrence matrix statistical parameters." *IEEE Transactions on Geoscience and Remote Sensing*, 33(2), 293-304.

Benediktsson, J., Swain, P., and Ersoy, O. K. (1990). "Neural network approaches versus statistical methods in classification of multi-source remote sensing data." *IEEE Transactions on Geoscience and Remote Sensing*, 28(4), 540-552.

Bernard, R., Martin, P. H., Thony, J. L., Vauclin, M., and Vidal-Madjar, D. (1982). "C-band radar for determining surface soil moisture." *Remote Sensing of Environment*, 12, 189-200.

Bindlish, R., and Barros, A. P. (2000). "Multi-frequency Soil Moisture Inversion from SAR Measurements with the Use of IEM." *Remote Sensing of Environment*, 71(1), 67-88.

Bindlish, R., and Barros, A. P. (2001). "Parameterization of vegetation backscatter in radar-based soil moisture estimation." *Remote Sensing of Environment*, 76, 130-137.

Bindlish, R., and Barros, A. P. (2002). "Subpixel variability of remotely sensed soil moisture: an inter-comparison study of SAR and ESTAR." *Remote Sensing of Environment*, 40(2), 326-337.

Blyth, K. (1997). "An Assessment of the Capabilities of the ERS Satellites' Active Microwave Instruments for Monitoring Soil Moisture Change." *Hydrology and Earth System Sciences*, 1, 159-174.

Boisvert, J., Gwyn, Q. H., Brisco, B., Major, D., and Brown, R. (1995a). "Evaluation of soil moisture estimation techniques and microwave penetration depth for radar applications." *Canadian Journal of Remote Sensing*, 21(2), 110-123.

Boisvert, J., Pultz, T., Brown, R., and Brisco, B. (1995b). "Potential of synthetic aperture radar for large-scale soil moisture monitoring: A review." *Canadian Journal of Remote Sensing*, 22(1), 2-13.

Brakke, T. W., Kanemasu, E. T., and Steiner, J. L. (1981). "Microwave radar response to canopy moisture, leaf-area index, and dry weight of wheat, corn and sorghum." *Remote Sensing of Environment*, 11, 207-220.

Burke, E. J., Shuttleworth, W. J., and French, A. N. (2001). "Using vegetation indices for soil-moisture retrievals from passive microwave radiometry." *Hydrology and Earth System Sciences*, 5(4), 671-677.

Burke, E. J., and Simmonds, L. P. (2001). "A simple parameterization for retrieving soil moisture from passive microwave data." *Hydrology and Earth System Sciences*, 5(1), 39-48.

Carpenter, G. A., Gopal, S., Macomber, S., Martens, S., Woodcock, C. E., and Franklin, J. (1999). "A neural network method for efficient vegetation mapping." *Remote Sensing of Environment*, 70, 326-338.

Ceccato, P., Flasse, S., and Gregoire, J. (2002). "Designing a spectral index to estimate vegetation water content from remote sensing data: Part 2. Validation and application." *Remote Sensing of Environment*, 82, 198-207.

Chakraborty, M., and Panigrahy, S. (2000). "A processing and software system for rice crop inventory using multi-date RADARSAT ScanSAR data." *ISPRS Journal of Photogrammetry and Remote Sensing*, 55(2), 119-128.

Chauhan, N., Miller, S., and Ardanuy, P. (2003). "Spaceborne soil moisture estimation at high resolution: a microwaveoptical/IR synergistic approach." *International Journal of Remote sensing*, 24(20), 4599–4622.

Chen, K. S., Yen, S. K., and Huang, W. P. (1995). "A simple model for retrieving bare soil moisture from radar-scattering coefficients." *Remote Sensing of Environment*, 54, 121–126.

Chiu, S. L. (1997). "An Efficient Method for Extracting Fuzzy Classification Rules from High Dimensional Data." *Journal of Advanced Computational Intelligence*, 1(1), 1-7.

Congalton, R. G. (1991). "A review of assessing the accuracy of classifications of remotely sensed data." *Remote Sensing of Environment*, 37, 35–46.

Crow, W. T., Drusch, M., and Wood, E. F. (2001). "An observation system simulation experiment for the impact of land surface heterogeneity on AMSR-E soil moisture retrievals." *IEEE Transactions on Geoscience and Remote Sensing*, 39(8), 1622-1632.

Crow, W. T., Ryu, D., and Famiglietti, J. S. (2005). "Upscaling of field-scale soil moisture measurements using distributed land surface modeling." *Advances in Water Resources*, 28, 1–14.

Dawson, M. S., Fung, A. K., and Manry, M. T. (1997). "A robust statistical-based estimator for soil moisture retrieval from radar measurements." *IEEE Transactions on Geoscience and Remote Sensing*, 35, 57-67.

Demirli, K., and Muthukumaran, P. (2000). "Higher order fuzzy system identification using subtractive clustering." *Journal of Intelligent and Fuzzy Systems*, 9, 129-158.

Dobson, M. C., Ulaby, F. T., LeToan, T., Beaudoin, A., Kasischke, E. S., and Christensen, N. (1992). "Dependence of radar backscatter on coniferous forest biomass." *IEEE Transactions on Geoscience and Remote Sensing*, 30, 412-415.

Doraiswamy, P. C., Hatfield, J. L., Jackson, T. J., Akhmedov, B., Prueger, J., and Stern, A. (2004). "Crop condition and yield simulations using Landsat and MODIS." *Remote Sensing of Environment*, 92, 548-559.

Du, Y., Ulaby, F. T., and Dobson, M. C. (2000). "Sensitivity to soil moisture by active and passive microwave sensors." *IEEE Transactions on Geoscience and Remote Sensing*, 38(1), 105-114.

Dubois, P. C., Zyl, J. V., and Engman, E. T. (1995). "Measuring soil moisture with imaging radars." *IEEE Transactions on Geoscience and Remote Sensing*, 33(4), 915-926.

Engman, E. T. (1991). "Application of microwave remote sensing of soil moisture for water resources and agriculture." *Remote Sensing of Environment*, 35, 213–226.

Engman, E. T., and Chauhan, N. (1995). "Status of microwave soil moisture measurements with remote sensing." *Remote Sensing of Environment*, 51, 189-198.

Entekhabi, D., H.Nakamura, and Njoku, E. G. (1994). "Solving the inverse problem for soil moisture and temperature profiles by sequential assimilation of multifrequency remotely sensed observations." *IEEE Transactions on Geoscience and Remote Sensing*, 32(2), 438-448.

Famiglietti, J. S., Devereaux, J. A., Laymon, C. A., Tsegaye, T., Houser, P. R., Jackson, T. J., Graham, S. T., Rodell, M., and Oevelen, P. J. (1999). "Ground-based investigation of soil moisture variability within remote sensing footprints during the Southern Great Plains 1997 (SGP97) Hydrology Experiment." *Water Resources Research*, 35(6), 1839–1851.

Farrar, T. J., Nicholson, S. E., and Lare, A. R. (1994). "The influence of soil type on the relationships between NDVI, rainfall, and soil moisture in semiarid Botswana. II. NDVI response to soil moisture." *Remote Sensing of Environment*, 50(2), 121-133.

Fassnacht, K. S., Gower, S. T., MacKenzie, M. D., Nordheim, E. V., and Lillesand, T. M. (1997). "Estimating the leaf area index of north central Wisconsin forests using the Landsat Thematic Mapper." *Remote Sensing of Environment*, 61, 229-245.

Fitzgerald, R. W., and Lees, B. G. (1994). "Assessing the classification accuracy of multi-source remote sensing data." *Remote Sensing of Environment*, 47, 362-368.

Foody, G. M. (2002). "Status of land cover classification accuracy assessment." *Remote Sensing of Environment*, 80, 185-201.

Foody, G. M., and Arora, M. K. (1997). "An evaluation of some factors affecting the accuracy of classification by an artificial neural network." *International Journal of Remote Sensing*, 18(4), 799-810.

Frate, F. D., Ferrazzoli, P., and Schiavon, G. (2003). "Retrieving soil moisture and agricultural variables by microwave radiometry using neural networks." *Remote Sensing of Environment*, 84, 174-183.

Fung, A. K., Li, Z., and Chen, K. S. (1992). "Backscattering from a randomly rough dielectric surface." *IEEE Transactions on Geoscience and Remote Sensing*, 30(6), 799-808.

Geng, H., Hugh, Q., Gwyn, J., Brisco, B., Boisvert, J., and Brown, R. (1996). "Mapping of Soil Moisture from C-Band Radar Images." *Canadian Journal of Remote Sensing*, 22(1), 117-126.

Ghedira, H., and Bernier, M. (2004). "The effect of Some Internal Neural Network Parameters on SAR Texture Classification Performance." *In proc. IEEE International Geosciences and Remote Sensing Symposium*, 6, 3845–3848.

Ghedira, H., Bernier, M., and Ouarda, T. B. M. J. (2000). "Application of neural networks for wetland classification in Radarsat SAR imagery." *IEEE International Geosciences and Remote Sensing Symposium, IGARSS'2000*, 2 675-677.

Ghedira, H., Lakhankar, T., Jahan, N., and Khanbilvardi, R. "Combination of Passive and Active Microwave Data for Soil Moisture Estimates." *IEEE International Geosciences and Remote Sensing Symposium. IGARSS'2004*, 2783 - 2786.

Ghinelli, B. M., and Bennett, J. C. "The application of artificial neural networks and standard statistical methods to SAR image classification." *IGARSS '97 'Remote Sensing - A Scientific Vision for Sustainable Development', IEEE Geoscience and Remote Sensing Conference, 3-8 August 1997*, 1211 - 1213.

Gilfilian, E., and Page, D. (1986). "Use of Multivariate Statistical Techniques to Associate Biologically Active Stressors with Observed Effects in Multiple Stressor Situations." *OCEANS*, 18, 953-959.

Glenn, N. F., and Carr, J. R. (2003). "The use of geo-statistics in relating soil moisture to RADARSAT-1 SAR data obtained over the Great Basin, Nevada, USA." *Computers and Geosciences*, 29, 577-586.

Gower, S. T., Kucharik, C. J., and Norman, J. M. (1999). "Direct and indirect estimation of leaf area index, fAPAR, and net primary production of terrestrial ecosystems." *Remote Sensing of Environment*, 70, 29–51.

Hall, F. G., Townshend, J. R., and Engman, E. T. (1995). "Status of remote sensing algorithms for estimation of land surface state parameters." *Remote Sensing of Environment*, 51(1), 138--156.

Haralick, R. M. (1979). "Statistical and structural approaches to texture." *Proceedings of the IEEE*, 67(5), 786-804.

Hayajneh, M. T., and Radaideh, S. M. (2003). "Modeling Surface Finish in End Milling Using Fuzzy Subtractive Clustering-Based System Identification Method." *Materials and Manufacturing Processes*, 18(4), 653-665.

Henderson, F. M., and Lewis, A. J. (1998). *Principles and Applications of Imaging Radar, Manual of Remote Sensing*, Wiley.

Jackson, T. J., Chen, D., Cosh, M., Li, F., Anderson, M., Walthall, C., Doraiswamy, P., and Hunt, E. R. (2004). "Vegetation water content mapping using Landsat data normalized difference water index (NDWI) for corn and soybean." *Remote Sensing of Environment*, 92, 475-482.

Jackson, T. J., and Schmugge, T. (1991). "Vegetation effects on the microwave emission of soils." *Remote Sensing of Environment*, 36, 203-212.

Jackson, T. J., Vine, D. L., Hsu, A. Y., Oldak, A., Starks, P., Swift, C., Isham, J., and Haken, M. (1999). "Soil moisture mapping at regional scales using microwave radiometry: the Southern Great Plains Hydrology Experiment." *IEEE Transactions on Geoscience and Remote Sensing*, 37, 2136-2151.

Jacobs, J. M., Mohanty, B. P., Hsu, E.-C., and Miller, D. (2004). "SMEX02: Field scale variability, time stability and similarity of soil moisture." *Remote Sensing of Environment*, 92, 436-446.

Janssen, L. L. F., and Wel, F. J. M. v. d. (1994). "Accuracy Assessment of Satellite Derived Land-Cover Data: A Review." *Photogrammetric Engineering & Remote Sensing*, 60(4), 419-426.

Jensen, J. R. (2000). *Remote Sensing of the Environment: An Earth Resource Perspective*, Prentice Hall.

Justice, C. O., Holben, B. N., and Gwynne, M. D. (1986). "Monitoring East African vegetation using AVHRR data." *International Journal of Remote Sensing*, 7, 1453-1474.

Kanellopoulos, I., and Wilkinson, G. (1997). "Strategies and best practice for neural network image classification." *International Journal of Remote Sensing*, 18(4), 711-725.

Karam, M. A., Fung, A. K., Lang, R. H., and Chauhan, N. S. (1992). "A Microwave Scattering Model for Layered Vegetation." *IEEE Transactions on Geoscience and Remote Sensing*, 30, 767-784.

Kasischke, E., Smith, K., Bourgeau-Chavez, L., Romanowicz, E., Brunzell, S., and Richardson, C. (2003). "Effects of seasonal hydrologic patterns in south Florida wetlands on radar backscatter measured from ERS-2 SAR imagery." *Remote Sensing of Environment*, 88(4), 423-441.

Kasischke, E. S., Melack, J. M., and Dobson, M. C. (1997). "The use of imaging radars for ecological applications - A Review." *Remote Sensing of Environment*, 59, 141-156.

Khoshgoftaar, T. M., Szabo, R. M., and Guasti, P. J. (1995). "Exploring the behaviour of neural network software quality models." *Software Engineering Journal*, 10(3), 89-96.

Kurvonen, L., and Hallikainen, M. (1999). "Textural information of multi-temporal ERS-1 and JERS-1 SAR images with applications to land and forest type recognition in boreal zone." *IEEE Transactions on Geoscience and Remote Sensing*, 37(2), 680-689.

Lippman, R. (1987). "An introduction to computing with neural nets." *IEEE ASSP Magazine*, 4, 4-22.

Low, H. K., Chuah, H. T., and Ewe, H. T. (1999). "A neural network land use classifier for SAR images using textural and fractal information." *Geocarto International*, 14(1), 66-73.

Mattikalli, N., Engman, E. T., Ahuja, L., and Jackson, T. J. (1998). "Microwave remote sensing of soil moisture for estimation of profile soil property." *International Journal of Remote Sensing*, 19(9), 1751–1767.

Meade, N., Hinzman, L., and Kane, D. (1999). "Spatial estimation of soil moisture using synthetic aperture radar in Alaska." *Advanced Space Research*, 24, 935-940.

Mo, T., Schmugge, T. J., and Jackson, T. J. (1984). "Calculations of radar backscattering coefficient of vegetation covered soils." *Remote Sensing of Environment*, 15, 119-133.

Moeremans, B., and Dautrebande, S. (2000). "Soil moisture evaluation by means of multi-temporal ERS SAR PRI images and interferometric coherence." *Journal of Hydrology*, 234, 162-169.

Mohanty, B. P., Shouse, P. J., Miller, D. A., and Genuchten, M. T. v. (2002). "Soil property database: Southern Great Plains 1997 Hydrology Experiment." *Water Resources Research*, 38(5).

Moran, M. S., Hymer, D. C., Qi, J., and Kerr, Y. (2002). "Comparison of ERS-2 SAR and Landsat TM imagery for monitoring agricultural crop and soil conditions." *Remote Sensing of Environment*, 79, 243-252.

Myneni, R. B., Hall, F. G., Sellers, P. J., and Marshak, A. L. (1995). "The interpretation of spectral vegetation indexes." *IEEE Transactions on Geoscience and Remote Sensing* 33, 481–486.

Narayan, U., Lakshmi, V., and Njoku, E. (2004). "Retrieval of soil moisture from passive and active L/S band sensor (PALS) observations during the soil moisture experiment in 2002 (SMEX02)." *Remote Sensing of Environment*, 92, 483-496.

Nedeljkovic, I. "Image classification based on fuzzy logic." *The International Archives of the Photogrammetry, Remote Sensing and Spatial Information Sciences*, 74-79.

Neusch, T., and Sties, M. (1999). "Application of the Dubois-model using experimental synthetic aperture radar data for the determination of soil moisture and surface roughness." *ISPRS Journal of Photogrammetry and Remote Sensing*, 54(4), 273-278.

O'Neill, P. E., Jackson, T. J., Chauhan, N. S., and Seyfried, M. S. (1993). "Microwave soil moisture estimation in humid and semiarid watersheds." *Advanced Space Research*, 13(5), 115-118.

Oh, Y., Sarabandi, K., and Ulaby, F. T. (1992). "An empirical model and an inversion technique for radar scattering from bare soil surfaces." *IEEE Transactions on Geoscience and Remote Sensing*, 30(2), 370–381.

Oldak, A., Jackson, T., and Pachepsky, Y. (2002). "Using GIS in passive microwave soil mapping and geostatistical analysis." *International Journal of Geographical Information Science*, 16, 681-689.

Paola, J., and Schowengerdt, R. A. (1995). "A review and analysis of back-propagation neural networks for classification of remotely-sensed multi-spectral imagery." *International Journal of Remote Sensing*, 16(16), 3033-3058.

Pultz, T., Leconte, R., Brown, R., and Brisco, B. (1990). "Quantitative soil moisture extraction from airborne SAR data." *Canadian Journal of Remote Sensing*, 16(3), 56-62.

Quesney, A., Hégarat-Mascle, S. L., Taconet, O., Vidal-Madjar, D., Wigneron, J. P., Loumagne, C., and Normand, M. (2000). "Estimation of watershed soil moisture index from ERS/SAR data." *Remote Sensing of Environment*, 72(3), 290-303.

Rao, K. S., Raju, S., and Wang, J. R. (1993). "Estimation of soil moisture and surface roughness parameters from backscattering coefficient." *IEEE Transactions on Geoscience and Remote Sensing*, 31(5), 1094-1099.

Richards, J. A. (1996). "Classifier performance and map accuracy." *Remote Sensing Environment*, 57, 161-166.

Robinson, N. (1966). *Solar Radiation*, Elsevier Publishing Compony, Amsterdam.

Roo, R. D. D., Du, Y., Ulaby, F. T., and Dobson, M. C. (2001). "A Semi-Empirical Backscattering Model at L-Band and C-Band for a Soybean Canopy with Soil Moisture Inversion." *IEEE Transactions on Geoscience and Remote Sensing*, 39(4), 864-872.

Rosnaya, P., Calvetb, J.-C., Kerra, Y., Wigneronc, J.-P., Lemaître d, F., Escorihuelaa, M., and et.al. (2006). "SMOSREX: A long term field campaign experiment for soil moisture and land surface processes remote sensing " *Remote Sensing of Environment* In Press.

Rumelhart, D. E., Hinton, G. E., and Williams, R. J. (1986). *Learning internal representation by error propagation, Parallel distributed processing: Exploration in the microstructure of cognition*, M.I.T., Cambridge Press (MA).

Sahebi, M. R., Bonn, F., and Bénié, G. B. (2004). "Neural networks for the inversion of soil surface parameters from synthetic aperture radar satellite data." *Canadian Journal of Civil Engineering*, 31(1), 95-108.

Satalino, G., Mattia, F., Davidson, M. W. J., Toan, T. L., Pasquariello, G., and Borgeaud, M. (2002). "On current limits of soil moisture retrieval from ERS-SAR data." *IEEE Transactions on Geoscience and Remote Sensing*, 40(11), 2438-2447.

Schmugge, T. J. (1998). "Application of passive microwave observation of surface soil moisture." *Journal of Hydrology*, 212-213, 188-197.

Schmugge, T. J., and Jackson, T. J. (1992). "A dielectric model of the vegetation effects on the microwave emission from soils." *IEEE Transactions on Geoscience and Remote Sensing*, 30, 757-760.

Schoups, G., Troch, P. A., and Verhoest, N. (1998). "Soil moisture influences on the radar backscattering of sugar beet fields." *Remote Sensing of Environment*, 65(2), 184–194.

Scipal, K., and Wagner, W. "Global Soil Moisture Data and Its Potential for Climatological and Meteorological Applications." *The 2004 Eumetsat Meteorological Satellite Conference,*, Prague, Czech Rebublic, May 31st – June 4th 2004.

Shi, J., Wang, J., Hsu, A., O'Neill, P., and Engman, E. T. (1997). "Estimation of bare surface soil moisture and surface roughness parameters using L-band SAR image data." *IEEE Transactions on Geoscience and Remote Sensing*, 35(5), 1254-1266.

Shoshany, M., Svoray, T., Curran, P. J., Foody, G. M., and Perevolotsky, A. (2000). "The relationship between ERS-2 SAR backscatter and soil moisture: Generalization from a humid to semi-arid transect." *International Journal of Remote Sensing*, 21(11), 2337-2343.

Smits, P. C., Dellepiane, S. G., and Schowengerdt, R. A. (1999). "Quality assessment of image classification algorithms for land-cover mapping: a review and a proposal for a cost-based approach." *International Journal of Remote Sensing*, 20(8), 1461-1486.

Soares, J. V., Renno, C. D., Formaggio, A. R., Costa, C. F. Y., and Frery, A. C. (1997). "An investigation of the selection of texture features for crop discrimination using SAR imagery." *Remote Sensing of Environment*, 59(2), 234-247.

Srivastava, H. S., Patel, P., Manchanda, M. L., and Adiga, S. (2003). "Use of multi-incidence angle RADARSAT-1 SAR data to incorporate the effect of surface roughness in soil moisture estimation." *IEEE Transactions on Geoscience and Remote Sensing* 41(7), 1638-1640.

Stehman, S. V. (1996). "Estimating the Kappa Coefficient and its variance under stratified random sampling." *Photogrammetric Engineering & Remote Sensing*, 62(4), 401-407.

Stehman, S. V. (1997a). "Estimating standard errors of accuracy assessment statistics under cluster sampling." *Remote Sensing of Environment*, 60, 258–269.

Stehman, S. V. (1997b). "Selecting and interpreting measures of thematic classification accuracy." *Remote Sensing of Environment*, 62, 77–89.

Svoray, T., and Shoshany, M. (2004). "Multi-scale analysis of intrinsic soil factors from SAR-based mapping of drying rates." *Remote Sensing of Environment*, 92(2), 233-246.

Taconet, O., Vidal-Madjar, D., Emblanch, C., and Normand, M. (1996). "Taking into account vegetation effects to estimate soil moisture from C-band radar measurements." *Remote Sensing of Environment*, 56, 52–56.

Takagi, T., and Sugeno, M. (1985). "Fuzzy identification of systems and its application to modeling and control." *IEEE Transactions on Systems, Man and Cybernetics*, SMC-15, 116-132.

Topouzelis, K., Karathanassi, V., Pavlakis, P., and Rokos, D. "Neural Networks for oil spill detection using ERS-SAR Data." *IEEE Transactions on geoscience, Istanbul, Turkey, July 2004*, 724-728.

Ulaby, F. T. (1974). "Radar measurement of soil moisture content." *IEEE Transaction on Antennas and Propagation*, AP-22(2), 257–265.

Ulaby, F. T., and Al-Rayes, M. A. (1987). "Microwave dielectric spectrum of vegetation Part II: Dual Dispersion Model." *IEEE Transactions on Geoscience and Remote Sensing*, GE-25, 550-557.

Ulaby, F. T., Dobson, M., and Bradley, G. (1981). "Radar reflectivity of bare and vegetation covered soil." *Advanced Space Research*, 1, 91-104.

Ulaby, F. T., Dubois, P. C., and Zyl, J. J. V. (1996). "Radar mapping of surface soil moisture." *Journal of Hydrology*, 184, 57-84.

Ulaby, F. T., Kouyate, F., Brisco, B., and Williams, T. H. L. (1986a). "Textural information in SAR images." *IEEE Transactions on Geoscience and Remote Sensing*, GE-24(2), 235-245.

Ulaby, F. T., Moore, R., and Fung, A. (1986b). *Microwave Remote Sensing Active and Passive From Theory to Applications*, Artech House Norwood MA.

Ulaby, F. T., Sarabandi, K., McDonald, K., Whitt, M., and Dobson, M. C. (1990). "Michigan Microwave Canopy Scattering Model." *International Journal of Remote Sensing*, 11(7), 1223-1253.

van-Zyl, J. J. (1993). "The Effects of Topography on the Radar Scattering from Vegetated Areas." *IEEE Transactions on Geoscience and Remote Sensing*, 31(1), 153-160.

Vine, D. M. L., Griffis, A., Swift, C. T., and Jackson, T. J. (1994). "ESTAR: A synthetic microwave radiometer for remote sensing applications." *Proceedings of the IEEE*, 82(12), 1787-1801.

Vine, D. M. L., Jackson, T. J., Swift, C. T., Haken, M., and Bidwell, S. (2001). "ESTAR measurements during the Southern Great Plains experiments." *IEEE Transactions on Geoscience and Remote Sensing*, 39, 1680-1685.

Walthall, C. L., Dulaney, W. P., Anderson, M. C., Norman, J. M., Fang, H., and Liang, S. (2004). "A comparison of empirical and neural network approaches for estimating corn and soybean leaf area index from Landsat ETM+ imagery." *Remote Sensing of Environment*, 92(4), 465-474.

Wang, C., Qi, J., Moran, S., and Marsett, R. (2004). "Soil moisture estimation in a semiarid rangeland using ERS-2 and TM imagery." *Remote Sensing of Environment*, 90, 178-189.

Wang, J. R., McMurtrey, J. E., Engman, E. T., Jackson, T. J., Schmugge, T. J., Gould, W. I., Fuchs, J. E., and Glazar, W. S. (1982). "Radiometric Measurements over Bare and Vegetated Fields at 1.4 Ghz and 5 Ghz Frequencies." *Remote Sensing of Environment*, 12, 295-311.

Wang, J. R., Schmugge, T. J., Shiue, J. C., and Engman, E. T. (1989). "Mapping surface soil moisture with L-band radiometric measurements." *Remote Sensing of Environment*, 27, 305-312.

Wang, Q., Adiku, S., Tenhunen, J., and Granier, A. (2005). "On the relationship of NDVI with leaf area index in a deciduous forest site." *Remote Sensing of Environment*, 94, 244–255.

Wang, Y., and Jamshidi, M. "Fuzzy logic applied in remote sensing image classification." *IEEE International Conference on Systems, Man and Cybernetics 10-13 Oct. 2004*, 6378-6382.

Western, A. W., and Bloschl, G. (1999). "On the spatial scaling of soil moisture." *Journal of Hydrology*, 217, 203-224.

Wickel, A. J., Jackson, T. J., and Wood, E. F. (2001). "Multi-temporal monitoring of soil moisture with Radarsat SAR during the 1997 Southern Great Plains hydrology experiment." *International Journal of Remote Sensing*, 22(8), 1571-1583.

Wood, E. F., Lin, D. S., Mamcini, M., Thongs, D., Troch, P. A., Jackson, T. J., Famiglietti, J. S., and Engman, E. T. (1993). "Inter-comparisons between passive and active microwave remote sensing and hydrological modeling for soil moisture." *Advanced Space Research*, 13(5), 167-175.

Zhao, K. G., Shi, J. C., Zhang, L. X., Jiang, L. M., Zhang, Z. J., Qin, J., Yao, Y. J., and Hu, J. C. "Retrieval of bare soil surface parameters from simulated data using neural networks combined with IEM." *IGARSS '03. IEEE Geoscience and Remote Sensing Symposium 21-25 July 2003*, 3881-3883.

Zribi, M., and Dechambre, M. (2002). "A new empirical model to retrieve soil moisture and roughness from C-band radar data." *Remote Sensing of Environment*, 84, 42-52.

Zribi, M., He´garat-Mascle, S. L., Ottl'e, C., Kammoun, B., and Guerin, C. (2003). "Surface soil moisture estimation from the synergistic use of the (multi-incidence and multi-resolution) active microwave ERS Wind Scatterometer and SAR data." *Remote Sensing of Environment*, 86, 30–41.